



Calhoun: The NPS Institutional Archive
DSpace Repository

Theses and Dissertations

1. Thesis and Dissertation Collection, all items

2021-06

TRANSONIC COMPRESSOR INLET FLOW FIELD ANALYSIS

Hearn, Patrick H.

Monterey, CA; Naval Postgraduate School

<https://hdl.handle.net/10945/67736>

This publication is a work of the U.S. Government as defined in Title 17, United States Code, Section 101. Copyright protection is not available for this work in the United States.

Downloaded from NPS Archive: Calhoun



Calhoun is the Naval Postgraduate School's public access digital repository for research materials and institutional publications created by the NPS community. Calhoun is named for Professor of Mathematics Guy K. Calhoun, NPS's first appointed -- and published -- scholarly author.

Dudley Knox Library / Naval Postgraduate School
411 Dyer Road / 1 University Circle
Monterey, California USA 93943

<http://www.nps.edu/library>



**NAVAL
POSTGRADUATE
SCHOOL**

MONTEREY, CALIFORNIA

THESIS

**TRANSONIC COMPRESSOR INLET FLOW FIELD
ANALYSIS**

by

Patrick H. Hearn

June 2021

Thesis Advisor:

Walter Smith

Co-Advisor:

Anthony J. Gannon

Approved for public release. Distribution is unlimited.

THIS PAGE INTENTIONALLY LEFT BLANK

REPORT DOCUMENTATION PAGE			<i>Form Approved OMB No. 0704-0188</i>	
Public reporting burden for this collection of information is estimated to average 1 hour per response, including the time for reviewing instruction, searching existing data sources, gathering and maintaining the data needed, and completing and reviewing the collection of information. Send comments regarding this burden estimate or any other aspect of this collection of information, including suggestions for reducing this burden, to Washington headquarters Services, Directorate for Information Operations and Reports, 1215 Jefferson Davis Highway, Suite 1204, Arlington, VA 22202-4302, and to the Office of Management and Budget, Paperwork Reduction Project (0704-0188) Washington, DC 20503.				
1. AGENCY USE ONLY (Leave blank)		2. REPORT DATE June 2021	3. REPORT TYPE AND DATES COVERED Master's thesis	
4. TITLE AND SUBTITLE TRANSONIC COMPRESSOR INLET FLOW FIELD ANALYSIS			5. FUNDING NUMBERS	
6. AUTHOR(S) Patrick H. Hearn				
7. PERFORMING ORGANIZATION NAME(S) AND ADDRESS(ES) Naval Postgraduate School Monterey, CA 93943-5000			8. PERFORMING ORGANIZATION REPORT NUMBER	
9. SPONSORING / MONITORING AGENCY NAME(S) AND ADDRESS(ES) Pratt and Whitney, Hartford, CT 06118			10. SPONSORING / MONITORING AGENCY REPORT NUMBER	
11. SUPPLEMENTARY NOTES The views expressed in this thesis are those of the author and do not reflect the official policy or position of the Department of Defense or the U.S. Government.				
12a. DISTRIBUTION / AVAILABILITY STATEMENT Approved for public release. Distribution is unlimited.			12b. DISTRIBUTION CODE A	
13. ABSTRACT (maximum 200 words) Achieving low stall speeds is desired for military aircraft to allow for improved flight performance. The purpose of this study was to accurately characterize the inlet flow field of a transonic compressor's inlet and observe if there were any flow field improvements due to rig modifications. Constant temperature hot-film anemometry was installed to obtain velocity measurements. Radial surveys were obtained at four separate azimuthal locations: 0°, -30°, 30°, and 120° to achieve an understanding of the flow field due to upstream components. Average turbulence intensity, flow field velocities, displacement thickness, momentum thickness, and shape factor were also computed and the experimental data was analyzed for compressor operations at 70%, and 85% power for near stall, intermediate, and choked conditions. A Computational Fluid Dynamic model was also created to compare the 85% choked simulation to the experimental results. This data set is essential for the evaluation of computational codes used for the simulation of transonic compressor rotors. These measurements will be utilized for future Computation Fluid Dynamic validation for separate work involving the redesign of the transonic compressor rig inlet as well as boundary and inlet conditions for ongoing simulation work.				
14. SUBJECT TERMS TCR, transonic compressor rig, CTA, constant temperature anemometry			15. NUMBER OF PAGES 121	
			16. PRICE CODE	
17. SECURITY CLASSIFICATION OF REPORT Unclassified	18. SECURITY CLASSIFICATION OF THIS PAGE Unclassified	19. SECURITY CLASSIFICATION OF ABSTRACT Unclassified	20. LIMITATION OF ABSTRACT UU	

THIS PAGE INTENTIONALLY LEFT BLANK

Approved for public release. Distribution is unlimited.

TRANSONIC COMPRESSOR INLET FLOW FIELD ANALYSIS

Patrick H. Hearn
Lieutenant, United States Navy
BS, University of Maryland College Park, 2012

Submitted in partial fulfillment of the
requirements for the degree of

MASTER OF SCIENCE IN MECHANICAL ENGINEERING

from the

**NAVAL POSTGRADUATE SCHOOL
June 2021**

Approved by: Walter Smith
Advisor

Anthony J. Gannon
Co-Advisor

Garth V. Hobson
Chair, Department of Mechanical and Aerospace Engineering

THIS PAGE INTENTIONALLY LEFT BLANK

ABSTRACT

Achieving low stall speeds is desired for military aircraft to allow for improved flight performance. The purpose of this study was to accurately characterize the inlet flow field of a transonic compressor's inlet and observe if there were any flow field improvements due to rig modifications. Constant temperature hot-film anemometry was installed to obtain velocity measurements. Radial surveys were obtained at four separate azimuthal locations: 0° , -30° , 30° , and 120° to achieve an understanding of the flow field due to upstream components. Average turbulence intensity, flow field velocities, displacement thickness, momentum thickness, and shape factor were also computed and the experimental data was analyzed for compressor operations at 70%, and 85% power for near stall, intermediate, and choked conditions. A Computational Fluid Dynamic model was also created to compare the 85% choked simulation to the experimental results. This data set is essential for the evaluation of computational codes used for the simulation of transonic compressor rotors. These measurements will be utilized for future Computation Fluid Dynamic validation for separate work involving the redesign of the transonic compressor rig inlet as well as boundary and inlet conditions for ongoing simulation work.

THIS PAGE INTENTIONALLY LEFT BLANK

TABLE OF CONTENTS

I.	INTRODUCTION.....	1
A.	OVERVIEW.....	1
B.	AIRCRAFT ENGINE STALL AND SURGE IMPORTANCE	1
C.	FLOW DISTORTION.....	2
D.	TURBULENCE.....	3
E.	FLOW FIELD MEASUREMENT TECHNIQUES	4
F.	RESEARCH OVERVIEW.....	7
II.	EXPERIMENTAL EQUIPMENT	9
A.	OVERVIEW	9
B.	HOT FILM ANEMOMETRY	9
C.	LOW SPEED TESTING.....	10
D.	NPS TRANSONIC COMPRESSOR TEST RIG.....	12
III.	DATA COLLECTION AND ANALYSIS	17
A.	CALIBRATION.....	17
B.	PROCEDURE	19
C.	COMPUTATIONAL SIMULATION.....	22
IV.	RESULTS	25
A.	WIND TUNNEL RESULTS	25
B.	TCR EXPERIMENTAL RESULTS	26
C.	COMPUTATIONAL RESULTS.....	39
V.	CONCLUSIONS	43
VI.	RECOMMENDATIONS.....	45
	APPENDIX A. HOT FILM CALIBRATION PROCEDURE.....	47
	APPENDIX B. HOT FILM DATA ACQUISITION PROCEDURE.....	51
	APPENDIX C. DATA ANALYSIS CODE.....	55
	APPENDIX D. ADDITIONAL TABLES AND GRAPHS.....	61
	LIST OF REFERENCES.....	99
	INITIAL DISTRIBUTION LIST	101

THIS PAGE INTENTIONALLY LEFT BLANK

LIST OF FIGURES

Figure 1.	Hot Wire Probe. Adapted from [12].	6
Figure 2.	Cylinder in Cross Flow	7
Figure 3.	Hot Film Probe	10
Figure 4.	IFA 300 Data Acquisition System	10
Figure 5.	Wind Tunnel	11
Figure 6.	Wind Tunnel Calibration Set Up	11
Figure 7.	Wind Tunnel with Mounted Traverse	12
Figure 8.	Transonic Test Rig Diagram	13
Figure 9.	TCR Rig Configuration	14
Figure 10.	Sensor Locations	15
Figure 11.	Hot Film Locations	15
Figure 12.	Hot Film Calibration Curve	18
Figure 13.	Density Correction Curve	18
Figure 14.	Alternate Calibration Method	19
Figure 15.	Test Configurations	21
Figure 16.	TCR CFX-Mesh	22
Figure 17.	TCR Cross Section CFX-Mesh	23
Figure 18.	Wind Tunnel Velocity Profile	25
Figure 19.	Wind Tunnel Turbulence Intensity	25
Figure 20.	Velocity Profile at 85% Power and Choked Condition	27
Figure 21.	Turbulence Profile at 85% Power and Choked Condition	27
Figure 22.	Velocity Profile at 85% Power and Intermediate Condition	28
Figure 23.	Turbulence Profile at 85% Power and Intermediate Condition	28
Figure 24.	Velocity Profile at 85% Power and Near Stall Condition	29

Figure 25.	Turbulence Profile at 85% Power and Near Stall Condition	29
Figure 26.	Velocity Profile at 70% Power and Choked Condition	30
Figure 27.	Turbulence Profile at 70% Power and Choked Condition.....	30
Figure 28.	Velocity Profile at 70% Power and Intermediate Condition	31
Figure 29.	Turbulence Profile at 70% Power and Intermediate Condition	31
Figure 30.	Velocity Profile at 70% Power and Near Stall Condition.....	32
Figure 31.	Turbulence Profile at 70% Power and Near Stall Condition	32
Figure 32.	Approximated Velocity Profile.....	33
Figure 33.	Power Spectrum 85% Power	35
Figure 34.	Power Spectrum 70% Power	36
Figure 35.	85% Power Spatial Contour Plot	36
Figure 36.	70% Power Spatial Contour Plot	37
Figure 37.	Power Spectrum at 85% Power at Nosecone.....	38
Figure 38.	85% Power Choked Condition Velocity Histogram.....	39
Figure 39.	CFD Velocity Distribution.....	40
Figure 40.	CFD Velocity Distribution near Traverse.....	40
Figure 41.	Comparison of CFD and Experimental Velocity Profiles	41
Figure 42.	Comparison of CFD and Experimental TI Profiles	41
Figure 43.	ThermalPro Calibration Setup	47
Figure 44.	ThermalPro Calibration Window.....	48
Figure 45.	Acquisition Sensor Setup Window	51
Figure 46.	Acquisition Conditions Setup.....	52
Figure 47.	Real-time display	53
Figure 48.	Velocity Analysis Window.....	53
Figure 49.	Velocity Analysis Statistics Window.....	54

LIST OF TABLES

Table 1.	Hot Film Sensor Specifications [14].....	9
Table 2.	Hot Film Calibration Data	17
Table 3.	Hot Film Data Locations.....	20
Table 4.	Mesh Statistics	22
Table 5.	Flow Characteristics.....	34
Table 6.	Wind Tunnel Calculations	61
Table 7.	Results for 85% Power Choked at 0°	62
Table 8.	Results for 85% Power Intermediate Condition at 0°	63
Table 9.	Results for 85% Power Near Stall at 0°	64
Table 10.	Results for 70% Power Choked at 0°	65
Table 11.	Results for 70% Power Intermediate Condition at 0°	66
Table 12.	Results for 70% Power Near Stall at 0°	67
Table 13.	Results for 85% Power Choked at -30°	68
Table 14.	Results for 85% Power Intermediate Condition at -30°	69
Table 15.	Results for 85% Power Near Stall at -30°	70
Table 16.	Results for 70% Power Choked at -30°	71
Table 17.	Results for 70% Power Intermediate Condition at -30°	72
Table 18.	Results for 70% Power Near Stall at -30°	73
Table 19.	Results for 85% Power Choked at 30°	74
Table 20.	Results for 85% Power Intermediate Condition at 30°	75
Table 21.	Results for 85% Power Near Stall at 30°	76
Table 22.	Results for 70% Power Choked at 30°	77
Table 23.	Results for 70% Power Intermediate Condition at 30°	78
Table 24.	Results for 70% Power Near Stall at 30°	79

Table 25.	Results for 85% Power Choked at 120°	80
Table 26.	Results for 85% Power Intermediate Condition at 120°	81
Table 27.	Results for 85% Power Near Stall at 120°	82
Table 28.	Results for 70% Power Choked at 120°	83
Table 29.	Results for 70% Power Intermediate Condition at 120°	84
Table 30.	Results for 70% Power Near Stall at 120°	85
Table 31.	Results for 85% Power Choked at 30° and Bellmouth Removed.....	86
Table 32.	Results for 85% Power Intermediate Condition at 30° and Bellmouth Removed	87
Table 33.	Results for 85% Power Near Stall at 30° and Bellmouth Removed.....	88
Table 34.	Results for 70% Power Choked at 30° and Bellmouth Removed.....	89
Table 35.	Results for 70% Power Intermediate Condition at 30° and Bellmouth Removed	90
Table 36.	Results for 70% Power Near Stall at 30° and Bellmouth Removed.....	91
Table 37.	Results for 85% Power Choked at 0° and Bellmouth Removed.....	92
Table 38.	Results for 85% Power Intermediate Condition at 0° and Bellmouth Removed	93
Table 39.	Results for 85% Power Near Stall at 0° and Bellmouth Removed.....	94
Table 40.	Results for 70% Power Choked at 0° and Bellmouth Removed.....	95
Table 41.	Results for 70% Power Intermediate Condition at 0° and Bellmouth Removed	96
Table 42.	Results for 70% Power Near Stall at 0° and Bellmouth Removed.....	97

LIST OF ACRONYMS AND ABBREVIATIONS

ANSYS	Analysis System
CFD	Computational Fluid Dynamics
CFX	Computational Fluid Flow
CTA	Constant Temperature Anemometry
IFA	Intelligent Flow Analyzer
LDV	Laser Doppler Velocimetry
NPS	Naval Postgraduate School
PIV	Particle Image Velocimetry
TPL	Turbopropulsion Lab

THIS PAGE INTENTIONALLY LEFT BLANK

NOMENCLATURE

E	Voltage	V
D	Diameter	m
d*	Displacement Thickness	m
h	Convection Heat Transfer Coefficient	$W m^{-2} K^{-1}$
H	Shape Factor	-
k	Turbulent Kinetic Energy Per Unit Mass	$m^2 s^{-2}$
k _f	Conductive Heat Transfer	$W m^{-1} K^{-1}$
k-ε	k-epsilon	-
L	Length	m
Nu	Nusselt Number	-
P	Pressure	Pa
P _o	Total Air Pressure	Pa
Re	Reynolds Number	-
St	Strouhal Number	-
T _{AMB}	Ambient Temperature	K
TI	Turbulent Intensity	-
TKE	Turbulent Kinetic Energy	$kg m^2 s^{-2}$
u	Local Velocity	$m s^{-1}$
u'	Velocity Variance	$m s^{-1}$
U _{FS}	Freestream Velocity	$m s^{-1}$
U _{Mean}	Mean Velocity	$m s^{-1}$
U _{Meas}	Measured Velocity	$m s^{-1}$
U _{Ref}	Reference Velocity	$m s^{-1}$
V	Velocity	$m s^{-1}$
ω	Frequency	Hz
θ	Momentum Thickness	mm

THIS PAGE INTENTIONALLY LEFT BLANK

ACKNOWLEDGMENTS

Completion of this research would not be possible without the dedication of several individuals. My advisors, Dr. Walter Smith, Dr. Anthony Gannon, and Dr. Garth Hobson, provided enormous support throughout my time at the Naval Postgraduate School. Not only do they have their own research, teaching, and other duties to fulfill, but they find the time to help answer my questions without hesitation and offer their support. The past year and a half has been especially difficult due to the pandemic, which has brought obstacles I did not foresee, but my advisors were flexible and provided input on how to continue to progress with thesis work. They also challenged me to expand my ability to think critically, put knowledge to practice, and solve complex problems, which is certain to help with my future endeavors.

In addition, I would not have completed much of this work without the assistance of Mr. John Gibson. John was always at the Turbopropulsion Lab early every morning to provide hands-on assistance and guidance even as he had his own duties to perform and students to assist.

The engineers at TSI were also instrumental to my progress throughout this project. They answered my many questions expeditiously. Without their help, it would have been difficult to integrate the hot film and traversing systems.

My fellow classmates were also instrumental in providing beneficial recommendations to my thesis and were also a steady source of motivation to study effectively and manage my time effectively. It was a unique experience having to learn remotely, but everyone was great at adapting to new methods of collaboration and communicating with one another.

THIS PAGE INTENTIONALLY LEFT BLANK

I. INTRODUCTION

A. OVERVIEW

There has been much experimental research performed to better understand and model turbulence inside a compressor. Transition of the flow's boundary layer may occur over a wide range and depends on the degree of turbulence [1]. The transition region's position has a direct influence on the compressor's performance. Understanding the turbulence behavior is necessary for two main reasons. The first is that many compressor rigs desire to obtain similar flow characteristics at the inlet as in-service compressors. This ensures validity of the rest of the rig and engine analysis. Another motivator for turbulence modeling, as discussed extensively by Camp and Shin, is to apply experimental results to sophisticated and complex CFD programs which are widely used by the engineering community to model systems and perform design and analysis [1].

The overall goal of this study is to successfully and accurately measure the flow field characteristics of a transonic compressor test rig inlet. One method is accomplished by utilizing hot film anemometry. By inserting a hot wire probe and sensor into the test rig, and monitoring power to maintain temperature, flow velocity measurements are obtained. In addition, with the velocity measurements, turbulence intensities and kinetic energies are calculated as a function of the distance from the outer wall.

B. AIRCRAFT ENGINE STALL AND SURGE IMPORTANCE

Today most large subsonic aircraft utilize turbine and turbojet engine principles. The first jet engine was developed, tested, and flown in 1938 by Heinkel and Von Ohain [2]. The jet engine revolutionized the aircraft industry by permitting aircraft to fly at higher speeds, greater altitudes, and make flying more practical and affordable.

Military aircraft engines are designed to operate at a specified flight envelope which allows for a small stall margin. By having a lower mass flow, engines would be capable of flying at lower speeds which would allow for more maneuverability and larger flight envelopes for landing and taking off. Papamarkos describes engine stall occurring when the demand for airflow exceeds the airflow being supplied by the compressor [3]. When

this occurs, the smooth air is disrupted causing turbulent flow and pressure fluctuations to occur within the turbine [3].

C. FLOW DISTORTION

Flow distortion is an important concept that aircraft engine designers must understand. Distorted flow occurs when an engine is subject to incoming flow that is nonuniform. Naval aircraft aboard aircraft carriers are subject to flow distortions that cause the aircraft's compressor to operate with a decreased stall margin [4]. Currently steam catapults are used aboard aircraft carriers to allow for the launching of aircraft over a short distance. Catapult steam leaks out and is sometimes ingested by the engines during takeoff [4]. Lieutenant Payne investigated "pop stall" which is the ingestion of steam leading to compressor stall. To study the effects of "pop stall," a steam boiler was utilized to simulate the catapult steam which was then introduced with the main air intake through a fast-acting solenoid valve. By relating the mass flows at steam induced stall and regular compressor stall, the stall margin decreased by 17% on the Sanger rotor [4].

Research has been conducted in the analysis of engine response to distorted flow fields due to the aircraft design. As aircraft continue to evolve and aircraft manufacturers continue to investigate methods for decreasing fuel consumption, many aircraft involve embedding the engine within the airframe which leads to a distorted flow. Modern military fighter aircraft, are fitted with turbofan engines which are embedded into the underbelly or sides of the aircraft fuselage. At Virginia Technical University, an inlet distortion generation program called a StreamVane was created to produce simultaneous pressure and swirl elements to create a desired inlet profile [5]. This profile is created by computational analysis of a boundary layer ingesting engine. The StreamVane creates this distorted field by creating a total pressure loss screen pattern and adjusting turning vanes which induce the swirl profile. A full-scale engine test was performed to compare the engine performance with and without flow distortion. It was concluded flow distortion caused a significant reduction in inlet mass flow rate and an increase in fuel consumption. Therefore, the engine experienced a decrease in performance and large efficiency impact [5]. Due to these adverse effects, developing and testing engines which can withstand flow

distortion and upstream turbulent sources will play a major role in future engine research and development.

D. TURBULENCE

Jet engines are also subject to turbulence which has been a difficult quantity to measure though there are some indications that it may be more systematic than previously indicated. Turbulent flow as described by Tennekes and Lumley is random, fluctuating, and disordered motion due to flow instabilities especially at larger Reynolds Numbers (Re) [6]. Turbulence is quantified by a simple mean value calculation as the Navier Stokes equations result in chaotic solutions. Though this is a practical way to perform turbulence analysis and provide an overall flow understanding, it is not the most accurate as every flow is unique and as a result variations in turbulence will exist [6].

Turbulent flow requires production and dissipated energy from the flow to continue its existence, according to Tennekes and Lumley [6]. This energy comes from a shear force in the mean flow. If an environment of no shear exists, the flow will transition to laminar. The distance this occurs is known as the diffusion length. If the velocity of the flow is known, the time scale of diffusion can be related to the length scale. The diffusion rate of turbulent flow is much higher as opposed to molecular diffusion, therefore obtaining measurements at a high frequency is important to perform flow analysis in a turbulent flow environment [6]. According to Bradshaw, turbulence can also be viewed as motion as a result of vortex stretching which causes velocity fluctuations [7]. This stretching and turbulent wavelength is caused and limited by the frictional forces and flow boundary conditions [7].

There are several parameters which are used in the field of fluid mechanics to quantify turbulence as discussed by Goldstein [8]. A common parameter is the turbulent kinetic energy (TKE). This is calculated by first determining the root mean-square components of velocity. The root mean-square components are determined by summing the squares of the difference between the actual velocity and mean velocity and then taking the average. The turbulent kinetic energy per unit mass (k) can then be calculated using

equation 2 which requires a summation of the velocity component variances u' , v' , and w' [8].

$$E_{Total} = E_M + E_{TURB} = .5(u + u')^2 = .5(u + u')(u + u') = .5(u^2 + u'u') \quad (1)$$

$$k = .5(u'^2 + v'^2 + w'^2) \quad (2)$$

Another common parameter is the turbulent intensity (TI) [8]. This is related to the kinetic energy and the mean velocity (U_{mean}) by

$$Ti = \frac{\left(\frac{2}{3} * k\right)^{.5}}{U_{mean}} \quad (3)$$

This is a useful variable as it allows for a comparison of turbulence at different locations and times. In turbulent flows, it is expected that the intensity will decrease exponentially from the turbulent source.

E. FLOW FIELD MEASUREMENT TECHNIQUES

Several methods of capturing the flow field through an engine have been implemented. It is important for these measurements to be accurate as technologies have been advancing in aircraft engines and so it is important that the manufactures are provided with reliable and accurate data to evaluate their simulation codes with. One of the most common methods for obtaining flow characteristics in turbomachinery is to utilize pressure-based measurements. These pressure based methods require a pressure probe to be inserted into the flow field. A common probe used in the aircraft industry is a pitot probe that is capable of obtaining total and static pressure measurements. By obtaining a static and total pressure measurement, a subsonic velocity can be calculated by utilizing Bernoulli's equation. If the flow upstream of the total pressure measurement is subsonic, fluid momentum and isentropic relations are used for calculations. However, in the case of supersonic flow, a normal shock will occur resulting in an entropy increase as the velocity decreases. This will result in a pressure increase and therefore this needs to be accounted for when performing flow analysis and calculations. Goldstein discusses several issues with this method due to the probe insertion which has the potential to influence the obtained

measurements [8]. One such effect could be caused by the proximity to a wall. As the pressure probe approaches a wall, streamlines are deflected by a probe-wall interaction. This is likely to occur when the distance between the probe and the wall is less than two times the diameter of the probe. Another issue is the wall of the instrument will create an asymmetrical flow around the tube leading to incorrect data. Also, the effective center of the tube will shift toward regions of higher velocity causing biased data to be obtained [8]. As a result, these devices are not optimal for high speed measurements especially in regards to turbulent flows and so other options are available and utilized for such flow analysis. This was especially apparent when performing a calibration and proof of concept in a small 3D printed wind tunnel and larger low speed wind tunnel as it took some time for air to accumulate through the pressure instrument and tubing which was connected to a manometer.

Sensitive pressure transducers, developed by Kulite Semiconductor Product, Inc are another method capable of obtaining flow measurements [9]. These sensors are more suitable for high frequency measurements as the sensor is highly sensitive and located directly in the flow. The instrument consists of 3 layers. The first layer consists of monocrystalline N-type silicon which has a diaphragm machined within the layer. The diaphragm thickness depends on the maximum pressure and is designed to witness 350–400 microinches per inch of strain at the maximum pressure. The second layer consists of silicon dioxide on top of the N-type diaphragm. This electrically isolated the N type material and P-type material. The final layer contains four strain gauges of P-type silicon organized in a Wheatstone bridge circuit. As the elements are exposed to a pressure force two of these strain gauges will see tension which causes the resistance to increase while the other two witness compression causing their resistance to decrease. The tension gauges are opposite of each other as are the compression ones. This causes the resistance change to be substantial which allows for a maximum output. The stress applied is directly proportional to the resistance imbalance across the Wheatstone circuit [9].

An additional measurement technique to counter undesired effects is Constant Temperature Anemometry (CTA) which was utilized in this research as it is robust, well understood, and trusted in the fluid mechanics field. A hot wire or film probe consisting of

a thin sensor aligned perpendicular to the direction of flow. This sensor is held in place between two prongs as seen in Figure 1. As air flows over the wire or film convection heat transfer occurs between the sensor and the flow as depicted in Figure 2. As the flow velocity increases more convection occurs causing the wire temperature to decrease [10]. The heat transfer can be described by the Nusselt Number (Nu) which is the ratio of convective heat transfer to conductive heat transfer resulting in being a function of the Reynolds Number (Re) and pressure ratio (Pr) as shown by equation 4. To keep the sensor at a constant temperature the current applied is balanced with the flow over the wire. This change in current is displayed as a voltage change which is recorded by Thermal Pro software [11]. Use of this experimental instrumentation has been proven in past research to include a ramjet engine by Ensign Alford at the Naval Postgraduate Turbopropulsion Laboratory (TPL) [12]. There are also more sophisticated hot wire probes which consist of multiple sensors at fixed angles. This allows for decomposition of the velocity components to allow for more accurate calculations and an improved understanding of the flow field as the velocity is composed of three directional components [11]. The single film sensor was utilized for this research as interest was in the axial flow direction.

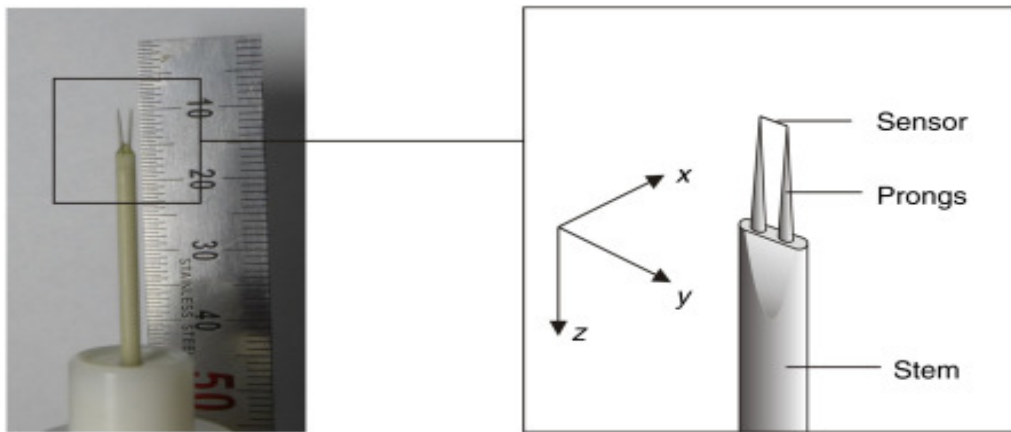


Figure 1. Hot Wire Probe. Adapted from [12].

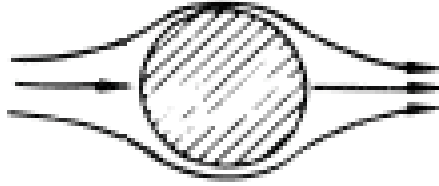


Figure 2. Cylinder in Cross Flow

$$Nu = \frac{hL}{k_f} = f(Re, Pr) \quad (4)$$

Particle Image Velocimetry (PIV) is a common imaging technique. Guimaraes describes this technique as small particles being introduced to the flow while ensuring a Stokes number of less than 1 exists [13]. This ensures that the particles will flow with the streamlines. A laser sheet is then used to illuminate the flow field with short pulses. Particle images are captured with a camera which is synchronized with the pulses. Images are then used to calculate the displacement of the particle which allows for a velocity to be calculated. Not only does PIV decrease the probe disturbance effect but it also allows for a large portion of the flow to be analyzed while a probe can only obtain measurements at a single location [13].

F. RESEARCH OVERVIEW

The goal of this study was to model the turbulence of the Naval Postgraduate School's (NPS) Transonic Compressor Rig's (TCR) inlet. This was performed by using constant temperature anemometry.

The Experimental Equipment section provides details of the hot film equipment which was necessary to obtain the required data. This equipment was used in both the TCR and a low speed wind tunnel. Information on the set up, integration, and operation of these devices is also provided.

The procedure section contains the process for obtaining the data. This includes the calibration method which was required to calibrate the hot film sensor. Calibration was accomplished by obtaining voltage readings and correlating them to velocity measurements

from pressure instrumentation in the free stream. A density correction was also necessary for the TCR which required a density correction plot which utilized the pressure in the flow field. The density correction curve was constructed by correlating the velocity and static inlet pressure. With these curves, it was possible to convert raw voltages to corrected velocities at the compressor inlet. The equations to convert the raw voltage to a density corrected velocity are provided. In addition to obtaining real data, a computational simulation was performed to model the flow. The setup is also explained.

Data was first obtained in the low speed wind tunnel. Afterwards, the equipment was transferred to the TCR. Measurements were taken at four separate locations for six flow field conditions at 70% and 85% power and repeated at two of these locations after removing the upstream bellmouth. Velocity and turbulence intensity plots were produced to compare the flow at the various locations. The computational results were also plotted against the experimental data for comparison.

Conclusions and recommendations are also discussed to provide information on the success and areas of improvement for this research. Also, methods to further expand this research are also discussed.

II. EXPERIMENTAL EQUIPMENT

A. OVERVIEW

The Naval Postgraduate Turbopropulsion Lab (TPL) is a part of the Department of Mechanical and Astronautical Engineering; this is where testing of the transonic compressor, data collection, and analysis is performed.

B. HOT FILM ANEMOMETRY

TSI's Intelligent Flow Analyzer (IFA) 300 Constant Temperature Anemometer and ThermalPro software were utilized to obtain hot film data. The IFA 300 was controlled by the ThermalPro software through a RS-232 connection and maintained the hot film sensor at a constant temperature by regulating the voltage. Voltage readings were sent through a terminal board and then to a data acquisition card which was installed within the computer. Figure 4 illustrates the schematic of this data acquisition system and the user interface of ThermalPro is shown in Appendices A and B which outline the procedures. The probe model utilized was TSI Model 1212-20, Regular Straight Probe, as shown in Figure 3, with a sensor orientation of 0° relative to the probe connection. The probe was connected to the IFA 300 by a coaxial cable. The probe's and sensor's specifications are summarized in Table 1 [14]. The sampling frequency was 100 KHz which was chosen from the low speed wind tunnel testing which resulted in the TI 95% confidence interval to be within 1% in the freestream.

Table 1. Hot Film Sensor Specifications [14]

Temperature Coefficient of Resistance	.00024 °C
Maximum Sustained Ambient Temperature	300°C
Maximum Sensor Operating Temperature	425°C
Material	Platinum
Sensor Area Width	25.4 umm
Sensor Area Length	.51 mm
Distance Between Supports	3.2 mm

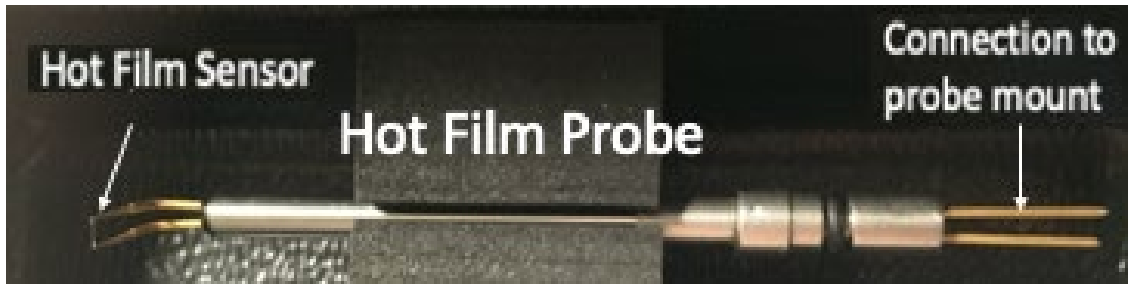


Figure 3. Hot Film Probe

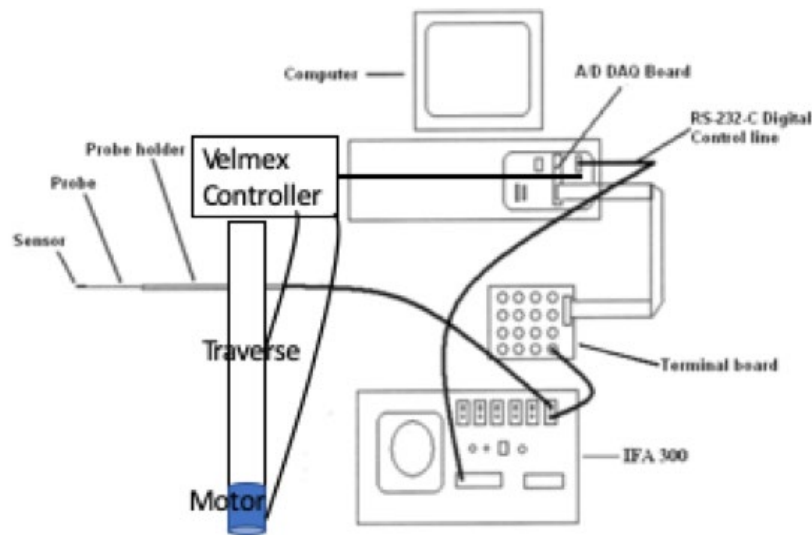


Figure 4. IFA 300 Data Acquisition System

A Velmex Motorized BiSlide traverse was mounted with a 2.5 VDC SLO-SYN Stepping Motor at a 90-degree offset to the outer casing and then connected to the probe holder by an aluminum arm so the hot film could be automatically repositioned by the Thermal-pro software. Traverse configuration can be observed in the proceeding sections.

C. LOW SPEED TESTING

A wind tunnel, Figures 5–7, was transferred from Watkins Hall to the Propulsion Lab to perform a proof of concept study for both the calibration and acquisition of hot film data. This allowed for insight in regards to noise levels and required frequency and sample size requirements. The tunnel was modified to hold the hot film probe and a pitot probe

simultaneously. The pitot probe was connected to an angled barometer along with a static pressure connection from the bottom of the tunnel. The wind tunnel was powered by an electrical motor which allowed for speed regulation and therefore acted as a throttle. The calibration began with the fan stationary to obtain a zero-velocity voltage reading and then voltage and differential pressure readings were taken at 70%, 80%, 90%, and 100% power. The differential pressure was converted to a velocity to be inputted to the ThermalPro software.



Figure 5. Wind Tunnel

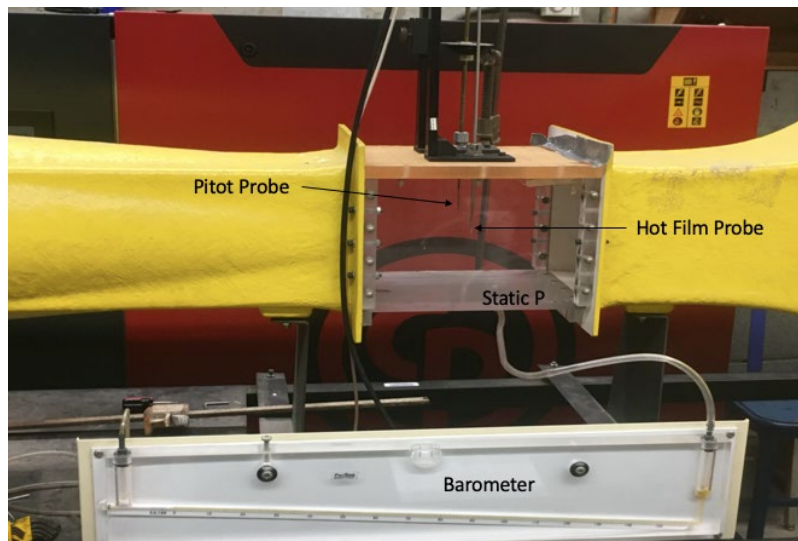


Figure 6. Wind Tunnel Calibration Set Up

After performing a calibration, the traverse was incorporated by mounting it behind the hot film probe holder and connecting it by an aluminum arm. This allowed for testing the control of the traverse and integrating all of the hardware components through the ThermalPro software.

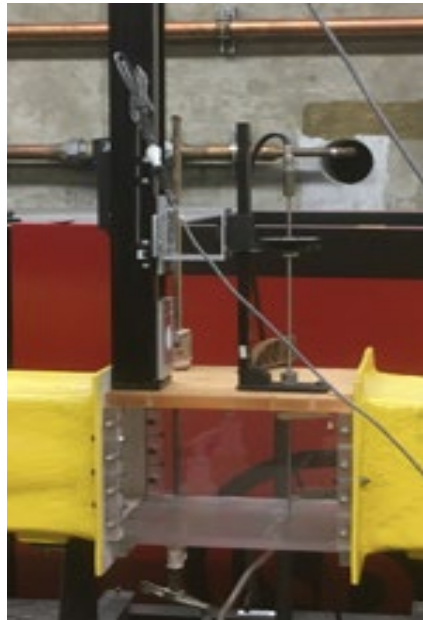


Figure 7. Wind Tunnel with Mounted Traverse

D. NPS TRANSONIC COMPRESSOR TEST RIG

The Transonic Compressor Test Rig (TCR) at the Naval Postgraduate School (NPS) has been utilized as a test platform for pioneering flow measurements. It was designed by Dr. Vavra of the Aerospace department and is still being used today. This rig has been used to test real world flow fields and compare them to computer simulations [15]. The TCR is manually operated in a separate room outside the test area. Figure 8 shows the TCR.

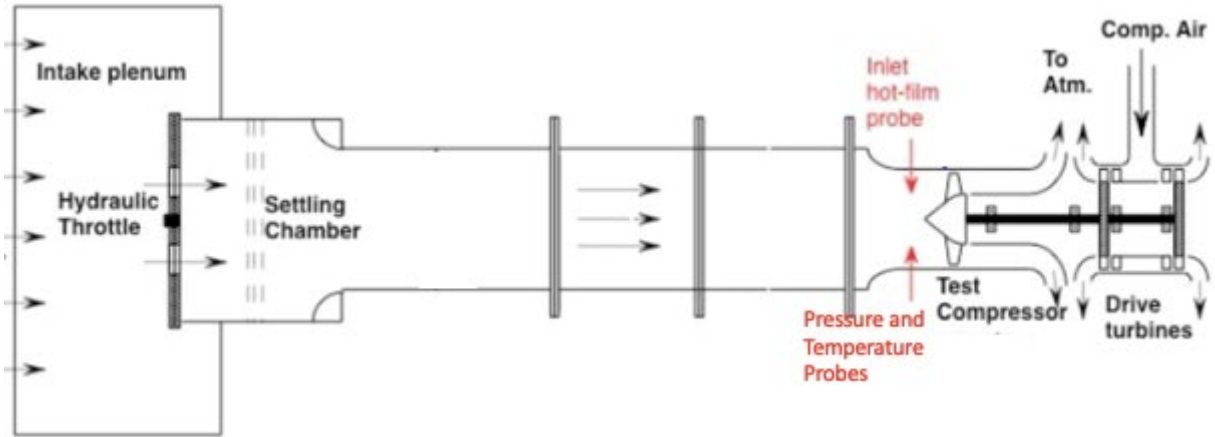


Figure 8. Transonic Test Rig Diagram

As described by Payne, the TCR is driven by compressed air, as seen on the right most part of Figure 8, from two opposing rotor turbine stages being driven by a 12-stage Allison-Chalmers axial compressor [4]. The compressor is capable of providing compressed air at 300 KPa at 5 Kilograms per second. An electric motor is used to adjust the turbine speed. A hydraulically actuated operating plate throttle controls the flow rate through the test compressor [4].

The traverse which was described previously was mounted to the outer casing. Figure 9 shows the equipment mounted to the TCR outer casing.



Figure 9. TCR Rig Configuration

The hot film sensor was inserted through the TCR casing by a steel rod which had a coaxial connection at the top. The sensor location was rotated four times for separate measurement angles as the inlet contained six holes at 60 degree offsets which could potentially lead to a non-uniform flow. This was performed to be sure the flow was axisymmetric for future modeling and analysis purposes. Two pressure instruments which were at offsetting angles were used for calibration purposes. Figure 10 shows the pressure and hot film sensor locations and Figure 11 shows the four hot film locations relative to the upstream throttle. The 0 and 120 degree locations are situated between the throttle holes which allow air flow to enter while the 30 and -30 degree locations are exposed to the inlet holes.



Figure 10. Sensor Locations

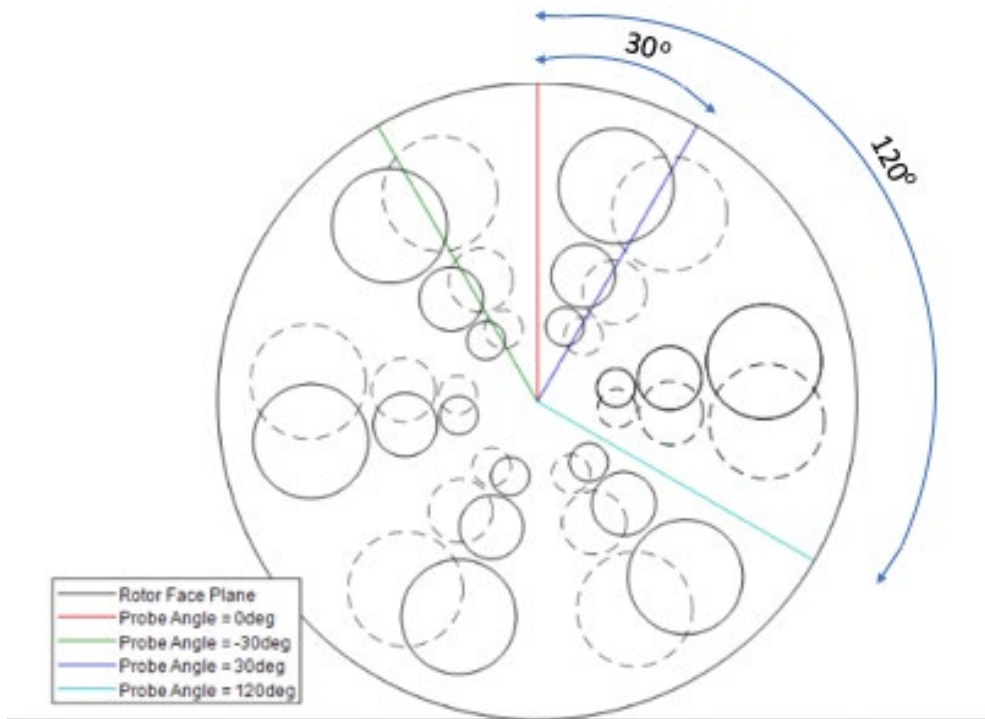


Figure 11. Hot Film Locations

THIS PAGE INTENTIONALLY LEFT BLANK

III. DATA COLLECTION AND ANALYSIS

A. CALIBRATION

With all of the hardware and software components set up properly, a calibration was performed. As the TCR was brought up to speed, several speeds were used to calibrate the hot film sensor while at a choked condition. By taking known velocity, pressure, and voltage readings calibration curves were constructed. A fourth-order curve was fitted using the velocity and voltage measurements to convert the raw voltage to velocity measurements. Pressure data was obtained to create a separate curve to calculate a corrected velocity, taking into account density changes. Table 2 provides calibration data which was then used to create a velocity calibration curve, Figure 12, and a density correction curve, Figure 13. Appendix A provides the detailed steps to perform the calibration through the ThermalPro software.

Table 2. Hot Film Calibration Data

Voltage [V]	Velocity [m/s]	Pressure [Pa]	Temperature [K]
2.92	41.73	98526.48	285.40
3.10	56.27	96449.55	285.00
3.23	71.39	93404.28	284.20
3.43	105.40	85972.19	285.70
3.47	113.63	83880.00	284.60
3.49	123.00	81533.00	288.30
3.53	132.38	79110.52	286.60
3.54	135.95	78195.41	284.50
3.54	137.93	77795.00	286.20

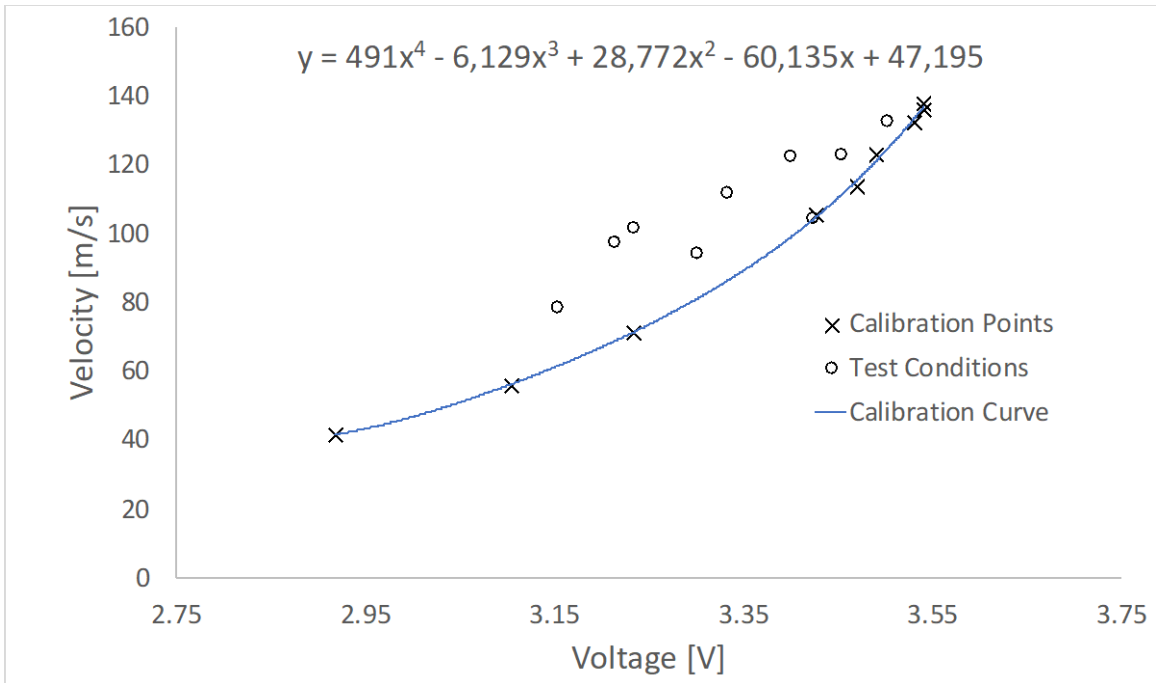


Figure 12. Hot Film Calibration Curve

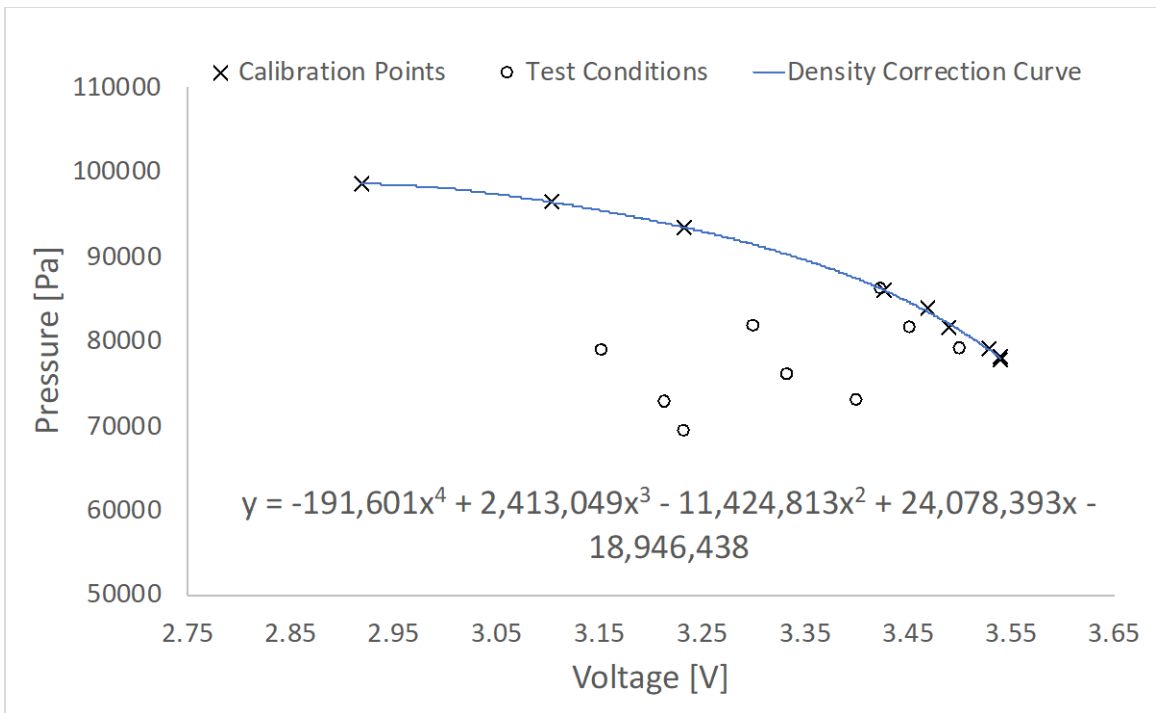


Figure 13. Density Correction Curve

An alternate method for calculating the velocity was also investigated as it allowed for a wider range of operating conditions to be used as the previous method only utilized a full open throttle. An additional intermediate and near stall point at 80% power were included. Voltage was plotted with the calibration velocity multiplied by the calibration pressure. This allowed the velocity to be calculated, from Figure 14, in a single step which produced near identical results as to the two step method.

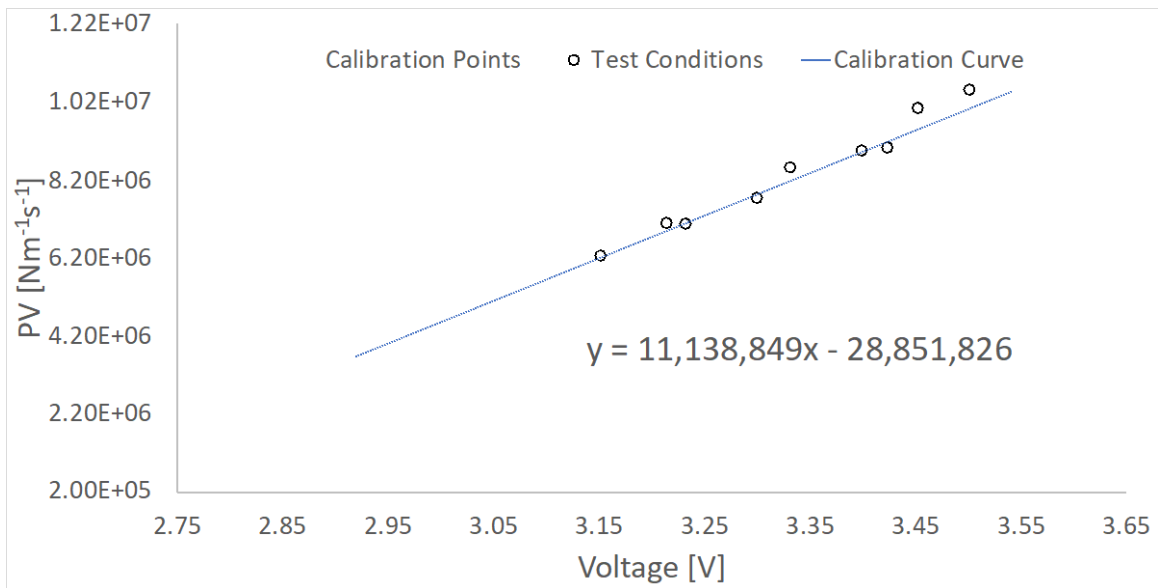


Figure 14. Alternate Calibration Method

B. PROCEDURE

After a calibration was performed, hot film data was acquired at predetermined locations with 6mm from the inner casing being used as a zero-reference point. Table 3 provides the locations which were inputted to ThermalPro so the traverse could control the position of the hot film sensor automatically. The front of the nose cone was 145.6 mm from the inner casing so 139.6 mm was inputted for Run #30 to capture this location.

Table 3. Hot Film Data Locations

Run #	X [mm]	Run #	X [mm]	Run #	X [mm]
2	0	12	2	22	30
3	0.1	13	2.5	23	40
4	0.2	14	3	24	50
5	0.3	15	3.5	25	60
6	0.4	16	4	26	75
7	0.5	17	5	27	90
8	0.75	18	7.5	28	105
9	1	19	10	29	125
10	1.25	20	15	30	139.6
11	1.5	21	20	31	141

For each location, hot film data was acquired at each predetermined position for the choked, an intermediate condition, and near stall for 70% and 85% power. Figure 15 outlines the compressor operating conditions. Initially the probe was mounted from the top (0°) of the TCR. Once hot film data was taken for the above conditions the experimental rig was adjusted to 30, -30, and 120 degree offsets. Then, the upstream bellmouth was removed and the process was repeated for the 0 and 30 degree locations. This was necessary as the test rig will be upgraded and was desired to have a characterization of the flow before and after the upgrade. This will allow for a comparison of performance as future modifications are implemented. Appendix B provides a detailed procedure for using ThermalPro to acquire data for each condition.

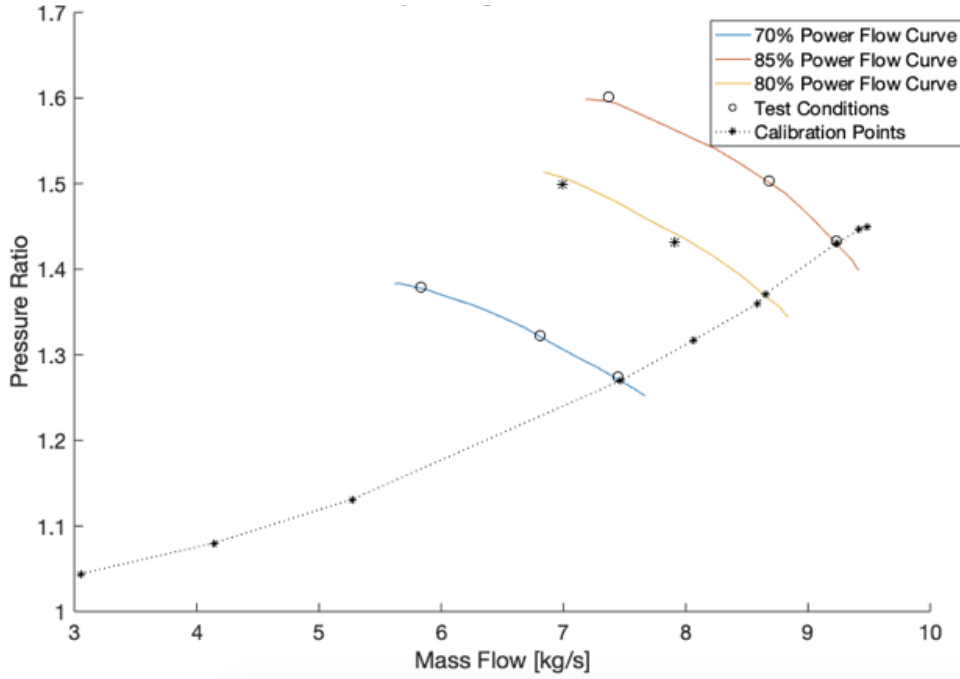


Figure 15. Test Configurations

After performing velocity calculations with the calibration curve, a density correction was required since the calibration curve was performed at the choked condition. Density correction was performed by using the density correction curve to determine the corresponding calibration pressure (P_{cal}). A corrected velocity (V_{cor}) was then calculated by equations 5–7 which also required the experimental pressure (P_{exp}) which was obtained from the static pressure ports during the traverse. Equation 5 was first used to convert the raw voltage (E) to a velocity (V). This velocity was corrected for density by extracting P_{cal} from equation 6 and then applying it to equation 7 along with V and P_{exp} .

$$V = A_1 E^4 + A_2 E^3 + A_3 E^2 + A_4 E + A \quad (5)$$

$$P_{cal} = B_1 E^4 + B_2 E^3 + B_3 E^2 + B_4 E + B \quad (6)$$

$$V_{cor} = V \frac{P_{cal}}{P_{exp}} \quad (7)$$

C. COMPUTATIONAL SIMULATION

The TCR inlet piping was modeled by use of ANSYS-CFX version 19.2. Drawings and physical measurements were utilized to create the nose cone, bell mouth, and 3 meters of upstream piping in SolidWorks. Then, the model was imported to generate a mesh in ANSYS-CFX. Table 4 provides the information in regards to the meshing of the tunnel and Figures 16 and 17 illustrate the resulting mesh.

Table 4. Mesh Statistics

Number of Nodes	3,257,155
Number of Elements	7,488,427
Number of Inflation Layers	33
First Layer Thickness	1 micrometer
Inflation Layer Expansion Ratio	1.2
Element Size	.01 meter
Yplus	.2
Max Size	.1 meter

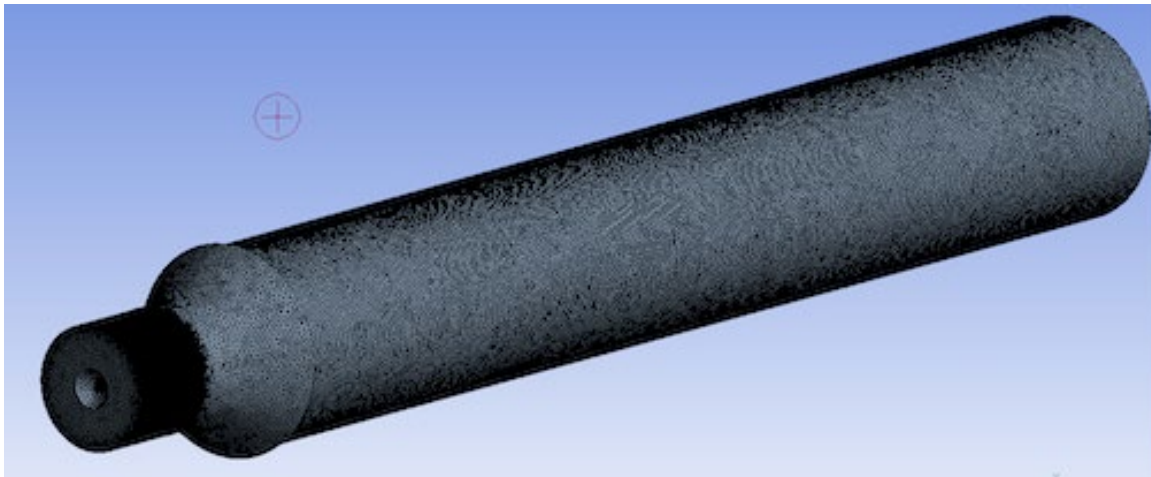


Figure 16. TCR CFX-Mesh

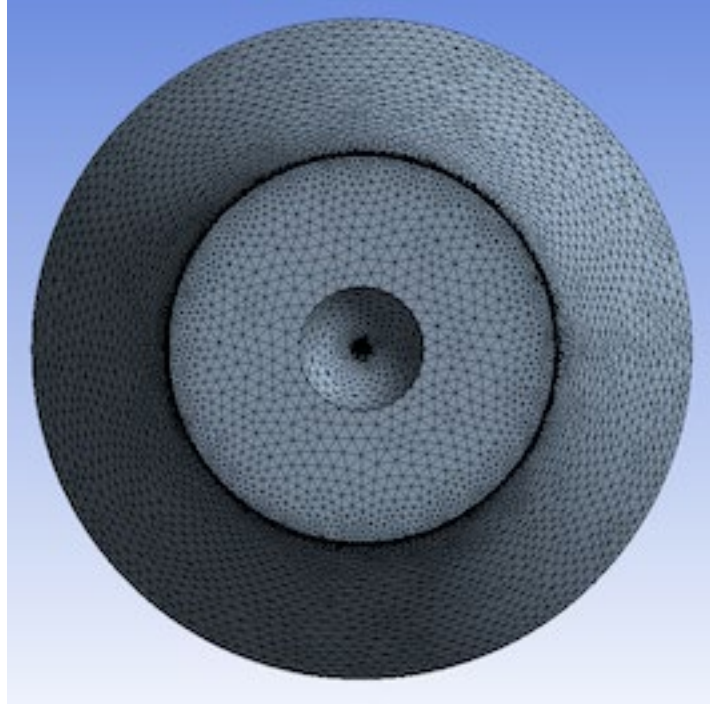


Figure 17. TCR Cross Section CFX-Mesh

After completing the mesh, CFX-Pre was used to match the experimental conditions for the 85% power choked condition. This included matching the RPM, static P at the compressor inlet, and upstream total pressure. To model the turbulence the k-Epsilon ($k-\epsilon$) model was chosen with an inlet intensity of 10% to match the experimental freestream TI as close as feasible.

THIS PAGE INTENTIONALLY LEFT BLANK

IV. RESULTS

A. WIND TUNNEL RESULTS

A wind tunnel velocity profile and turbulence intensity was calculated along with 95% confidence intervals. Figures 18 and 19 illustrate the velocity and turbulence intensity profiles and Table 6 provides the calculated numerical results.

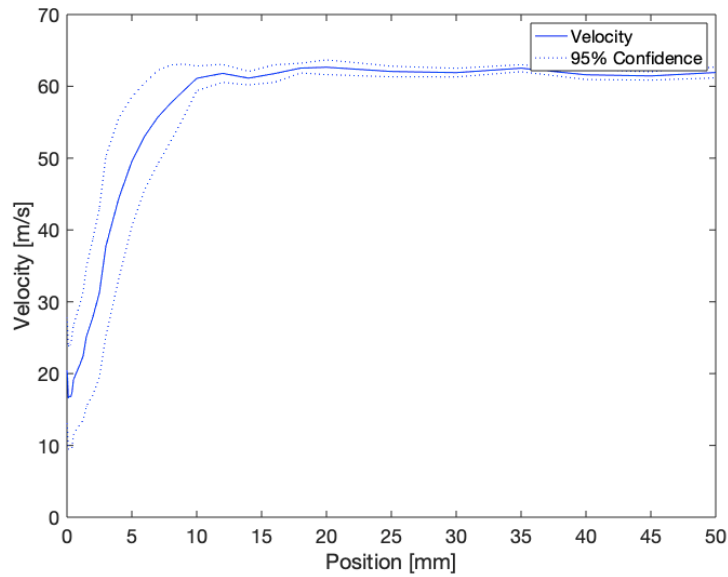


Figure 18. Wind Tunnel Velocity Profile

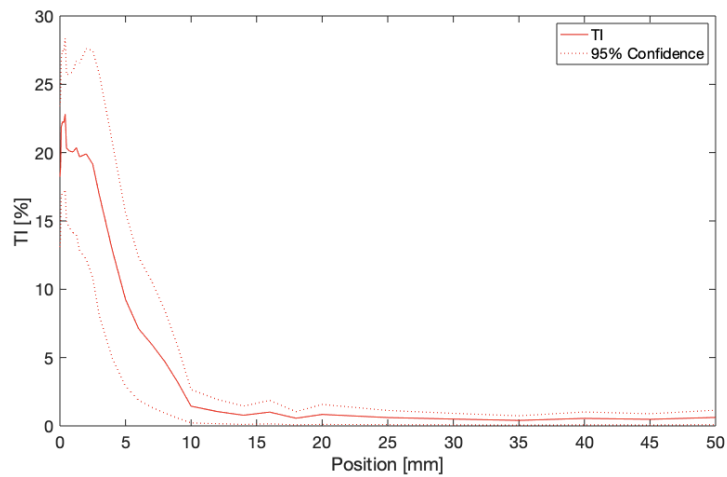


Figure 19. Wind Tunnel Turbulence Intensity

B. TCR EXPERIMENTAL RESULTS

Hot film measurements were obtained at 85% and 70% power for choked, an intermediate, and near stall conditions. This was repeated at four circumferential locations; 0, -30, 30, and 120°. The normalized velocity, ratio of local velocity (u) to freestream velocity (U_{FS}) which was corrected for TSI standard conditions as calculated by equations 8 and 9, and turbulence intensity was calculated at each location and then plotted, Figures 20 - 31, for comparison purposes.

$$U_{FS} = U_{Meas} \frac{T_{AMB}}{273+21.1} \frac{101325}{P_o} \quad (8)$$

$$Normalized\ Velocity = \frac{u}{U_{FS}} \quad (9)$$

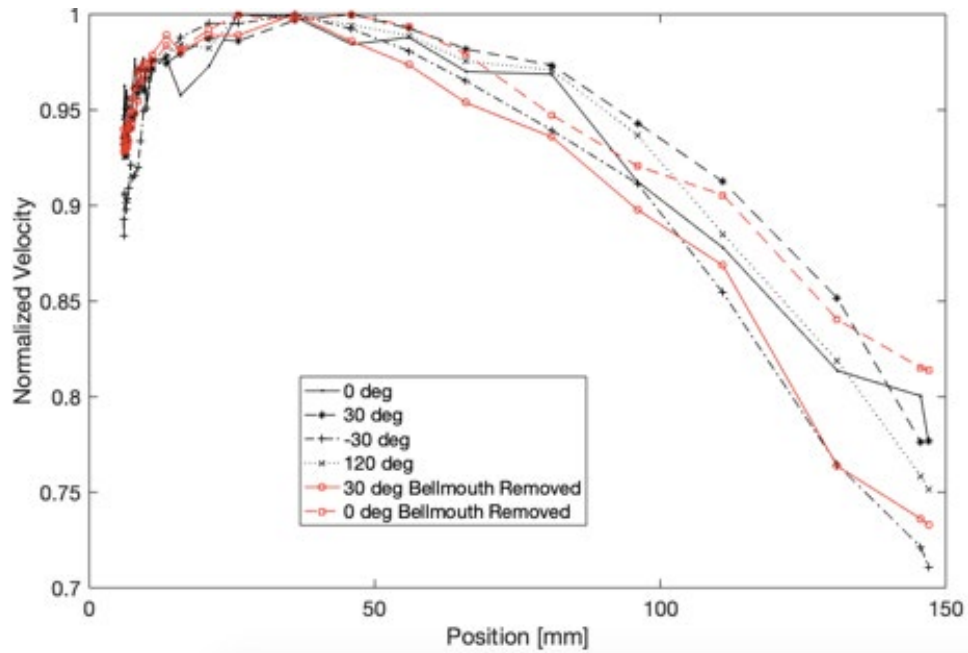


Figure 20. Velocity Profile at 85% Power and Choked Condition

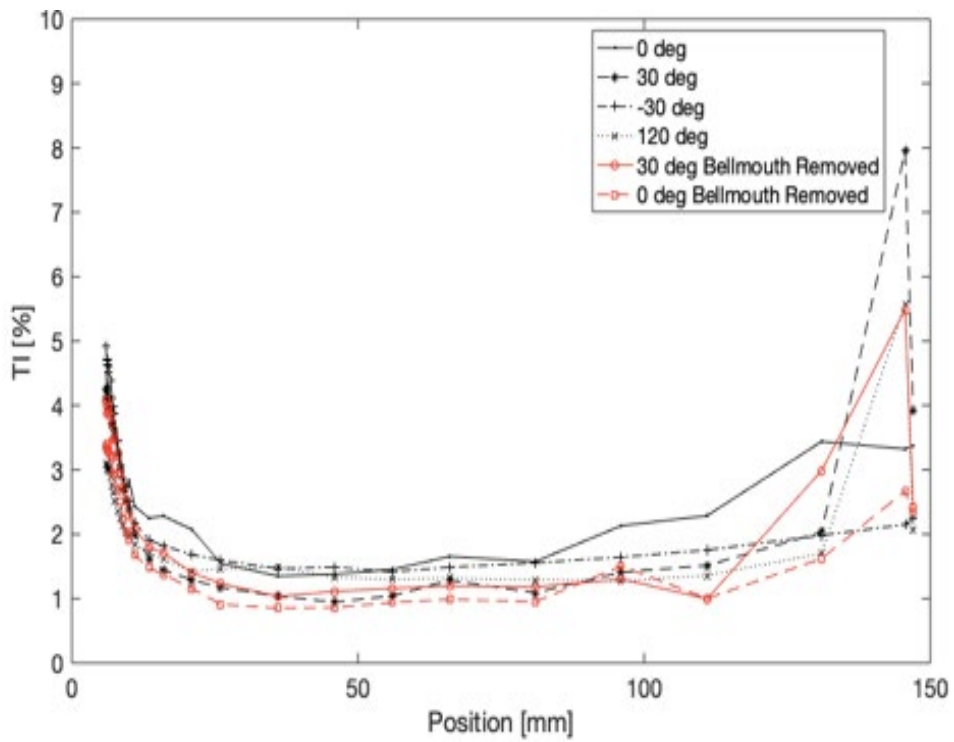


Figure 21. Turbulence Profile at 85% Power and Choked Condition

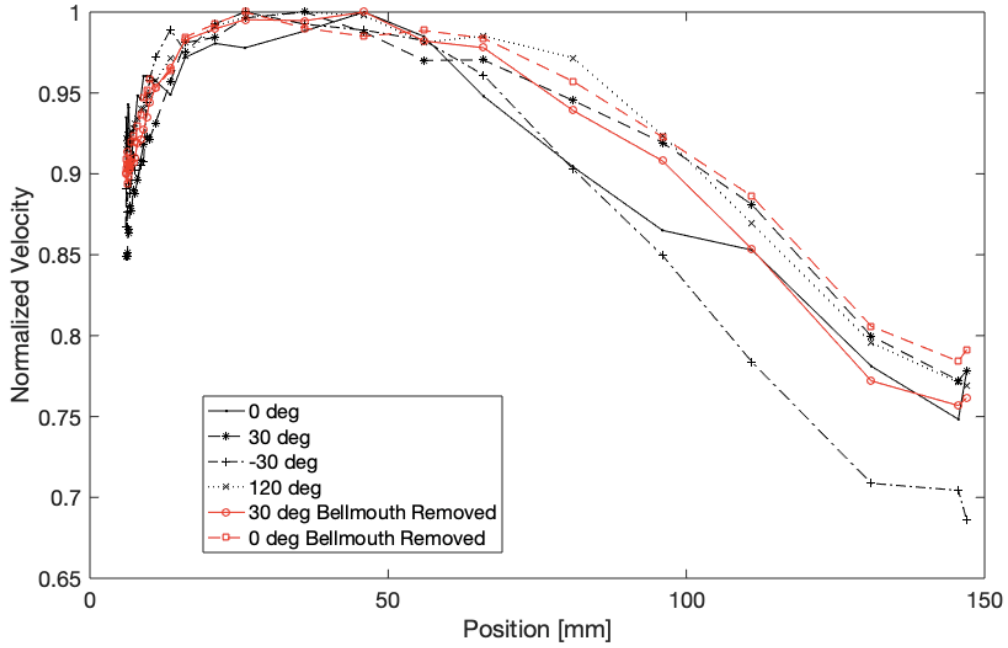


Figure 22. Velocity Profile at 85% Power and Intermediate Condition

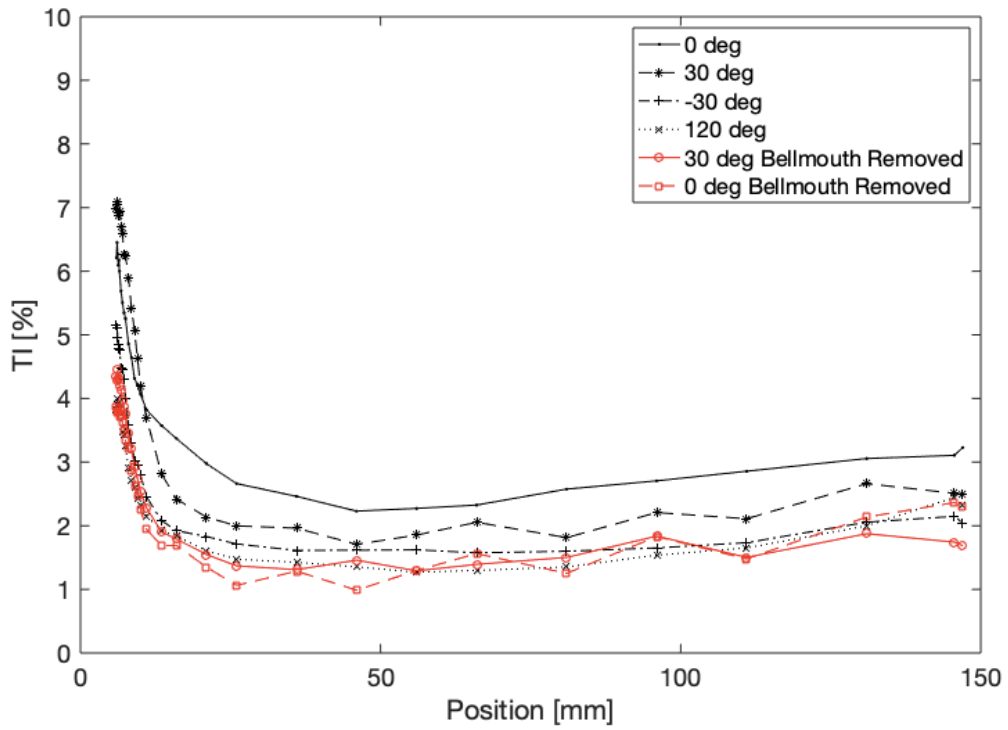


Figure 23. Turbulence Profile at 85% Power and Intermediate Condition

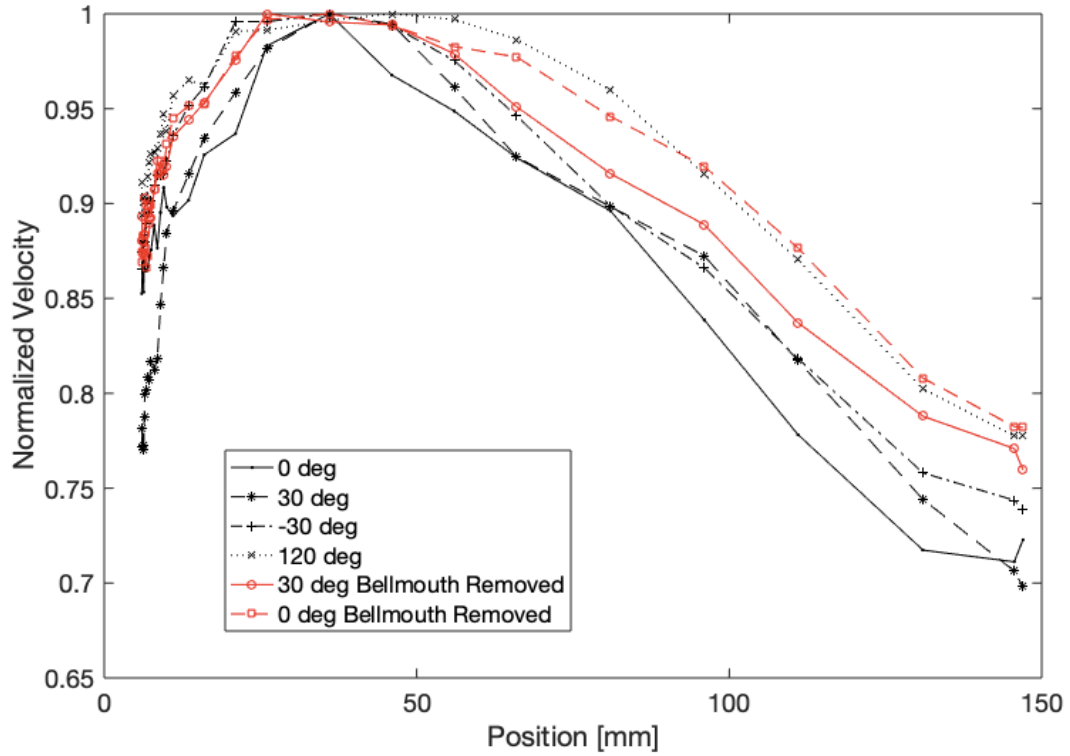


Figure 24. Velocity Profile at 85% Power and Near Stall Condition

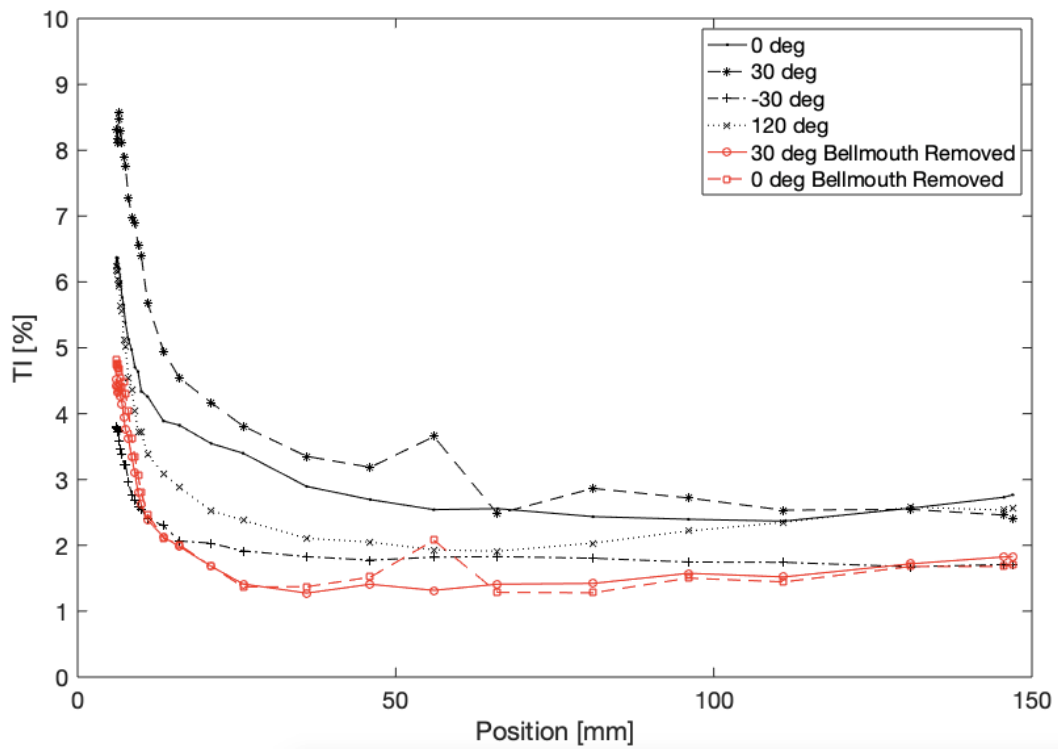


Figure 25. Turbulence Profile at 85% Power and Near Stall Condition

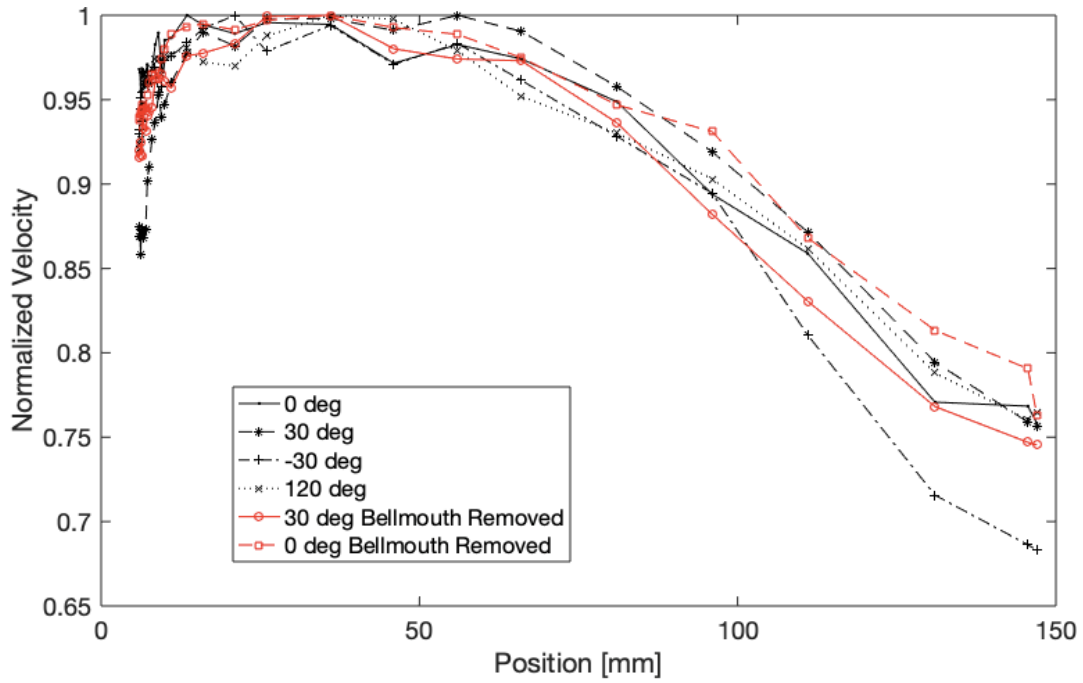


Figure 26. Velocity Profile at 70% Power and Choked Condition

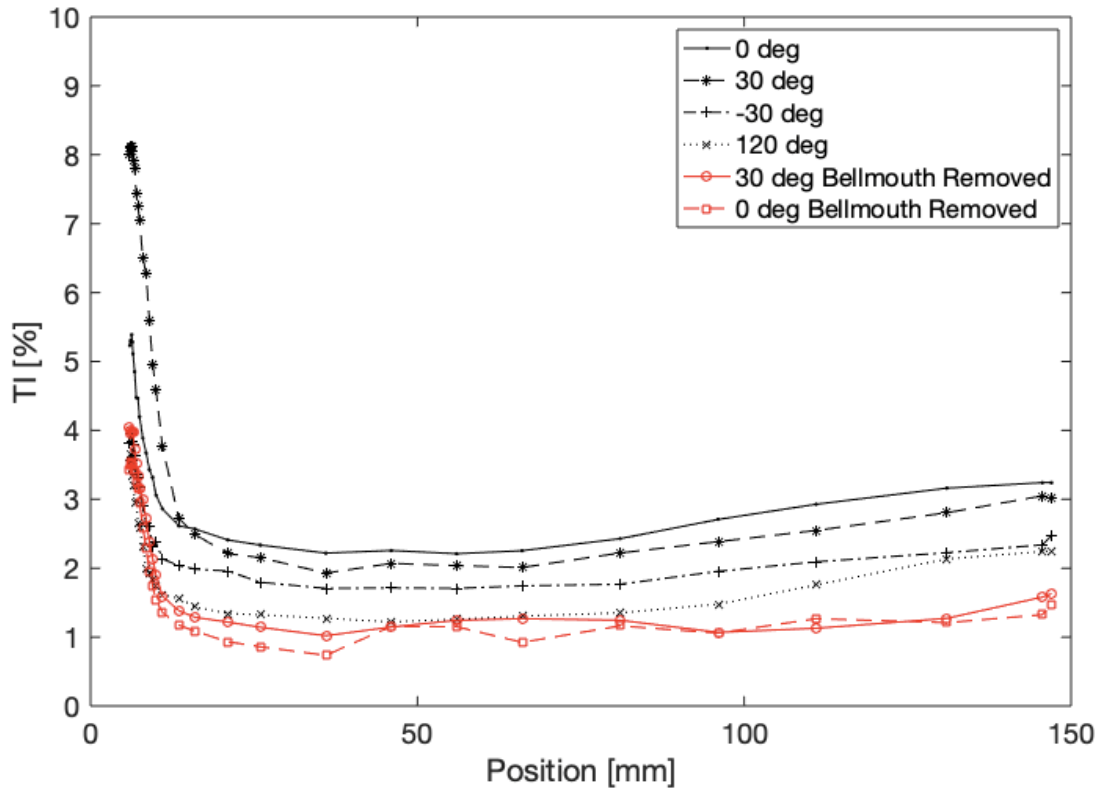


Figure 27. Turbulence Profile at 70% Power and Choked Condition

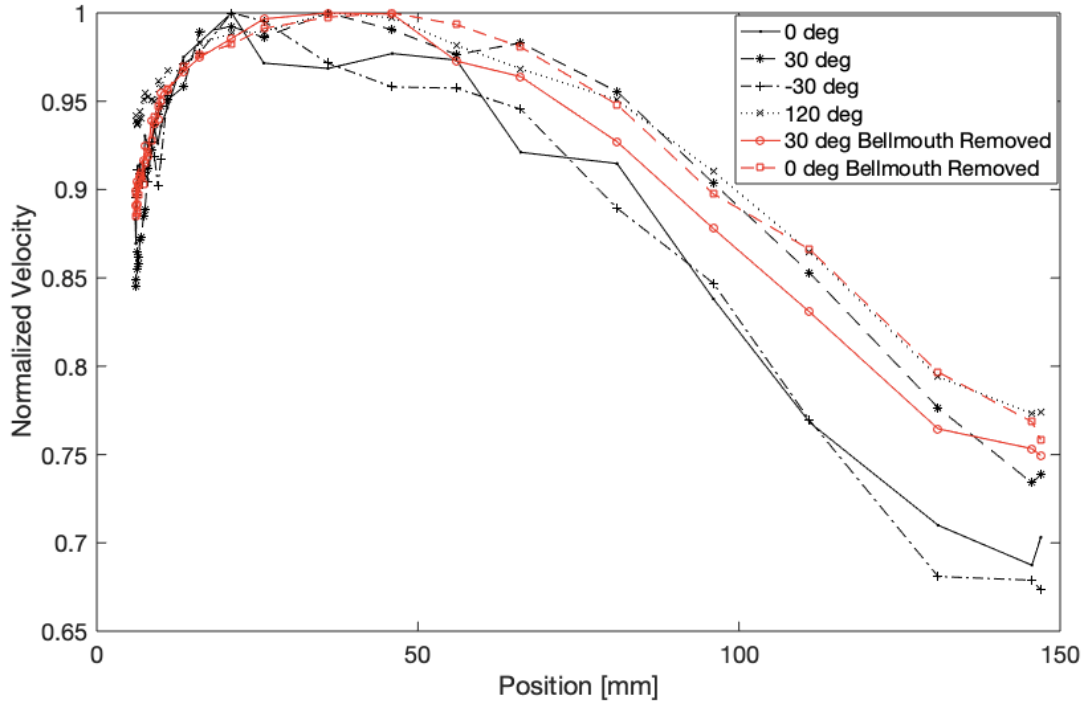


Figure 28. Velocity Profile at 70% Power and Intermediate Condition

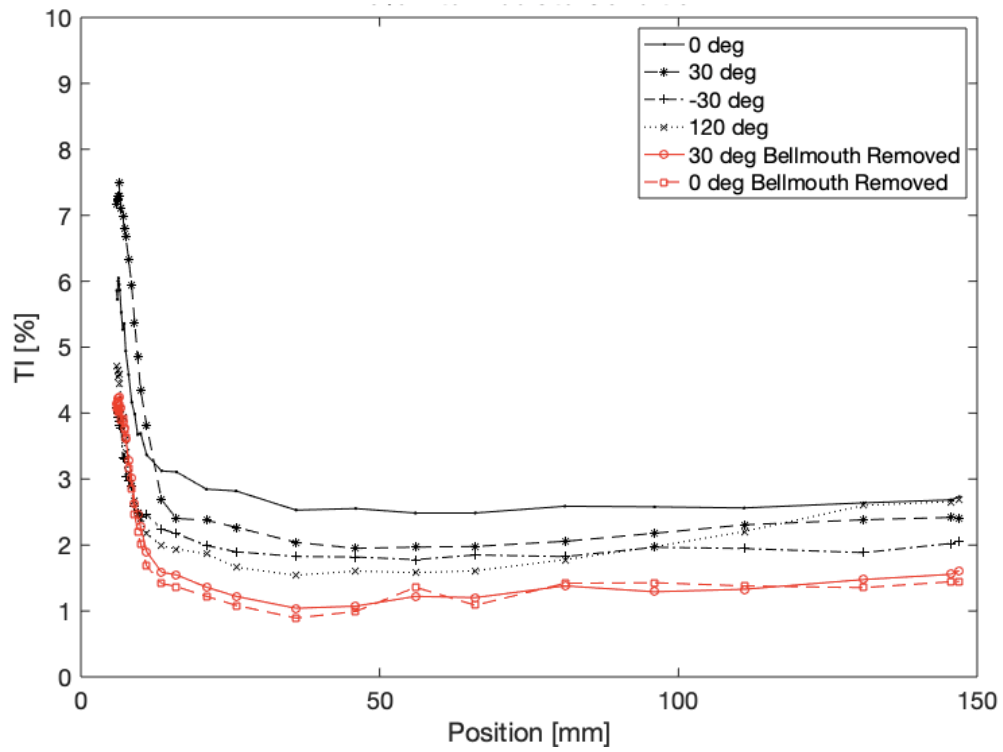


Figure 29. Turbulence Profile at 70% Power and Intermediate Condition

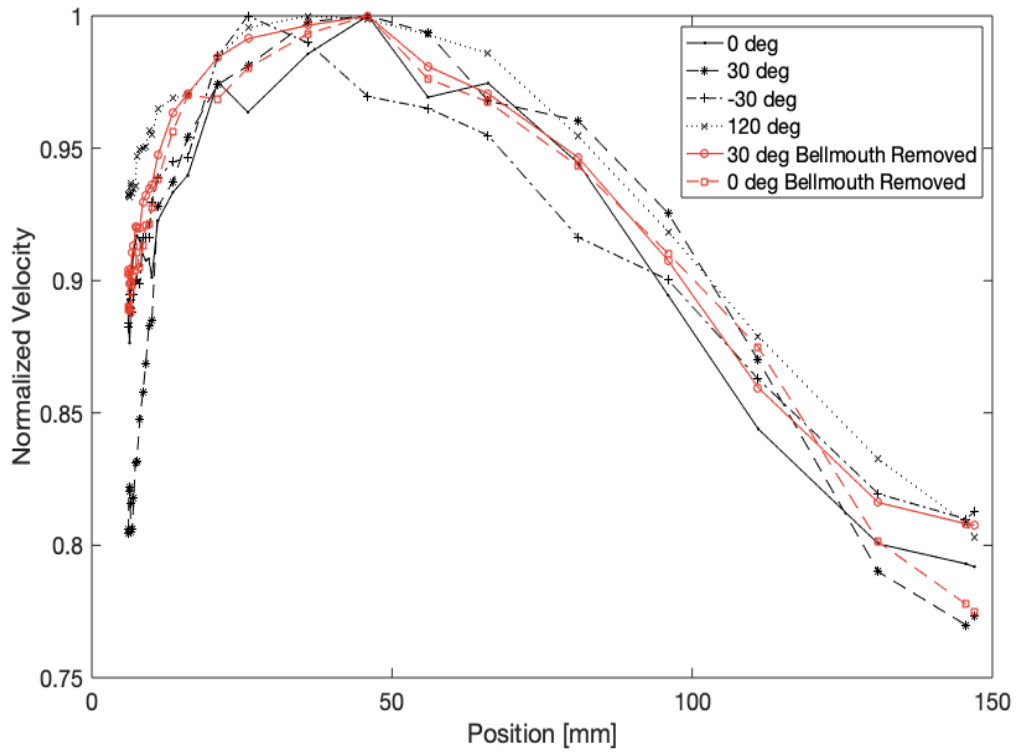


Figure 30. Velocity Profile at 70% Power and Near Stall Condition

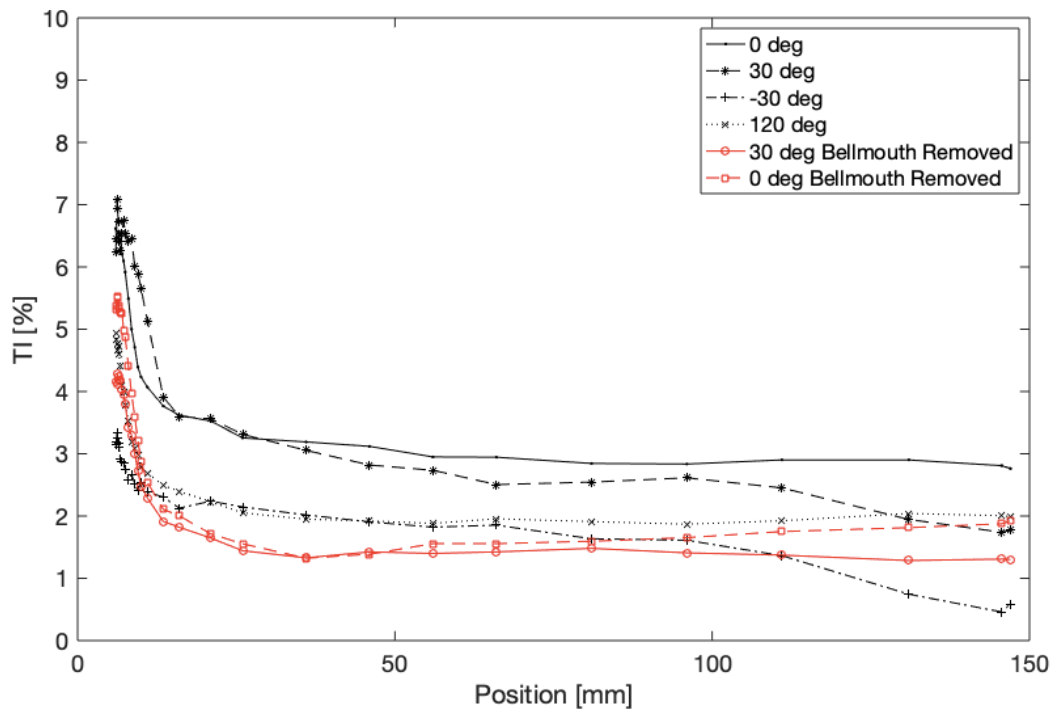


Figure 31. Turbulence Profile at 70% Power and Near Stall Condition

Figure 32 shows an approximated velocity profile by fitting the experimental data points to allow for the displacement thickness (d^*), momentum thickness (θ), and shape factor (H) to be tabulated. Since data was obtained starting at 6mm from the wall to protect the hot film sensor, the entire profile, from the wall to freestream, was approximated with the existing data by a power function. This was necessary as these values required integrating from the wall to the freestream location of 36mm achieved with equations 10–12 which were obtained from Tennekes and Lumley [6]. By calculating d^* , θ , and H , the nature of the flow can be characterized as turbulent or laminar [6]. These results are shown in Table 5.

$$d^* = \int_0^d \left(1 - \frac{u}{U}\right) dy \quad (10)$$

$$\theta = \int_0^d \frac{u}{U} \left(1 - \frac{u}{U}\right) dy \quad (11)$$

$$H = \frac{d^*}{\theta} \quad (12)$$

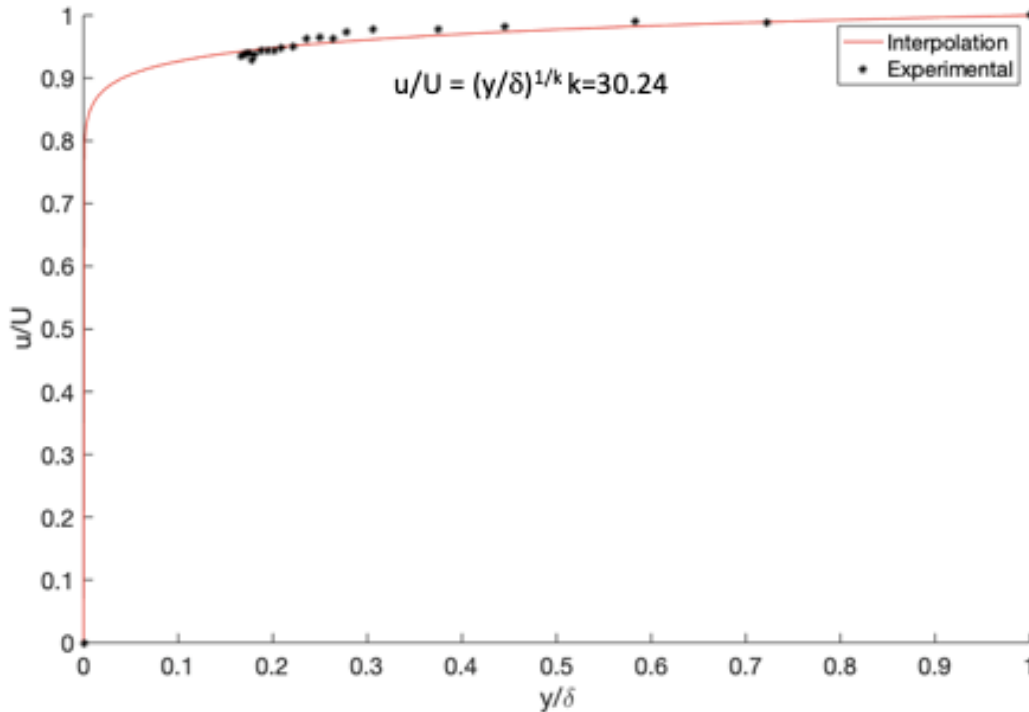


Figure 32. Approximated Velocity Profile

Table 5. Flow Characteristics

Condition	Position [deg]	d* [mm]	θ [mm]	H
85% Choked	0	1.064	0.987	1.078
85% Choked	30	1.166	1.078	1.082
85% Choked	-30	1.854	1.659	1.118
85% Choked	120	1.152	1.065	1.081
85% Choked	30 (Bell removed)	1.110	1.028	1.079
85% Choked	0 (Bell removed)	1.252	1.153	1.086
85% Intermediate	0	1.257	1.157	1.086
85% Intermediate	30	2.565	2.213	1.159
85% Intermediate	-30	2.122	1.873	1.133
85% Intermediate	120	1.561	1.417	1.102
85% Intermediate	30 (Bell removed)	1.779	1.598	1.113
85% Intermediate	0 (Bell removed)	1.771	1.591	1.113
85% Near Stall	0	2.830	2.407	1.176
85% Near Stall	30	4.116	3.264	1.261
85% Near Stall	-30	2.304	2.015	1.144
85% Near Stall	120	1.753	1.576	1.112
85% Near Stall	30 (Bell removed)	2.236	1.962	1.140
85% Near Stall	0 (Bell removed)	2.391	2.082	1.149
70% Choked	0	0.694	0.651	1.066
70% Choked	30	2.166	1.907	1.135
70% Choked	-30	1.010	0.939	1.075
70% Choked	120	1.125	1.041	1.080
70% Choked	30 (Bell removed)	1.377	1.261	1.092
70% Choked	0 (Bell removed)	1.010	0.940	1.075
70% Intermediate	0	1.931	1.721	1.122
70% Intermediate	30	2.444	2.121	1.152
70% Intermediate	-30	1.987	1.766	1.125
70% Intermediate	120	1.199	1.107	1.084
70% Intermediate	30 (Bell removed)	1.852	1.657	1.117
70% Intermediate	0 (Bell removed)	1.879	1.679	1.119
70% Near Stall	0	1.940	1.729	1.122
70% Near Stall	30	3.524	2.887	1.221
70% Near Stall	-30	2.219	1.949	1.139
70% Near Stall	120	1.322	1.214	1.089
70% Near Stall	30 (Bell removed)	1.791	1.608	1.114
70% Near Stall	0 (Bell removed)	1.997	1.774	1.126

Power spectrum plots, Figures 33 and 34, and spatial contour plots, Figures 35 and 36, were created through a Fast Fourier Transform. The blade passing frequency was observed as 9350 Hz corresponding to the blade passing frequency at 85% power and 7700 Hz corresponding to 70% power. As the frequency increases, the magnitude decreases with the exemption of corresponding blade passing frequencies, indicating the signal is primarily composed of frequencies related to the rotor's blades rotation. The spatial contour plots indicate a slight shift in magnitude near the blade passing frequencies as the probe traverses from the tip to the nosecone.

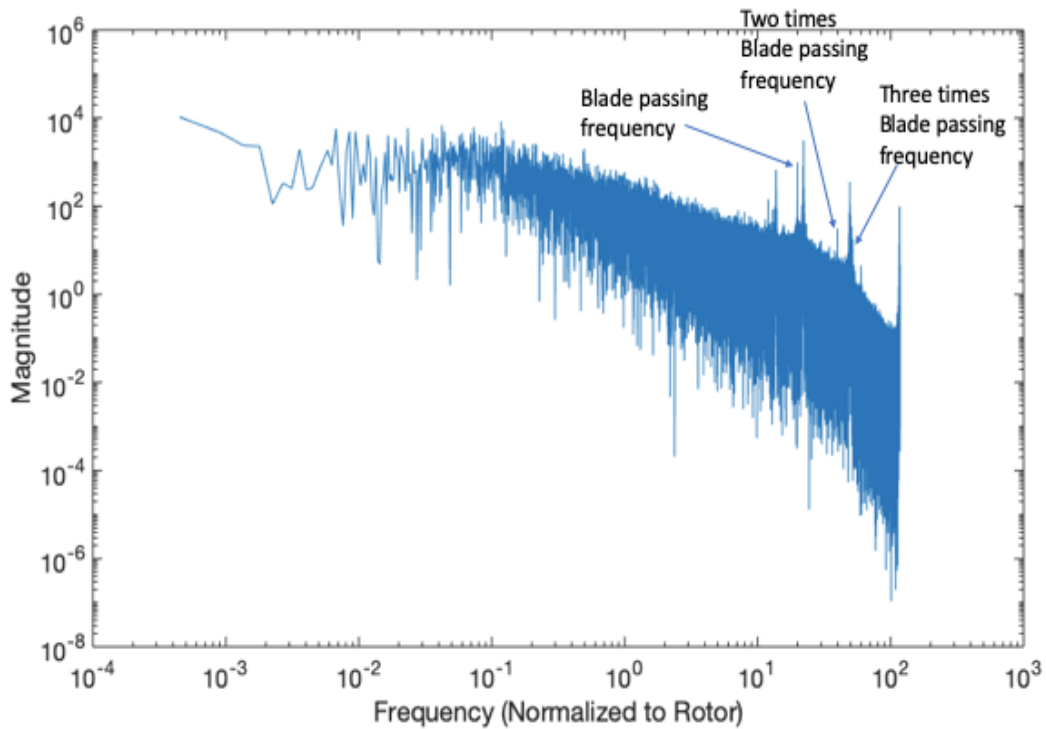


Figure 33. Power Spectrum 85% Power

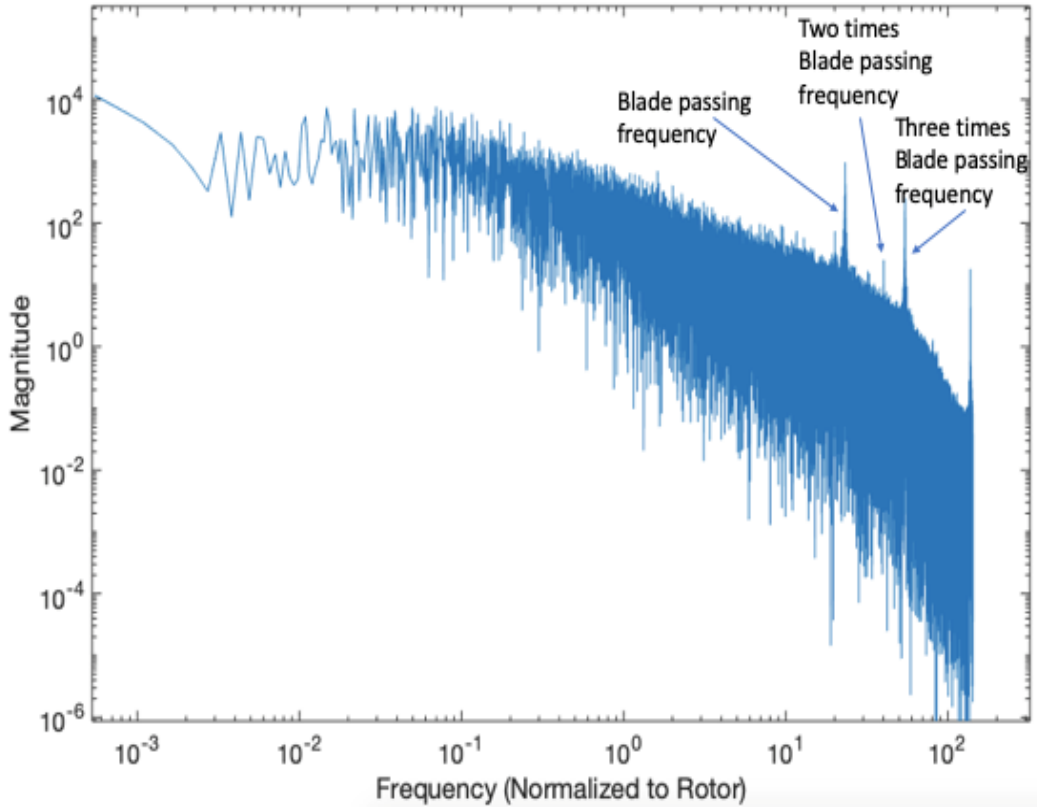


Figure 34. Power Spectrum 70% Power

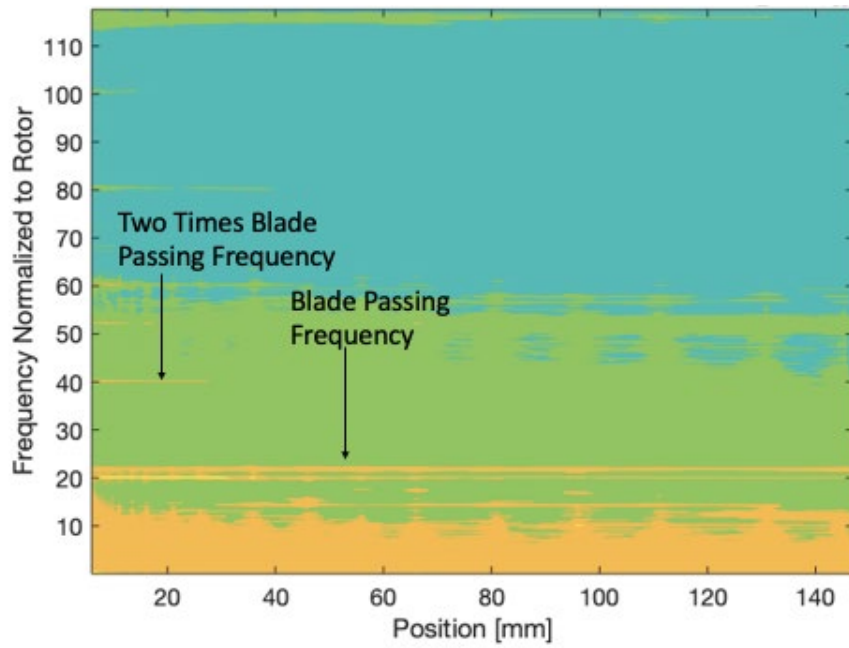


Figure 35. 85% Power Spatial Contour Plot

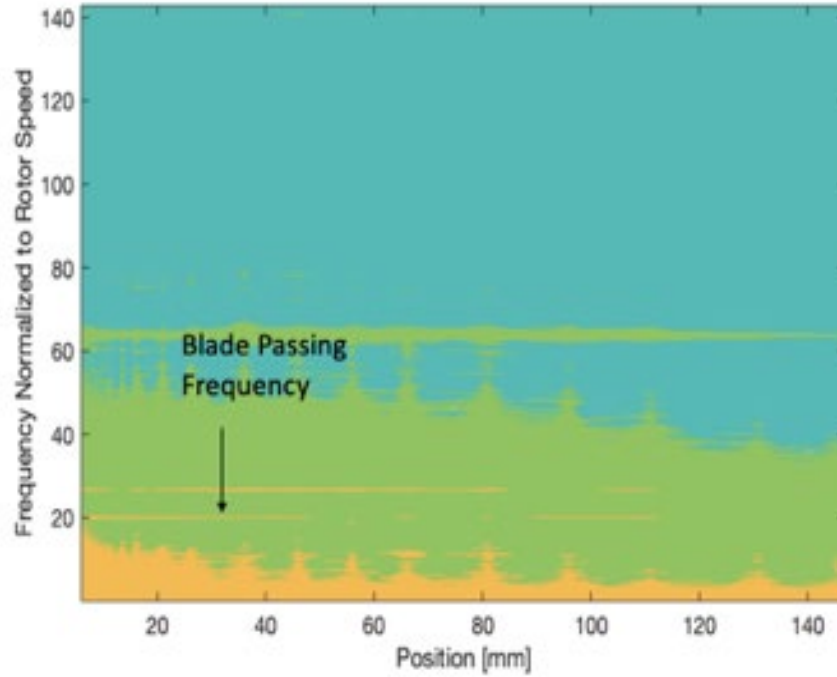


Figure 36. 70% Power Spatial Contour Plot

The TI significantly increased at the nosecone for the 85% power choked condition. The Power spectrum, Figure 37, supported the presence of vortex shedding as the Strouhal number (St) was calculated to be .24 by using equation 13 [8]. A frequency (ω) of 5500 Hz was used since this is the first major spike from the power spectrum. A 4.6 mm diameter (D) was used as this is the width of the hot film probe which attaches to the steel rod and U_{mean} of 105 m/s was obtained from the calculated velocity profile.

$$St = \frac{\omega D}{U_{Mean}} \quad (13)$$

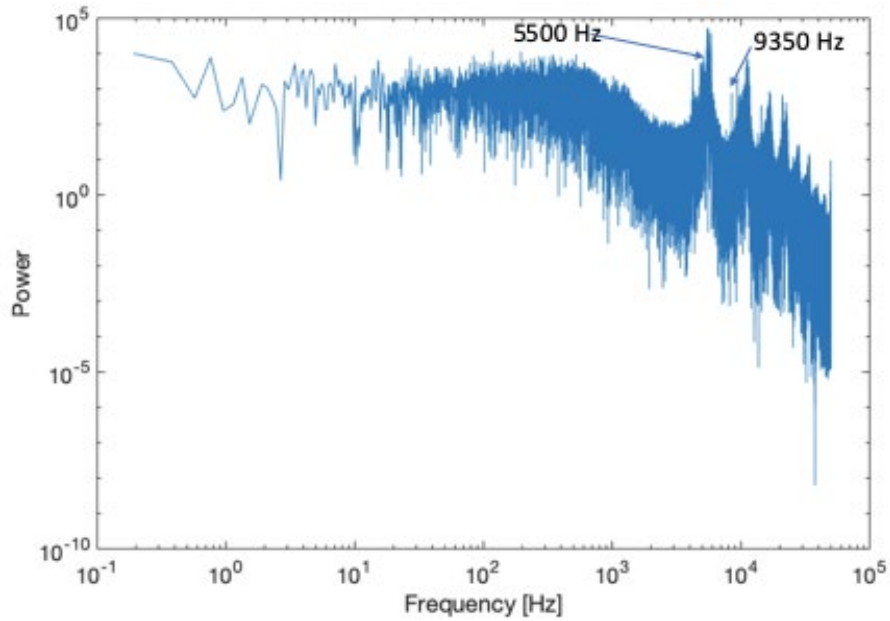


Figure 37. Power Spectrum at 85% Power at Nosecone

Histogram plots were also created to illustrate the distribution of velocity. This was desired to show the velocity distribution for each location being symmetric about the mean value and demonstrate no presence of outliers. This also confirmed proper gain and offset settings within the ThermalPro software as gaps were absent from these plots. Figure 38 shows a typical velocity profile at the 85% Power choked condition in the low turbulence intensity region of the radial survey.

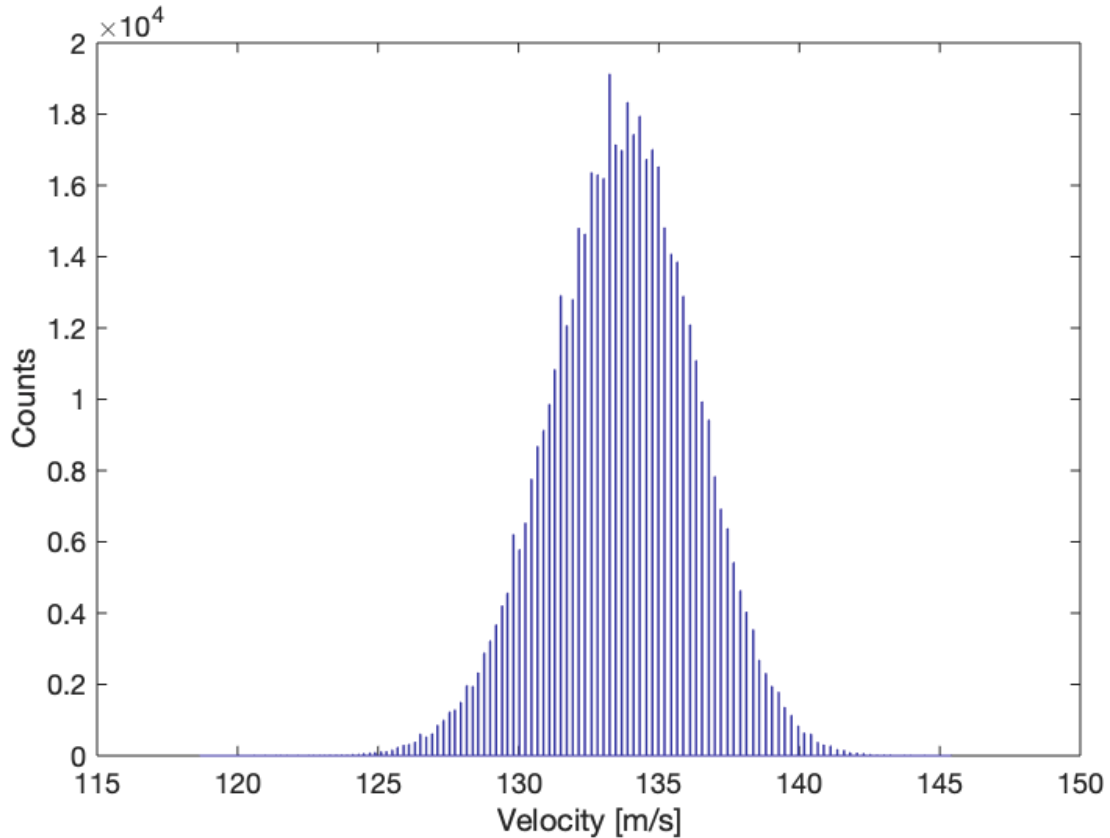


Figure 38. 85% Power Choked Condition Velocity Histogram

C. COMPUTATIONAL RESULTS

CFD results were over plotted with the experimental data at 85% Power choked condition. Figures 39 and 40 show a cross sectional view of the model illustrating the pressure and axial velocity profile. Figure 41 shows the CFD velocity decreasing slightly more as the profile approaches the nose cone. The TI, plotted in Figure 42, demonstrates a slightly different TI profile than the experimental results. The CFD results are higher near the wall and lower in the free stream. The CFD does have a slight increase as it approaches the nose cone however it is not as pronounced. During the actual compressor run, vortex shedding was occurring at this location due to an extended steel rod in the flow field causing large velocity fluctuations and therefore a more pronounced TI increase.

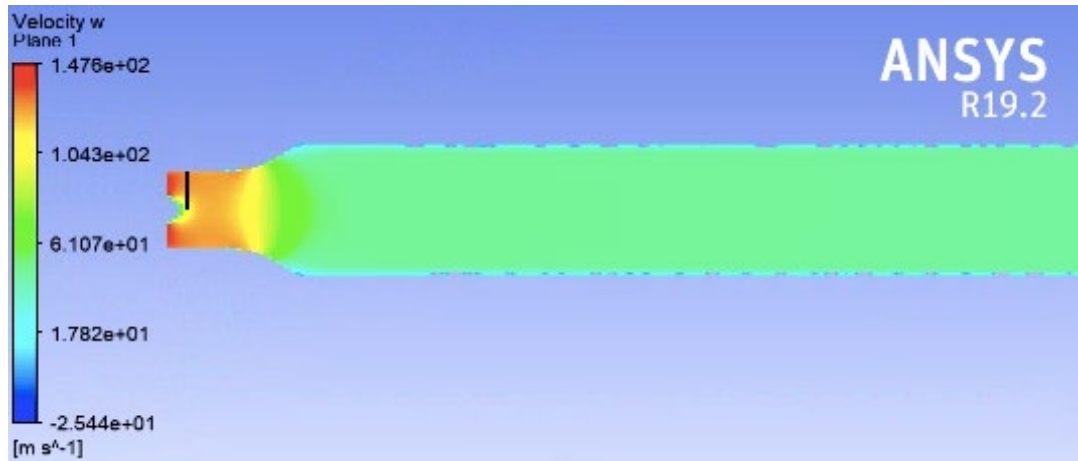


Figure 39. CFD Velocity Distribution

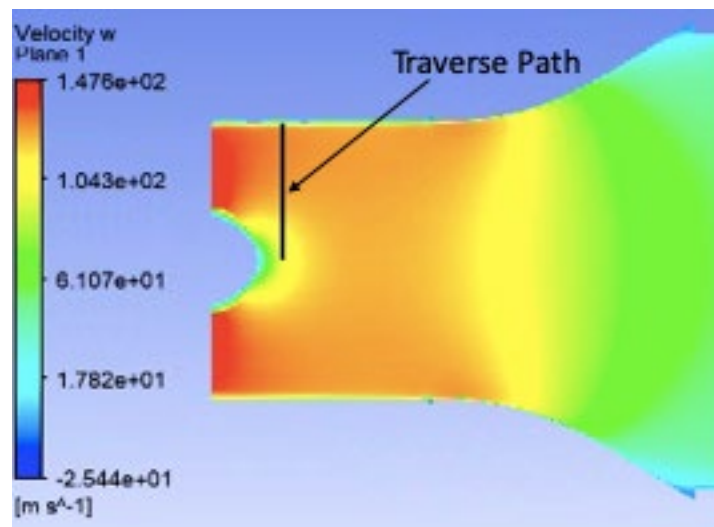


Figure 40. CFD Velocity Distribution near Traverse

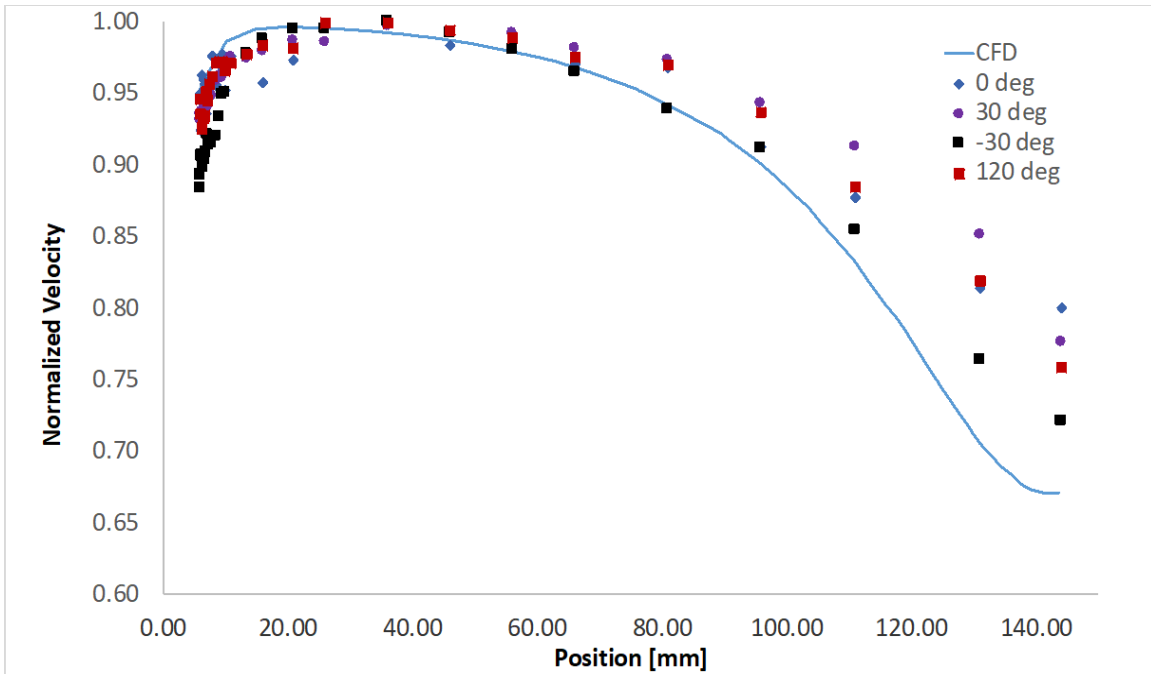


Figure 41. Comparison of CFD and Experimental Velocity Profiles

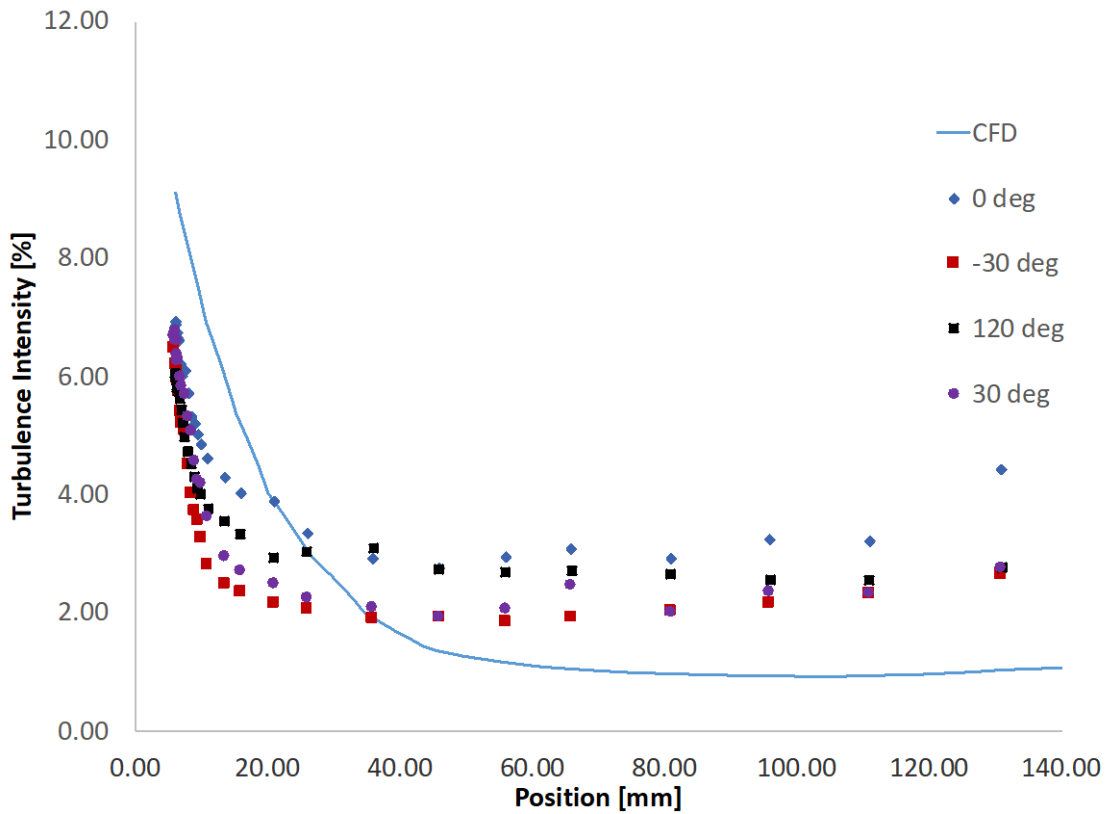


Figure 42. Comparison of CFD and Experimental TI Profiles

THIS PAGE INTENTIONALLY LEFT BLANK

V. CONCLUSIONS

Hot film data was successfully obtained at the desired power and various conditions. To accomplish this, a new data acquisition system was configured and integrated with a traverse which was tested on a small wind tunnel. After successful test runs, the system was transferred to the TCR.

Hot film data was then obtained at the desired power and throttle configurations allowing for the analysis and computation of velocity and turbulence intensity profiles. These profiles all demonstrated similar characteristics, however there were slight variations in magnitude. The freestream TI calculations varied between 2 and 4 percent. It is suspected that this variance could be due to variance within the TCR due to the upstream throttle configuration. After, removing the upstream bellmouth, the TI had a noticeable decrease which is likely due the removal of a potential disturbance to the flow. Voltage oscillations were also noticeable during the calibration procedure which could potentially lead to further error which should be investigated. Overall, the assumption of an axisymmetric inlet is reasonable as shown by the data.

With velocity profiles for each location and condition, a velocity curve was fitted with the data. The curve allowed for the calculation of d^* , θ , and H . Since the H values were between 1 and 1.2 the flow was concluded to be turbulent.

In addition, a separate calibration method was introduced (equation 4). A single equation will help simplify the conversion of voltages to density corrected velocities.

Computational results were also obtained and compared to the experimental results. The velocity profile illustrated a similar profile to the experimental profiles from the wall and most of the freestream at which point the velocity decreased slightly more than the experimental velocities. The TI was also compared and demonstrated a different profile. The actual TI near the nosecone was significantly higher due to vortex shedding as there was a noticeable increase in the signal's magnitude at 5500 Hz whereas the rest of the flow field only had noticeable increases at blade passing frequencies. Additional, computational analysis will be required to improve the turbulence model.

THIS PAGE INTENTIONALLY LEFT BLANK

VI. RECOMMENDATIONS

Though the flow field and turbulence intensity was modeled successfully, there are several improvements and alternate methods which could be incorporated to improve this research and enhance the accuracy. The hot film data was only obtained from a single axial location; just in front of the inlet rotor. To achieve an improved understanding of the overall system, more turbulence data and information could be obtained from upstream of the inlet to observe the amount of turbulence decay. This would allow for a better understanding of any initial turbulence created by the inlet throttle and bell mouth pieces.

Additionally, the hot film sensors used to analyze the flow field only allowed for the flow to be analyzed in one dimension. There do exist hot film sensors which contain multiple wires and at angled offsets to allow for the analysis of flow in all three dimensions.

There are other methods which could also be explored to acquire additional turbulence information. These include PIV and Laser Doppler Velocimetry (LDV) experimental devices which would allow for the following of a particular particle which would allow for better understanding of flow direction while also obtaining information on upstream locations.

THIS PAGE INTENTIONALLY LEFT BLANK

APPENDIX A. HOT FILM CALIBRATION PROCEDURE

1. Turn on the IFA300
2. Open the ThermalPro software. Once open the top of the screen should confirm the IFA 300 cabinet being connected and number of available channels.
3. Select “Calibration” and then “Probe Data” from the pulldown menu. The Calibration screen as seen from Figure 43 should appear.

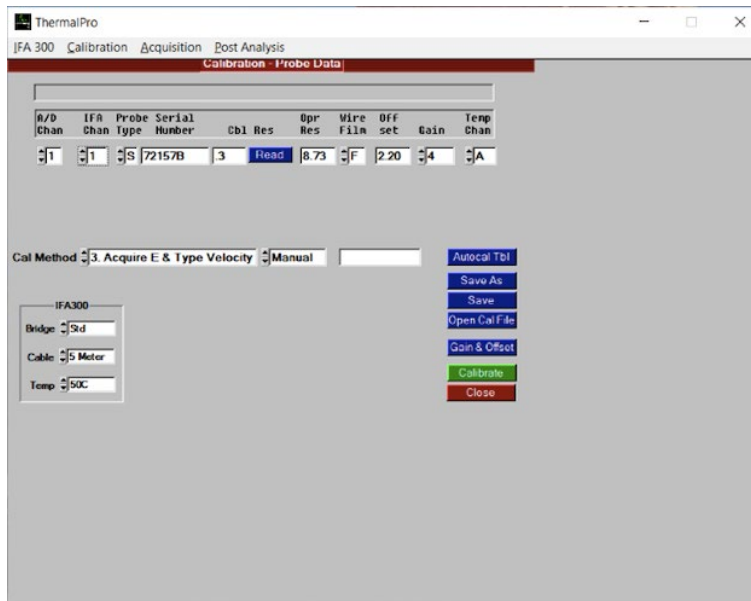


Figure 43. ThermalPro Calibration Setup

4. Then, select “Open Cal File.”
5. Next enter and verify all applicable parameters on the screen to include IFA channel, probe type, resistance, and wire film. For the “Cal Method” select the third available option; “Acquire E & Type Velocity.” For the Cable Resistance, if not already performed, a shorting probe needs to be inserted in place of the sensor. Then, click READ to obtain a cable resistance which should then be used in the cable resistance block. The shorting probe should now be replaced with the hot film sensor. Input a gain of 3 and offset of 2.5.
6. Next to the Cal Method window select “Manual” as the method for prompting the software to perform the calibration.
7. In the lower left verify the following is selected in the IFA 300 window: Std Bridge, 30 Meter cable, and 50C for temperature. These are the default parameters.

8. Then click on “Save As.” Input the sensor serial number as the file name before saving. The Serial number should appear under Serial Number.
9. Click on calibrate and the Conditions screen, Figure 44, should appear.

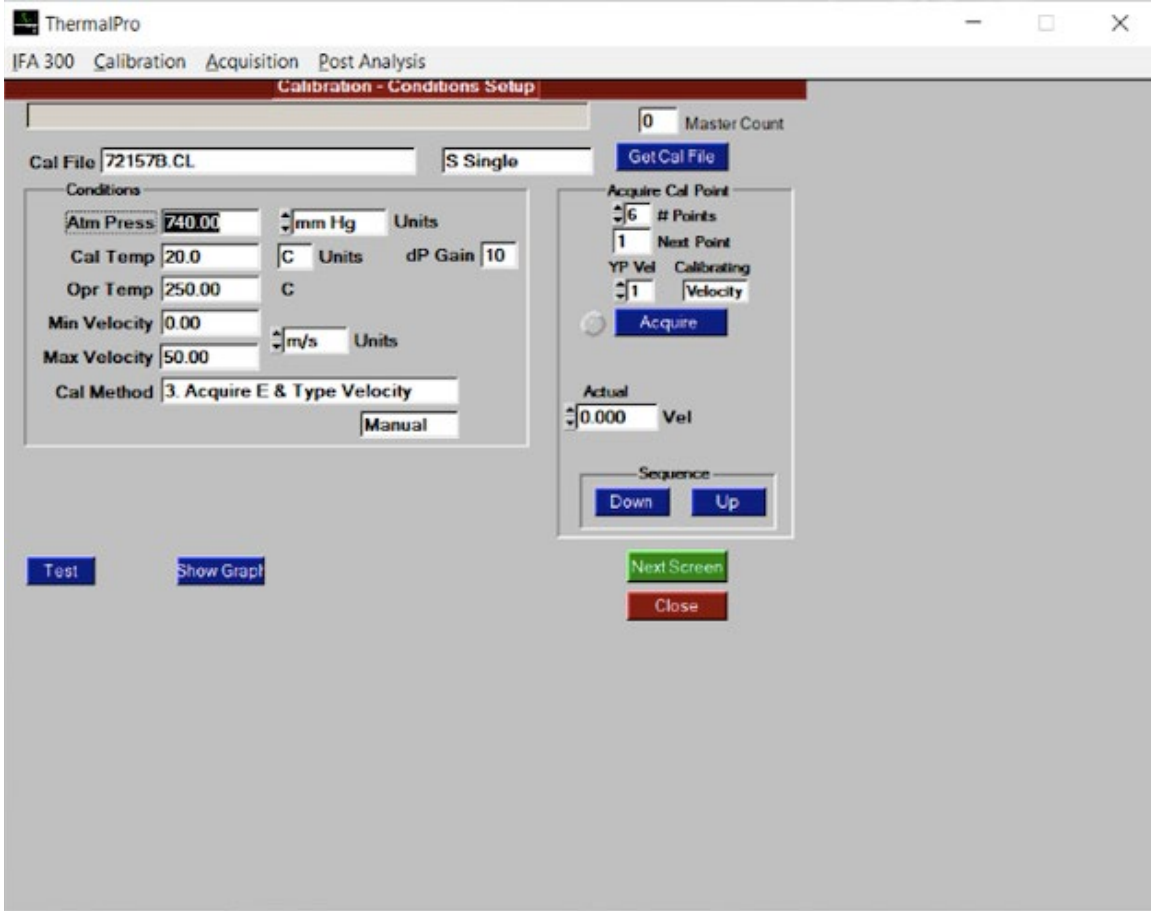


Figure 44. ThermalPro Calibration Window

10. Under the Conditions block type in the maximum expected velocity the probe to encounter and the sensor’s operating temperature.
11. Under the Acquire Cal Point block, type in the number of calibration points. It is recommended to perform 17 points for calibration but 8 is sufficient if spaced correctly.
12. Now if not already done, place the sensor in the flow field.
13. For the first calibration point set the differential pressure and flow velocity to zero and type 0 into the Vel box.
14. Click on Acquire to allow the system to acquire a voltage measurement.
15. After the system acquires the first point, increase the velocity to the next value and type in the new velocity into the Vel box.
16. Repeat steps 14 and 15 until all calibration points are obtained.

17. Click on Next Screen and a window with the resulting calibration data should appear.
18. Click on Curves to perform and generate a polynomial curve fit. A screen with a graph should appear.
19. Observe the graph and if the curve increases smoothly and monotonically, then the calibration process is successfully completed. If satisfied with the calibration record the polynomial coefficients and then click Close to save the calibration curve.
20. If not satisfied with the calibration curve erroneous points may be removed by selecting delete line or modified by selecting edit line.

THIS PAGE INTENTIONALLY LEFT BLANK

APPENDIX B. HOT FILM DATA ACQUISITION PROCEDURE

1. Turn on the IFA300
2. Open the ThermalPro software. Once open the top of the screen should confirm the IFA 300 cabinet being connected and number of available channels.
3. If not already performed, perform a calibration of the sensor to be utilized.
4. With a completed calibration, under the Acquisition list, select Probe Table which will open the Acquisition page, Figure 45, for the experiment.

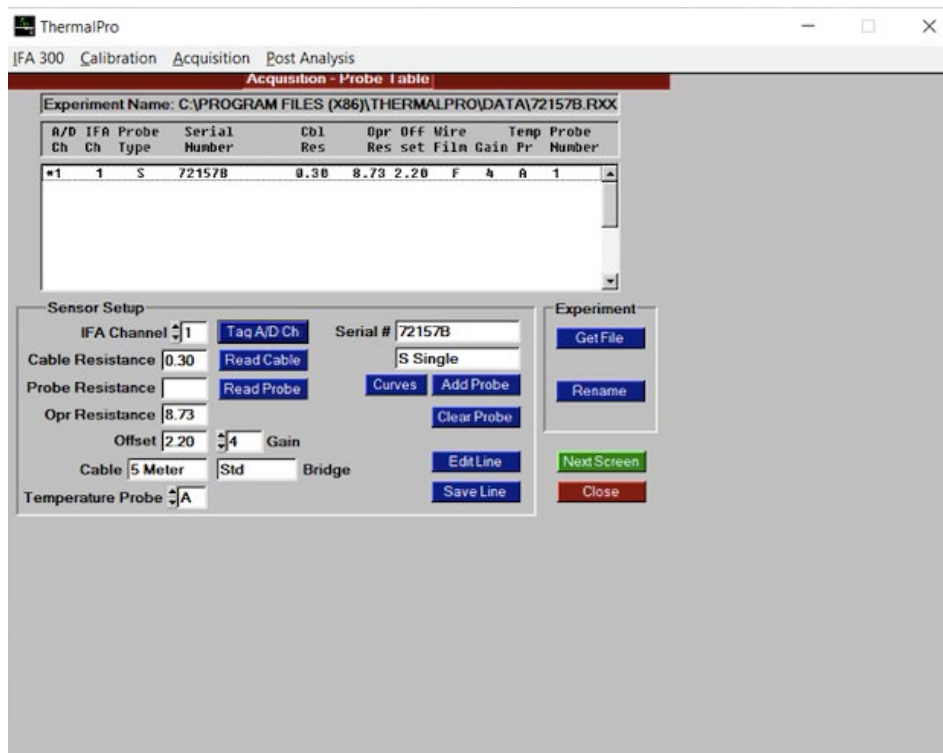


Figure 45. Acquisition Sensor Setup Window

5. Click on Get File and type in a name for the raw data files which will be created later. Then click on OK.
6. Then, click on Add Probe to add the probe which was most recently calibrated to the experiment.
7. Double click on the probe added to set as the first probe.
8. Press Edit Line and if needed make changes to any of the parameters pertaining to the sensor and once finished click Save Line.
9. Once finished with adding and editing sensors click Next Screen which will allow for the conditions setup window, Figure 46, to appear as seen below.

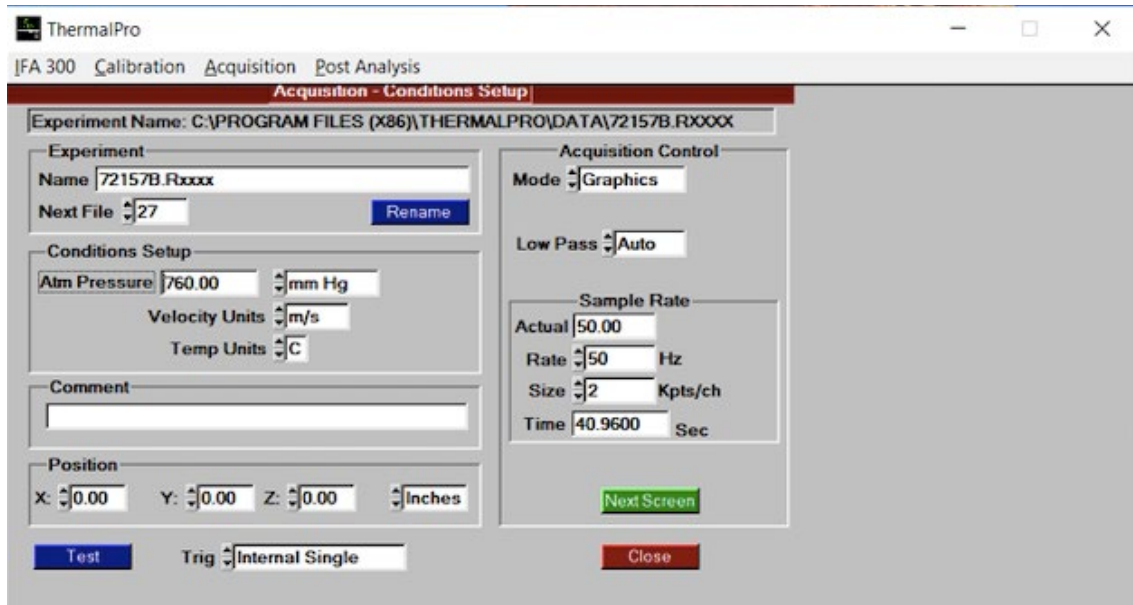


Figure 46. Acquisition Conditions Setup

10. On this screen verify the experiment name, next file, and conditions are as desired from previous steps.
11. Select Internal Single from the Trig option list and set the sample rate to 100 KHz and the size to 5.2 Kpts/ch.
12. If it is desired to perform a verification of the sensors, click on Test to observe voltage readings for each channel. Once satisfied with all the parameters and a traverse will not be used click Next Screen to open the real-time display screen, Figure 47. If utilizing a traverse skip to step 15.
13. To obtain data click the Trigger button. The sample rate and number of data points can also be modified on this screen before triggering an event.
14. Once finished obtaining data, click Close.

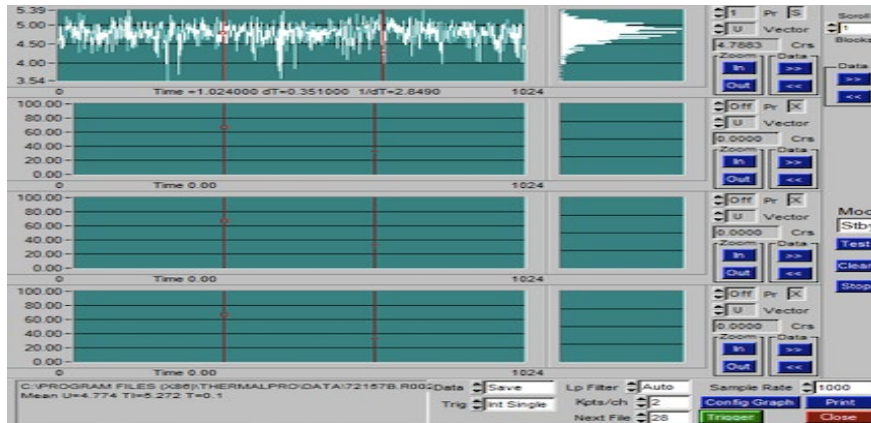


Figure 47. Real-time display

15. To obtain data with a traverse select traverse control from the IFA 300 drop down menu while still on the Conditions Setup Page. Then, select the traverse matrix to be used. Data will be automatically taken at each predetermined location once the trigger button is pressed. The real-time display will not be available and between each run the name of the experiment needs to be changed.
16. To perform post analysis, select Velocity Analysis from the Post Analysis header which will open the Analysis – Velocity window, Figure 48.
17. If the file to be analyzed is not displayed click on Get File and select the file from the list and then click OK. If there is more than one file, select the first file in the sequence and then search to display all the files.

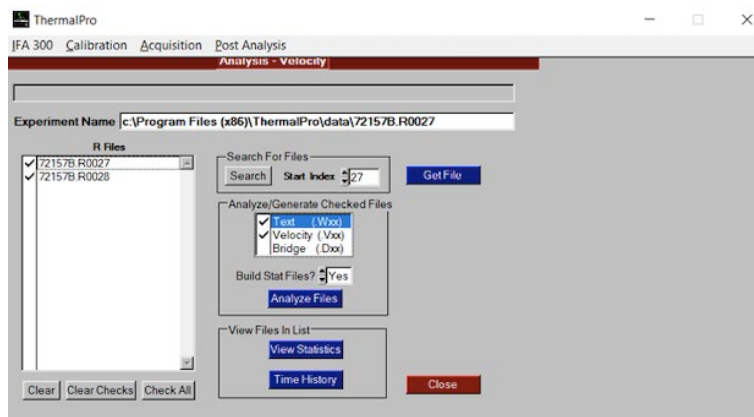


Figure 48. Velocity Analysis Window

18. With check marks next to the files to be analyzed, select Text and Velocity as the files to be generated. The text file is a .WXX extension and contains

columns of time and velocity which can be imported via MATLAB coding to perform data analysis. If instead voltage files are desired select Bridge in replace of Velocity to generate .EXX files which have voltage in the second column.

19. Click on Analyze files which will generate the files.
20. To observe statistics of the files selected click on View Statistics which will open the Statistics window, Figure 49, with statistical information for the files.

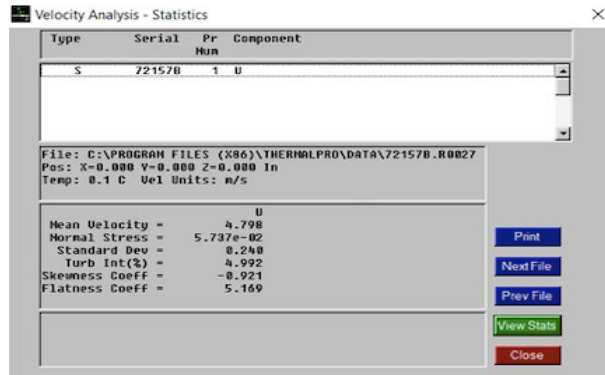


Figure 49. Velocity Analysis Statistics Window

21. Once finished click Close to exit the Statistics and then Velocity Analysis pages.

APPENDIX C. DATA ANALYSIS CODE

The following MATLAB script was utilized to perform the velocity calibration, density correction, analysis, and create plots from the text files created by the ThermalPro Post Analysis.

```
%%Calibration Generator
voltage=[2.864 3.035 3.170 3.286 3.382 3.418 3.442 3.452 3.432];
velocity=[41.9 56.3 71.99 104.18 113.19 123.7 132.67 135.77 136.84];
pressure=[98414 96302 93458 86364 84068 81396 79115 78270 78083];
filename='CALIBRATION.xlsx';
p=polyfit(voltage,velocity,4);
p2=polyfit(voltage,pressure,4);
PE=79228;
A=[p(1) p(2) p(3) p(4) p(5) PE p2(1) p2(2) p2(3) p2(4) p2(5)];
writematrix(A,filename,"FileType","spreadsheet","Range","A1","Sheet","16APR85CHOKED')

%%HOT FILM ANALYSIS CODE%%
%%Required input variables: f,l,y,file name, and ext (.E:voltage .W:velocity). Recommend
commenting out undesired outputs after for loop calculations. Default is to create excel file,
flow field plots, and sample PSD, raw data, Contour, Waterfall, Histogram,
and, autocorrel plots for multiple files while displaying results and plotting raw data, PSD,
and Histogram, for single file
tic

%Required User Inputs
all={'2APR85CHOKED','16APR85CHOKED',
'8APR85CHOKED','142APR85CHOKED','10MAY85CHOKED','6MAY85CHOKED','2APR85I
NTERMED','16APR85INTERMED','8APR85INTERMED','14APR85INTERMED','10MAY85I
NTERMED','6MAY85INTERMED','2APR85STALL','16APR85STALL','8APR85STALL','14AP
R85STALL','10MAY85STALL','6MAY85STALL','2APR70CHOKED','16APR70CHOKED','8A
PR70CHOKED','14APR70CHOKED','10MAY70CHOKED','6MAY70CHOKED','2APR70INTE
RMED','16APR70INTERMED','8APR70INTERMED','14APR70INTERMED','10MAY70INTE
RMED','6MAY70INTERMED','2APR70STALL','16APR70STALL','8APR70STALL','14APR70
STALL','10MAY70STALL','6MAY70STALL'};
files={'16APR85CHOKED'};
ext='.E';
f = 2;l = 31;%first and last file #

%%Positions inputted to thermal pro traverse matrix
% (for graphing and results purposes)
```

```

y=[6 6.1 6.2 6.3 6.4 6.5 6.75 7 7.25 7.5 8 8.5 9 9.5 10 11 13.5 16 21 26 36 46 56 66 81 96
111 131 145.6 147];

%%Initializing zero vectors for values to be calculated in for loop
N=1+l-f;%N: total files j: indexing results in case f not = 1.
u=zeros(1,N);uprime=u;ke=u;Tl=u;
rmsconf=u;uconf=u;rootmean=u;

for k=1:length(files)
filename=char(files(k))

%%Obtaining velocity calibration and density correcting coefficients and experimental pressure
(PE)
calfile='CALIBRATION.xlsx';
file=[xlsread('' sprintf(calfile) '' ',' ,sprintf(filename),'')];
a = eval(file);j=1;

for s = f:1:l

%%Reading in raw voltage data files (.EXXXX) and converting to %velocity 1st column is
time 2nd is voltage or (.WXXXX) for inputing %velocity directly

if s>9
file = ['dlmread('' sprintf(filename),sprintf(ext),sprintf('00'),num2str(s),'')];
else
file = ['dlmread('' sprintf(filename),sprintf(ext),sprintf('000'),num2str(s),'')];
end

data = eval(file);

if ext == '.E'
voltage=data(:,2);
avgvoltage=mean(voltage);
velocity=zeros(1,length(voltage));
PE=a(6);

velocity=a(1).*voltage.^4+a(2).*voltage.^3+a(3).*voltage.^2+a(4).*voltage+a(5);
PC=a(7).*avgvoltage.^4+a(8).*avgvoltage.^3+a(9).*avgvoltage.^2+a(10).*avgvoltage+a(11);
velocity=(PC/PE).*velocity;
%velocity=(a(7).*voltage.^4+a(8).*voltage.^3+a(9).*voltage.^2+a(10).*voltage+a(11))/PE;

else
velocity=data(:,2);
end

```

```

%%Mean Velocity, Turbulence, Confidence, FFT Calculations
u(j)=a(1).*avgvoltage.^4+a(2).*avgvoltage.^3+a(3).*avgvoltage.^2+a(4).*avgvoltage+a(5);
u(j)=(PC/PE)*u(j);

uprime(j) = sqrt(sum((velocity-u(j)).^2)/length(velocity)); %%std [m/s]
ke(j) = .5*uprime(j)^2 ;%Turbulence KE [m^2/s^2]
TI(j) = uprime(j)/u(j)*100;%Turbulence Intensity [%]
rootmean(j)=sqrt(uprime(j)^2+u(j)^2);
uconf(j)=1.96*uprime(j);%95% Velocity Confidence Interval
rmsconf(j)=1.96*sqrt(sum((velocity-u(j)).^2)/(2*length(velocity)));%95% RMD Confidence
Interval
Y = fft(velocity); Y(1) = [];
n = length(Y)-1;
P= (abs(Y(1:n/2)).^2)/n;
W(j,:)=log10(P');
fs=1/data(2,1);
fr = (1:n/2)*fs/(25500*n/60);

j=1+j

end

%%Plotting Flow Field, TI, and Contour
if N>1
plot(y,u,'-',y,u+uconf,':',y,u-uconf,':', 'Color,' b')
xlabel('Position [mm]');ylabel('Mean Velocity [m/s]');title('Velocity Profile');

figure
plot(y,TI,'-',y,TI+rmsconf,':', 'Color,' r')
xlabel('Position [mm]');ylabel('TI [%]');title('Turbulence Intensity');

figure
contour(W)
xlabel('count');ylabel('frequency [Hz]');zlabel('log10(Power)');

end

%Outputting Calculations to excel file if multiple files
if N>1
a=['Position [mm]', 'Umean [m/s]', 'TI[%]', 'STD', 'RMS', 'U 95% Confidence Interval', 'TI 95%
Confidence Interval'];
A=[y' u' TI' uprime' rootmean' uconf' rmsconf'];
writematrix(filename,'TCR
Results2APR','FileType',"spreadsheet","Sheet",filename,"Range",'A1')

```

```

writematrix(a,'TCR Results2APR','FileType','spreadsheet','Sheet',filename,'Range','A2')
writematrix(A,'TCR Results2APR','FileType','spreadsheet','Sheet',filename,'Range','A3')
end
%%For single file displaying resulting calculations
if N==1

figure
plot(data(:,1),voltage)
xlabel('Time [sec]');ylabel('Voltage [V]');title('Raw Data');

%Power Spectrum
Y = fft(velocity); Y(1) = [];
n = length(Y)-1;
P = (abs(Y(1:n/2)).^2)/n;
fs=1/data(2,1);
fr = (1:n/2)*fs/(n);
figure
loglog(fr,P);
xlabel('Frequency [Hz]');ylabel('Power');title({'Power Spectrum','});

%Autocorrelation

lag=length(velocity)-1;
r=zeros(lag,1);
xmean=mean(velocity);
for k=1:1:lag
r(k)=sum((velocity(k+1:lag)-xmean).*(velocity(1:lag-k)-xmean))/sum((velocity(1:lag)-xmean).^2);
end
t=1:1:lag;
fs=1/data(2,1);
t=t/fs;
figure
plot(t,r)
xlabel('time [sec]');ylabel('autocorrelation');title('autocorrelation');

%Histogram
figure
hist(velocity,1000)
xlabel('Velocity [m/s]');ylabel('Counts');title({'Velocity Distribution','});

disp('Average Velocity [m/s] is: ');disp(u)
disp('Tubulent Kinetic Energy is:');disp(ke);
disp('Turbulent Intensity is [%]:');disp(TI);

```

```

disp('Standard Deviation is:');disp(uptime);
disp('95% Confidence Interval [m/s] is:');disp(1.96*uptime);
disp('Root Mean Square is:');disp(rootmean);
disp('RMS 95% Confidence [%] is:');disp(1.96*rmsconf);
end

end
toc

%Approximating displacement thickness, momentum thickness, and shape
tic
clear all
%Required User Inputs
all={'2APR85CHOKED', '16APR85CHOKED',
'8APR85CHOKED', '14APR85CHOKED', '10MAY85CHOKED', '6MAY85CHOKED', '2APR85I
NTERMED', '16APR85INTERMED', '8APR85INTERMED', '14APR85INTERMED', '10MAY85I
NTERMED', '6MAY85INTERMED', '2APR85STALL', '16APR85STALL', '8APR85STALL', '14AP
R85STALL', '10MAY85STALL', '6MAY85STALL', '2APR70CHOKED', '16APR70CHOKED', '8A
PR70CHOKED', '14APR70CHOKED', '10MAY70CHOKED', '6MAY70CHOKED', '2APR70INTE
RMED', '16APR70INTERMED', '8APR70INTERMED', '14APR70INTERMED', '10MAY70INTE
RMED', '6MAY70INTERMED', '2APR70STALL', '16APR70STALL', '8APR70STALL', '14APR70
STALL', '10MAY70STALL', '6MAY70STALL'};
files=all; %{'16APR85CHOKED'};
ext='E';
f = 2;l = 22;%first and last file #

%%Positions inputted to thermal pro traverse matrix
% (for graphing and results purposes)
y=[0 6 6.1 6.2 6.3 6.4 6.5 6.75 7 7.25 7.5 8 8.5 9 9.5 10 11 13.5 16 21 26 36];

%%Initializing zero vectors for values to be calculated in for loop
N=l;u=zeros(1,l);

for r=1:length(files)
filename=char(files(r))

%Obtaining velocity calibration and density correction coefficients and experimental pressure
(PE)
calfile='CALIBRATION.xlsx';
file=[xlsread(sprintf(calfile) "%", "%", sprintf(filename), "")];
a = eval(file);j=2;

for s = f:l

```



```

%%Reading in raw voltage data files (.EXXXX) and converting to velocity
%%1st column is time 2nd is voltage or (.WXXXX) for inputting velocity directly

if s>9
file = ['dlmread('' sprintf(filename),sprintf(ext),sprintf('00'),num2str(s),'')'];
else
file = ['dlmread('' sprintf(filename),sprintf(ext),sprintf('000'),num2str(s),'')'];
end

data = eval(file);
voltage=data(:,2);
avgvoltage=mean(voltage);
PE=a(6);
u(j)=a(1).*avgvoltage.^4+a(2).*avgvoltage.^3+a(3).*avgvoltage.^2+a(4).*avgvoltage+a(5);
PC=a(7).*avgvoltage.^4+a(8).*avgvoltage.^3+a(9).*avgvoltage.^2+a(10).*avgvoltage+a(11);
u(j)=(PC/PE)*u(j);
j=1+j
end

[q s]=createFit(y/max(y),u/max(u))
yy=0:.001:1;
uu=yy.^(1./q.k);

%Flow Characteristics

deltastar(r)=trapz(yy,1-uu/max(uu))*36
theta(r)=trapz(yy,(uu/max(uu).*(1-uu/max(uu))))*36
shape(r)=deltastar(r)/theta(r)

figure
hold on
plot(y/maxy,u/max(u),'r',yy,uu,'k')
xlabel('y/d');ylabel('u/U');legend('Experimental','Interpolation');

end
flow2=[deltastar' theta' shape'];
writematrix(flow,'Flow Characteristics',
"filetype","spreadsheet","Sheet","flowcharacteristics","Range","B2")
toc

```

APPENDIX D. ADDITIONAL TABLES AND GRAPHS

Table 6. Wind Tunnel Calculations

Position [mm]	Uavg [m/s]	Tl [%]	STD	RMS	95% U Conf	95% RMS Conf
0	20.48	18.242	3.74	20.82	7.32	5.17
0.05	19.36	18.88	3.66	19.7	7.17	5.07
0.1	16.59	21.87	3.63	16.98	7.11	5.03
0.2	16.87	22.27	3.76	17.29	7.36	5.21
0.3	16.75	22.2	3.72	17.16	7.29	5.16
0.4	17.51	22.82	4	17.96	7.83	5.54
0.5	19.12	20.33	3.89	19.52	7.62	5.39
0.75	20.23	20.1	4.07	20.63	7.97	5.64
1	21.26	20.05	4.26	21.68	8.36	5.91
1.25	22.47	20.36	4.5	22.93	8.97	6.34
1.5	25.18	19.69	4.96	25.66	9.72	6.87
2	27.89	19.91	5.55	28.44	10.88	7.7
2.5	31.24	19.16	5.99	31.81	11.74	8.3
3	37.73	16.91	6.38	38.26	12.51	8.84
4	44.44	12.84	5.71	44.8	11.18	7.908
5	49.54	9.26	4.59	49.76	9	6.36
6	53.09	7.11	3.78	53.23	7.4	5.23
7	55.7	5.97	3.32	55.8	6.51	4.61
8	57.67	4.7	2.71	57.74	5.31	3.76
9	59.4	3.17	1.88	59.43	3.69	2.61
10	61.12	1.44	0.88	61.13	1.72	1.22
12	61.81	1.05	0.64	61.18	1.26	0.89
14	61.14	0.78	0.48	61.14	0.94	0.67
16	61.78	1.01	0.62	61.78	1.22	0.86
18	62.54	0.56	35	62.54	0.68	0.48
20	62.66	0.84	0.53	62.67	1.03	0.73
25	62.07	0.61	0.38	62.07	0.74	0.52
30	61.91	0.5	0.31	61.91	0.6	0.42
35	62.53	0.4	0.25	62.53	0.49	0.34
40	61.61	0.55	0.34	61.61	0.66	0.47
45	61.45	0.48	0.29	61.45	0.58	0.41
50	61.93	0.62	0.38	61.93	0.75	0.53

Table 7. Results for 85% Power Choked at 0°

Position[mm]	Umean[m/s]	TI[%]	STD	RMS	U 95% Confidence Interval	TI 95% Confidence Interval
6	123.01	6.83	8.41	123.29	16.48	11.65
6.1	126.51	6.94	8.78	126.81	17.21	12.17
6.2	128.09	6.89	8.83	128.39	17.30	12.24
6.3	124.64	6.76	8.42	124.92	16.51	11.67
6.4	126.33	6.65	8.40	126.61	16.47	11.65
6.5	127.75	6.67	8.51	128.03	16.69	11.80
6.75	127.24	6.61	8.41	127.51	16.49	11.66
7	124.56	6.22	7.75	124.80	15.19	10.74
7.25	125.46	6.03	7.56	125.69	14.82	10.48
7.5	126.56	6.11	7.73	126.79	15.16	10.72
8	129.94	5.72	7.43	130.15	14.56	10.29
8.5	127.18	5.32	6.76	127.36	13.25	9.37
9	129.10	5.21	6.73	129.27	13.18	9.32
9.5	130.01	5.01	6.52	130.17	12.78	9.04
10	126.74	4.87	6.18	126.89	12.11	8.56
11	129.92	4.62	6.01	130.06	11.78	8.33
13.5	129.98	4.31	5.60	130.10	10.97	7.76
16	127.43	4.03	5.13	127.53	10.06	7.11
21	129.46	3.91	5.06	129.56	9.91	7.01
26	133.06	3.36	4.47	133.14	8.77	6.20
36	132.89	2.92	3.88	132.95	7.60	5.37
46	130.98	2.76	3.61	131.03	7.08	5.00
56	131.46	2.96	3.90	131.52	7.64	5.40
66	129.08	3.10	4.00	129.14	7.84	5.55
81	128.89	2.92	3.77	128.95	7.38	5.22
96	121.42	3.26	3.96	121.49	7.77	5.49
111	116.82	3.24	3.78	116.88	7.41	5.24
131	108.27	4.43	4.80	108.37	9.40	6.65
145.6	106.50	4.22	4.50	106.60	8.81	6.23
147	103.26	4.19	4.33	103.35	8.49	6.00

Table 8. Results for 85% Power Intermediate Condition at 0°

Position[mm]	Umean[m/s]	TI[%]	STD	RMS	U 95% Confidence Interval	TI 95% Confidence Interval
6	108.08	7.53	8.14	108.39	15.96	11.28
6.1	111.74	7.95	8.89	112.09	17.42	12.32
6.2	108.69	7.62	8.28	109.01	16.23	11.47
6.3	109.61	7.43	8.14	109.91	15.96	11.28
6.4	112.70	7.65	8.62	113.03	16.89	11.94
6.5	112.49	7.41	8.34	112.80	16.35	11.56
6.75	109.30	6.93	7.58	109.57	14.85	10.50
7	108.19	6.68	7.23	108.44	14.18	10.02
7.25	110.74	6.56	7.26	110.98	14.24	10.07
7.5	111.09	6.48	7.19	111.32	14.10	9.97
8	113.35	6.06	6.86	113.56	13.45	9.51
8.5	113.10	5.79	6.55	113.29	12.83	9.07
9	114.79	5.45	6.25	114.96	12.26	8.67
9.5	114.80	5.32	6.11	114.96	11.97	8.46
10	114.79	5.15	5.91	114.94	11.58	8.19
11	114.45	4.83	5.53	114.58	10.84	7.67
13.5	113.43	4.50	5.10	113.54	9.99	7.07
16	116.18	4.32	5.01	116.29	9.83	6.95
21	117.21	3.84	4.50	117.30	8.81	6.23
26	116.89	3.42	4.00	116.96	7.85	5.55
36	118.13	3.20	3.78	118.19	7.41	5.24
46	119.53	2.94	3.51	119.58	6.88	4.86
56	117.73	2.95	3.47	117.78	6.80	4.81
66	113.31	2.92	3.31	113.36	6.49	4.59
81	108.09	3.15	3.40	108.15	6.67	4.72
96	103.40	3.25	3.36	103.45	6.59	4.66
111	101.95	3.42	3.49	102.00	6.83	4.83
131	93.36	3.62	3.38	93.42	6.62	4.68
145.6	89.44	3.68	3.29	89.51	6.45	4.56
147	93.00	3.82	3.56	93.07	6.97	4.93

Table 9. Results for 85% Power Near Stall at 0°

Position[mm]	Umean[m/s]	TI[%]	STD	RMS	U 95% Confidence Interval	TI 95% Confidence Interval
6	78.94	7.53	5.95	79.17	11.66	8.24
6.1	80.51	7.66	6.17	80.75	12.09	8.55
6.2	80.51	7.58	6.10	80.75	11.96	8.46
6.3	79.02	7.65	6.05	79.25	11.85	8.38
6.4	80.75	7.50	6.06	80.98	11.87	8.39
6.5	80.05	7.46	5.97	80.27	11.70	8.27
6.75	80.05	7.22	5.78	80.26	11.33	8.01
7	80.27	6.95	5.58	80.47	10.93	7.73
7.25	80.83	6.81	5.50	81.01	10.79	7.63
7.5	81.08	6.48	5.26	81.25	10.30	7.29
8	82.28	6.18	5.08	82.44	9.96	7.04
8.5	81.16	6.00	4.87	81.31	9.55	6.75
9	82.90	5.67	4.70	83.04	9.21	6.51
9.5	84.12	5.58	4.69	84.25	9.19	6.50
10	83.17	5.23	4.35	83.28	8.52	6.03
11	82.74	5.14	4.25	82.84	8.33	5.89
13.5	83.50	4.68	3.91	83.59	7.66	5.42
16	85.71	4.59	3.93	85.80	7.70	5.45
21	86.75	4.24	3.68	86.82	7.22	5.10
26	91.03	4.04	3.68	91.10	7.21	5.10
36	92.60	3.43	3.18	92.65	6.23	4.41
46	89.61	3.21	2.88	89.65	5.64	3.98
56	87.85	3.04	2.67	87.89	5.23	3.70
66	85.57	3.07	2.62	85.61	5.14	3.64
81	82.98	2.94	2.44	83.01	4.78	3.38
96	77.66	2.93	2.27	77.69	4.45	3.15
111	72.06	2.91	2.10	72.09	4.11	2.91
131	66.42	3.02	2.01	66.46	3.94	2.78
145.6	65.85	3.18	2.09	65.89	4.10	2.90
147	66.93	3.29	2.20	66.96	4.31	3.05

Table 10. Results for 70% Power Choked at 0°

Position[mm]	Umean[m/s]	TI[%]	STD	RMS	U 95% Confidence Interval	TI 95% Confidence Interval
6	99.86	6.59	6.58	100.08	12.89	9.12
6.1	99.68	6.67	6.64	99.90	13.02	9.21
6.2	98.52	6.59	6.49	98.73	12.72	8.99
6.3	98.96	6.74	6.67	99.18	13.08	9.25
6.4	99.90	6.64	6.64	100.12	13.01	9.20
6.5	99.57	6.43	6.40	99.77	12.54	8.87
6.75	98.79	6.07	5.99	98.97	11.75	8.31
7	99.73	5.64	5.63	99.89	11.03	7.80
7.25	100.15	5.64	5.65	100.31	11.07	7.83
7.5	98.92	5.27	5.21	99.06	10.21	7.22
8	99.83	4.92	4.91	99.95	9.63	6.81
8.5	101.38	4.72	4.79	101.49	9.39	6.64
9	102.08	4.46	4.55	102.18	8.92	6.30
9.5	99.80	4.24	4.23	99.89	8.29	5.86
10	101.64	3.99	4.05	101.72	7.94	5.61
11	101.77	3.75	3.82	101.85	7.49	5.29
13.5	103.16	3.48	3.59	103.22	7.04	4.98
16	102.58	3.40	3.49	102.64	6.84	4.84
21	102.04	3.17	3.24	102.09	6.34	4.49
26	102.72	3.10	3.19	102.77	6.24	4.42
36	102.61	2.95	3.03	102.65	5.93	4.19
46	100.23	2.93	2.93	100.27	5.75	4.06
56	101.37	2.90	2.94	101.41	5.76	4.08
66	100.50	2.93	2.94	100.54	5.77	4.08
81	97.88	3.09	3.02	97.93	5.92	4.19
96	92.22	3.31	3.06	92.27	5.99	4.23
111	88.61	3.53	3.13	88.67	6.13	4.33
131	79.51	3.74	2.98	79.57	5.83	4.12
145.6	79.27	3.84	3.04	79.33	5.96	4.22
147	78.22	3.84	3.00	78.28	5.88	4.16

Table 11. Results for 70% Power Intermediate Condition at 0°

Position[mm]	Umean[m/s]	TI[%]	STD	RMS	U 95% Confidence Interval	TI 95% Confidence Interval
6	80.41	6.93	5.57	80.60	10.93	7.73
6.1	79.17	6.78	5.37	79.35	10.52	7.44
6.2	82.25	7.09	5.83	82.46	11.43	8.08
6.3	81.89	7.15	5.86	82.09	11.48	8.12
6.4	83.18	7.03	5.84	83.38	11.46	8.10
6.5	82.17	6.93	5.69	82.37	11.16	7.89
6.75	83.27	6.53	5.44	83.44	10.66	7.53
7	82.09	6.22	5.11	82.25	10.01	7.08
7.25	82.65	6.33	5.23	82.81	10.26	7.25
7.5	84.74	5.83	4.94	84.88	9.69	6.85
8	84.09	5.41	4.55	84.21	8.91	6.30
8.5	84.29	4.92	4.15	84.40	8.13	5.75
9	85.07	4.71	4.01	85.17	7.85	5.55
9.5	84.34	4.34	3.66	84.41	7.18	5.07
10	85.22	4.36	3.72	85.30	7.29	5.15
11	86.16	3.99	3.44	86.23	6.73	4.76
13.5	88.78	3.71	3.29	88.84	6.46	4.57
16	89.54	3.70	3.31	89.60	6.49	4.59
21	91.06	3.40	3.09	91.11	6.06	4.29
26	88.47	3.35	2.96	88.52	5.81	4.11
36	88.20	3.00	2.65	88.24	5.19	3.67
46	88.96	3.04	2.70	89.01	5.29	3.74
56	88.63	2.95	2.62	88.67	5.13	3.63
66	83.87	2.94	2.47	83.91	4.84	3.42
81	83.30	3.06	2.55	83.34	5.00	3.53
96	76.32	3.07	2.34	76.36	4.59	3.25
111	69.95	3.09	2.16	69.98	4.24	3.00
131	64.65	3.23	2.09	64.68	4.09	2.90
145.6	62.59	3.30	2.06	62.62	4.05	2.86
147	64.03	3.35	2.15	64.07	4.21	2.97

Table 12. Results for 70% Power Near Stall at 0°

Position[mm]	Umean[m/s]	TI[%]	STD	RMS	U 95% Confidence Interval	TI 95% Confidence Interval
6	60.37	6.62	4.00	60.50	7.83	5.54
6.1	59.66	6.47	3.86	59.79	7.57	5.35
6.2	59.54	6.46	3.85	59.67	7.54	5.33
6.3	59.26	6.46	3.83	59.38	7.50	5.30
6.4	59.70	6.57	3.92	59.83	7.69	5.44
6.5	60.63	6.57	3.99	60.76	7.81	5.52
6.75	61.19	6.51	3.98	61.32	7.81	5.52
7	61.64	6.20	3.82	61.76	7.49	5.30
7.25	61.80	6.10	3.77	61.92	7.39	5.22
7.5	62.00	5.92	3.67	62.10	7.19	5.08
8	61.88	5.49	3.40	61.98	6.66	4.71
8.5	61.51	5.00	3.08	61.59	6.03	4.26
9	61.37	4.71	2.89	61.44	5.67	4.01
9.5	61.41	4.39	2.70	61.46	5.29	3.74
10	60.94	4.23	2.58	60.99	5.05	3.57
11	62.39	4.07	2.54	62.44	4.98	3.52
13.5	63.10	3.77	2.38	63.15	4.66	3.29
16	63.54	3.62	2.30	63.58	4.51	3.19
21	65.93	3.53	2.32	65.97	4.56	3.22
26	65.15	3.25	2.12	65.19	4.16	2.94
36	66.64	3.19	2.13	66.68	4.17	2.95
46	67.61	3.12	2.11	67.65	4.13	2.92
56	65.53	2.95	1.93	65.56	3.79	2.68
66	65.90	2.94	1.94	65.92	3.80	2.69
81	63.85	2.84	1.82	63.88	3.56	2.52
96	60.48	2.84	1.71	60.50	3.36	2.38
111	57.06	2.90	1.66	57.09	3.24	2.29
131	54.13	2.90	1.57	54.15	3.08	2.18
145.6	53.62	2.81	1.51	53.64	2.95	2.09
147	53.54	2.76	1.48	53.57	2.90	2.05

Table 13. Results for 85% Power Choked at -30°

Position[mm]	Umean[m/s]	TI[%]	STD	RMS	U 95% Confidence Interval	TI 95% Confidence Interval
6	123.00	6.48	7.97	123.26	15.63	11.05
6.1	121.82	6.20	7.55	122.05	14.80	10.46
6.2	124.73	6.21	7.74	124.97	15.17	10.73
6.3	124.92	6.09	7.61	125.15	14.92	10.55
6.4	123.74	5.96	7.37	123.96	14.45	10.22
6.5	124.19	6.05	7.51	124.42	14.73	10.41
6.75	124.51	5.77	7.18	124.71	14.07	9.95
7	125.21	5.41	6.78	125.39	13.28	9.39
7.25	126.92	5.21	6.61	127.09	12.95	9.16
7.5	126.00	5.09	6.41	126.16	12.56	8.88
8	126.15	4.53	5.71	126.27	11.19	7.92
8.5	126.74	4.02	5.10	126.84	10.00	7.07
9	128.62	3.74	4.82	128.71	9.44	6.67
9.5	130.84	3.58	4.69	130.92	9.18	6.49
10	130.99	3.29	4.31	131.06	8.45	5.98
11	133.71	2.83	3.79	133.76	7.43	5.25
13.5	134.77	2.49	3.35	134.81	6.57	4.64
16	136.14	2.37	3.23	136.17	6.33	4.47
21	137.14	2.19	3.00	137.17	5.88	4.16
26	137.11	2.08	2.85	137.14	5.58	3.94
36	137.79	1.90	2.62	137.81	5.14	3.63
46	136.72	1.93	2.64	136.75	5.18	3.66
56	135.14	1.85	2.49	135.17	4.89	3.46
66	132.98	1.94	2.58	133.00	5.07	3.58
81	129.44	2.04	2.64	129.46	5.18	3.66
96	125.60	2.17	2.72	125.63	5.33	3.77
111	117.72	2.33	2.74	117.75	5.37	3.80
131	105.33	2.66	2.80	105.37	5.48	3.88
145.6	99.39	2.89	2.87	99.43	5.62	3.98
147	97.96	3.00	2.94	98.01	5.76	4.08

Table 14. Results for 85% Power Intermediate Condition at -30°

Position[mm]	Umean[m/s]	TI[%]	STD	RMS	U 95% Confidence Interval	TI 95% Confidence Interval
6	102.74	6.87	7.06	102.98	13.83	9.78
6.1	105.44	6.81	7.18	105.69	14.08	9.95
6.2	102.70	6.61	6.79	102.93	13.31	9.41
6.3	103.76	6.38	6.62	103.97	12.97	9.17
6.4	106.80	6.46	6.90	107.02	13.51	9.56
6.5	105.82	6.34	6.71	106.03	13.16	9.30
6.75	105.12	5.99	6.29	105.31	12.33	8.72
7	106.10	5.94	6.31	106.29	12.36	8.74
7.25	107.94	5.75	6.21	108.12	12.16	8.60
7.5	106.81	5.34	5.70	106.96	11.17	7.90
8	106.15	4.79	5.09	106.27	9.98	7.05
8.5	107.19	4.41	4.73	107.29	9.27	6.55
9	107.46	4.03	4.34	107.54	8.50	6.01
9.5	111.84	3.94	4.41	111.93	8.64	6.11
10	113.44	3.73	4.24	113.51	8.30	5.87
11	115.08	3.27	3.77	115.15	7.38	5.22
13.5	117.14	2.78	3.25	117.19	6.38	4.51
16	115.49	2.57	2.97	115.53	5.82	4.11
21	117.56	2.44	2.87	117.60	5.63	3.98
26	118.42	2.29	2.71	118.45	5.31	3.75
36	117.53	2.15	2.53	117.56	4.96	3.51
46	117.09	2.16	2.53	117.12	4.95	3.50
56	116.34	2.17	2.52	116.37	4.94	3.49
66	113.81	2.11	2.40	113.84	4.70	3.32
81	106.91	2.15	2.29	106.93	4.50	3.18
96	100.60	2.22	2.23	100.63	4.37	3.09
111	92.80	2.32	2.15	92.82	4.22	2.98
131	83.92	2.71	2.28	83.95	4.46	3.16
145.6	83.41	2.83	2.36	83.44	4.63	3.27
147	81.24	2.68	2.17	81.27	4.26	3.01

Table 15. Results for 85% Power Near Stall at -30°

Position[mm]	Umean[m/s]	TI[%]	STD	RMS	U 95% Confidence Interval	TI 95% Confidence Interval
6	72.10	4.46	3.22	72.17	6.30	4.46
6.1	72.88	4.52	3.29	72.95	6.46	4.57
6.2	73.40	4.49	3.30	73.48	6.46	4.57
6.3	73.27	4.44	3.25	73.34	6.38	4.51
6.4	73.29	4.28	3.14	73.36	6.14	4.35
6.5	73.63	4.50	3.31	73.71	6.50	4.59
6.75	74.12	4.18	3.09	74.18	6.07	4.29
7	74.58	4.10	3.06	74.65	5.99	4.23
7.25	74.66	3.93	2.93	74.72	5.75	4.07
7.5	75.15	3.96	2.97	75.21	5.83	4.12
8	75.82	3.66	2.78	75.87	5.44	3.85
8.5	76.25	3.42	2.61	76.29	5.11	3.61
9	76.27	3.34	2.54	76.31	4.99	3.53
9.5	76.30	3.20	2.44	76.34	4.79	3.38
10	76.88	3.18	2.44	76.92	4.79	3.39
11	77.98	3.02	2.36	78.02	4.62	3.27
13.5	79.31	2.92	2.32	79.34	4.54	3.21
16	80.13	2.64	2.11	80.16	4.14	2.93
21	83.00	2.63	2.18	83.03	4.28	3.03
26	82.99	2.48	2.06	83.02	4.04	2.85
36	83.34	2.37	1.98	83.36	3.87	2.74
46	82.83	2.30	1.90	82.85	3.73	2.64
56	81.28	2.34	1.90	81.30	3.73	2.64
66	78.86	2.32	1.83	78.88	3.59	2.54
81	74.90	2.23	1.67	74.92	3.27	2.31
96	72.18	2.09	1.51	72.19	2.96	2.09
111	68.21	1.96	1.34	68.22	2.62	1.86
131	63.18	1.62	1.02	63.19	2.01	1.42
145.6	61.98	1.55	0.96	61.98	1.89	1.33
147	61.59	1.51	0.93	61.60	1.82	1.29

Table 16. Results for 70% Power Choked at -30°

Position[mm]	Umean[m/s]	TI[%]	STD	RMS	U 95% Confidence Interval	TI 95% Confidence Interval
6	93.12	5.09	4.74	93.24	9.28	6.56
6.1	93.32	5.27	4.92	93.45	9.64	6.82
6.2	94.55	5.27	4.99	94.68	9.77	6.91
6.3	95.19	5.12	4.87	95.31	9.55	6.75
6.4	93.82	4.77	4.47	93.92	8.76	6.20
6.5	95.57	5.05	4.83	95.70	9.47	6.69
6.75	96.68	4.83	4.67	96.79	9.16	6.48
7	96.18	4.48	4.31	96.28	8.45	5.98
7.25	96.76	4.41	4.27	96.85	8.37	5.92
7.5	96.16	4.24	4.08	96.24	7.99	5.65
8	96.10	3.86	3.71	96.18	7.27	5.14
8.5	97.05	3.53	3.43	97.11	6.72	4.75
9	95.52	3.49	3.33	95.58	6.53	4.62
9.5	95.84	3.08	2.95	95.89	5.79	4.09
10	97.48	3.17	3.09	97.53	6.06	4.28
11	97.69	2.86	2.79	97.73	5.47	3.87
13.5	98.48	2.72	2.68	98.51	5.25	3.71
16	99.32	2.65	2.64	99.36	5.17	3.65
21	100.11	2.62	2.62	100.15	5.13	3.63
26	97.98	2.40	2.35	98.01	4.61	3.26
36	99.51	2.28	2.27	99.54	4.45	3.14
46	97.21	2.29	2.23	97.24	4.37	3.09
56	98.44	2.28	2.25	98.47	4.40	3.11
66	96.26	2.33	2.25	96.28	4.40	3.11
81	92.93	2.37	2.20	92.96	4.32	3.05
96	89.56	2.62	2.35	89.59	4.60	3.26
111	81.14	2.80	2.27	81.17	4.46	3.15
131	71.65	2.93	2.10	71.68	4.12	2.91
145.6	68.70	3.05	2.10	68.73	4.11	2.91
147	68.39	3.22	2.20	68.43	4.32	3.06

Table 17. Results for 70% Power Intermediate Condition at -30°

Position[mm]	Umean[m/s]	TI[%]	STD	RMS	U 95% Confidence Interval	TI 95% Confidence Interval
6	76.15	5.34	4.07	76.26	7.97	5.63
6.1	75.81	5.14	3.89	75.91	7.63	5.40
6.2	75.99	5.24	3.98	76.10	7.80	5.51
6.3	77.18	5.27	4.07	77.29	7.98	5.64
6.4	76.47	5.00	3.82	76.56	7.49	5.30
6.5	76.31	5.06	3.86	76.40	7.57	5.35
6.75	76.99	4.95	3.81	77.09	7.47	5.28
7	76.72	4.37	3.36	76.80	6.58	4.65
7.25	77.06	4.35	3.35	77.13	6.57	4.65
7.5	77.03	3.99	3.07	77.09	6.02	4.26
8	76.59	3.91	3.00	76.65	5.88	4.16
8.5	78.48	3.83	3.01	78.54	5.89	4.16
9	77.80	3.43	2.67	77.85	5.22	3.69
9.5	76.40	3.28	2.51	76.44	4.91	3.47
10	77.66	3.22	2.50	77.70	4.90	3.46
11	80.72	3.28	2.65	80.77	5.19	3.67
13.5	82.25	3.00	2.46	82.29	4.83	3.41
16	82.77	2.90	2.40	82.81	4.71	3.33
21	84.70	2.67	2.26	84.73	4.43	3.13
26	84.31	2.54	2.14	84.33	4.20	2.97
36	82.28	2.44	2.01	82.31	3.93	2.78
46	81.14	2.43	1.97	81.17	3.86	2.73
56	81.09	2.37	1.92	81.11	3.77	2.67
66	80.08	2.46	1.97	80.10	3.87	2.73
81	75.33	2.41	1.81	75.35	3.55	2.51
96	71.74	2.56	1.84	71.76	3.60	2.55
111	65.16	2.44	1.59	65.18	3.11	2.20
131	57.67	2.12	1.22	57.69	2.40	1.70
145.6	57.50	2.27	1.31	57.51	2.56	1.81
147	57.03	2.28	1.30	57.04	2.55	1.80

Table 18. Results for 70% Power Near Stall at -30°

Position[mm]	Umean[m/s]	TI[%]	STD	RMS	U 95% Confidence Interval	TI 95% Confidence Interval
6	55.35	3.15	1.74	55.37	3.42	2.42
6.1	55.25	3.18	1.76	55.28	3.45	2.44
6.2	55.73	3.34	1.86	55.76	3.65	2.58
6.3	56.02	3.26	1.82	56.05	3.58	2.53
6.4	55.87	3.17	1.77	55.90	3.48	2.46
6.5	55.68	3.10	1.73	55.71	3.39	2.40
6.75	55.58	2.92	1.62	55.60	3.18	2.25
7	56.01	2.88	1.62	56.04	3.17	2.24
7.25	56.32	2.85	1.60	56.34	3.14	2.22
7.5	56.35	2.75	1.55	56.37	3.04	2.15
8	56.26	2.57	1.45	56.27	2.84	2.01
8.5	57.35	2.66	1.53	57.37	2.99	2.12
9	57.34	2.52	1.45	57.36	2.83	2.00
9.5	57.37	2.40	1.38	57.38	2.70	1.91
10	58.19	2.55	1.48	58.21	2.90	2.05
11	58.76	2.39	1.40	58.78	2.75	1.94
13.5	59.14	2.30	1.36	59.15	2.67	1.89
16	59.26	2.13	1.26	59.27	2.47	1.75
21	61.64	2.24	1.38	61.66	2.71	1.91
26	62.60	2.15	1.34	62.61	2.63	1.86
36	61.96	2.02	1.25	61.97	2.45	1.73
46	60.69	1.91	1.16	60.70	2.27	1.60
56	60.41	1.82	1.10	60.42	2.16	1.52
66	59.77	1.85	1.11	59.78	2.17	1.54
81	57.36	1.63	0.94	57.37	1.84	1.30
96	56.35	1.61	0.91	56.36	1.78	1.26
111	54.01	1.36	0.74	54.01	1.44	1.02
131	51.29	0.74	0.38	51.30	0.75	0.53
145.6	50.70	0.46	0.23	50.70	0.46	0.32
147	50.87	0.59	0.30	50.87	0.59	0.41

Table 19. Results for 85% Power Choked at 30°

Position[mm]	Umean[m/s]	TI[%]	STD	RMS	U 95% Confidence Interval	TI 95% Confidence Interval
6	124.50	6.71	8.35	124.78	16.37	11.57
6.1	124.99	6.77	8.46	125.28	16.57	11.72
6.2	125.23	6.61	8.28	125.50	16.22	11.47
6.3	125.20	6.62	8.29	125.48	16.24	11.49
6.4	123.77	6.37	7.88	124.02	15.44	10.92
6.5	124.82	6.26	7.81	125.07	15.31	10.82
6.75	125.66	6.30	7.92	125.91	15.51	10.97
7	125.80	5.99	7.54	126.03	14.78	10.45
7.25	125.66	5.84	7.33	125.87	14.38	10.17
7.5	126.28	5.70	7.20	126.49	14.11	9.97
8	126.67	5.34	6.76	126.85	13.25	9.37
8.5	128.14	5.07	6.50	128.30	12.73	9.00
9	128.59	4.58	5.89	128.73	11.54	8.16
9.5	128.34	4.26	5.46	128.46	10.70	7.57
10	129.70	4.19	5.43	129.81	10.64	7.52
11	130.37	3.62	4.72	130.45	9.26	6.55
13.5	130.22	2.96	3.86	130.27	7.57	5.35
16	130.89	2.71	3.55	130.94	6.96	4.92
21	131.95	2.51	3.31	131.99	6.49	4.59
26	131.75	2.27	2.99	131.78	5.86	4.14
36	133.21	2.09	2.78	133.24	5.46	3.86
46	133.62	1.94	2.59	133.65	5.08	3.59
56	132.64	2.07	2.75	132.67	5.39	3.81
66	131.19	2.46	3.23	131.23	6.32	4.47
81	130.07	2.01	2.62	130.09	5.13	3.63
96	126.03	2.35	2.96	126.07	5.81	4.11
111	121.92	2.33	2.84	121.96	5.57	3.94
131	113.79	2.77	3.16	113.83	6.18	4.37
145.6	103.73	9.96	10.33	104.25	20.24	14.31
147	103.82	4.88	5.06	103.94	9.92	7.02

Table 20. Results for 85% Power Intermediate Condition at 30°

Position[mm]	Umean[m/s]	TI[%]	STD	RMS	U 95% Confidence Interval	TI 95% Confidence Interval
6	100.37	8.37	8.40	100.72	16.47	11.64
6.1	100.41	8.52	8.55	100.78	16.76	11.85
6.2	100.37	8.45	8.48	100.73	16.62	11.75
6.3	100.62	8.23	8.29	100.96	16.24	11.48
6.4	102.08	8.32	8.50	102.43	16.65	11.77
6.5	102.36	8.35	8.54	102.71	16.74	11.84
6.75	104.04	8.10	8.43	104.38	16.51	11.68
7	103.74	7.95	8.25	104.06	16.16	11.43
7.25	105.23	7.57	7.96	105.53	15.61	11.04
7.5	104.98	7.54	7.91	105.27	15.51	10.97
8	105.95	7.13	7.56	106.22	14.81	10.47
8.5	107.41	6.58	7.07	107.65	13.85	9.80
9	108.55	6.16	6.69	108.75	13.11	9.27
9.5	109.07	5.63	6.14	109.24	12.03	8.51
10	108.94	5.11	5.56	109.08	10.90	7.71
11	110.12	4.52	4.98	110.23	9.75	6.90
13.5	113.17	3.52	3.98	113.24	7.80	5.51
16	115.99	3.08	3.58	116.04	7.01	4.96
21	116.38	2.73	3.18	116.43	6.23	4.40
26	117.80	2.58	3.04	117.84	5.96	4.21
36	118.23	2.54	3.00	118.27	5.88	4.16
46	116.76	2.19	2.55	116.79	5.00	3.54
56	114.69	2.34	2.68	114.72	5.26	3.72
66	114.73	2.60	2.98	114.77	5.84	4.13
81	111.76	2.25	2.52	111.79	4.94	3.49
96	108.69	2.71	2.94	108.73	5.76	4.07
111	104.15	2.55	2.65	104.19	5.20	3.68
131	94.54	3.17	3.00	94.59	5.88	4.15
145.6	91.32	2.99	2.73	91.36	5.35	3.78
147	92.01	2.97	2.73	92.05	5.36	3.79

Table 21. Results for 85% Power Near Stall at 30°

Position[mm]	Umean[m/s]	TI[%]	STD	RMS	U 95% Confidence Interval	TI 95% Confidence Interval
6	72.53	9.89	7.18	72.89	14.07	9.95
6.1	73.48	9.93	7.30	73.84	14.30	10.11
6.2	72.62	9.66	7.02	72.96	13.75	9.72
6.3	72.37	9.73	7.05	72.72	13.81	9.76
6.4	74.01	10.23	7.57	74.39	14.84	10.49
6.5	75.16	10.14	7.62	75.54	14.93	10.56
6.75	75.40	9.93	7.49	75.77	14.68	10.38
7	75.99	9.72	7.39	76.35	14.48	10.24
7.25	75.89	9.47	7.19	76.23	14.09	9.96
7.5	76.76	9.31	7.14	77.09	14.00	9.90
8	76.38	8.73	6.67	76.67	13.07	9.24
8.5	76.93	8.36	6.43	77.20	12.61	8.92
9	79.56	8.28	6.59	79.83	12.91	9.13
9.5	81.39	7.88	6.42	81.64	12.58	8.89
10	83.15	7.68	6.39	83.39	12.52	8.85
11	84.22	6.82	5.74	84.41	11.26	7.96
13.5	86.04	5.94	5.11	86.20	10.02	7.08
16	87.84	5.45	4.78	87.97	9.38	6.63
21	90.11	4.98	4.49	90.22	8.80	6.22
26	92.25	4.55	4.20	92.34	8.23	5.82
36	94.00	3.99	3.76	94.08	7.36	5.20
46	93.49	3.80	3.55	93.56	6.96	4.92
56	90.35	4.37	3.94	90.44	7.73	5.47
66	86.90	2.97	2.58	86.94	5.07	3.58
81	84.45	3.45	2.91	84.50	5.70	4.03
96	82.01	3.28	2.69	82.05	5.27	3.73
111	76.82	3.07	2.36	76.85	4.62	3.26
131	69.94	3.04	2.12	69.98	4.16	2.94
145.6	66.40	2.84	1.88	66.43	3.69	2.61
147	65.63	2.74	1.80	65.65	3.52	2.49

Table 22. Results for 70% Power Choked at 30°

Position[mm]	Umean[m/s]	TI[%]	STD	RMS	U 95% Confidence Interval	TI 95% Confidence Interval
6	86.60	9.62	8.33	87.00	16.33	11.55
6.1	87.22	9.79	8.54	87.63	16.74	11.84
6.2	85.59	9.73	8.33	86.00	16.32	11.54
6.3	86.63	9.78	8.47	87.04	16.60	11.74
6.4	86.95	9.68	8.42	87.35	16.50	11.67
6.5	87.02	9.54	8.30	87.41	16.27	11.50
6.75	86.57	9.38	8.12	86.95	15.92	11.26
7	87.00	8.92	7.76	87.34	15.21	10.76
7.25	89.86	8.76	7.87	90.21	15.43	10.91
7.5	90.74	8.55	7.76	91.07	15.21	10.75
8	92.39	7.90	7.30	92.68	14.31	10.12
8.5	93.38	7.67	7.16	93.66	14.03	9.92
9	94.94	6.86	6.51	95.16	12.76	9.03
9.5	93.68	6.05	5.67	93.85	11.11	7.86
10	94.41	5.62	5.31	94.56	10.40	7.35
11	95.74	4.64	4.44	95.84	8.71	6.16
13.5	97.44	3.43	3.35	97.50	6.56	4.64
16	98.70	3.18	3.14	98.75	6.15	4.35
21	97.88	2.81	2.75	97.92	5.39	3.81
26	99.45	2.77	2.75	99.49	5.40	3.82
36	99.51	2.49	2.47	99.54	4.85	3.43
46	98.79	2.66	2.63	98.83	5.15	3.64
56	99.69	2.64	2.63	99.72	5.15	3.64
66	98.74	2.58	2.55	98.78	4.99	3.53
81	95.49	2.78	2.65	95.52	5.20	3.68
96	91.63	2.92	2.68	91.67	5.25	3.71
111	86.89	3.07	2.67	86.93	5.22	3.69
131	79.21	3.34	2.65	79.25	5.19	3.67
145.6	75.66	3.64	2.75	75.71	5.39	3.81
147	75.41	3.59	2.71	75.46	5.31	3.75

Table 23. Results for 70% Power Intermediate Condition at 30°

Position[mm]	Umean[m/s]	TI[%]	STD	RMS	U 95% Confidence Interval	TI 95% Confidence Interval
6	76.34	8.57	6.54	76.62	12.82	9.06
6.1	76.70	8.67	6.65	76.99	13.03	9.22
6.2	77.23	8.63	6.67	77.51	13.07	9.24
6.3	78.10	8.69	6.79	78.40	13.30	9.41
6.4	77.46	8.94	6.92	77.77	13.57	9.60
6.5	77.86	8.71	6.78	78.15	13.29	9.40
6.75	78.74	8.48	6.67	79.02	13.08	9.25
7	78.88	8.33	6.57	79.15	12.87	9.10
7.25	79.93	8.10	6.47	80.19	12.68	8.97
7.5	80.25	7.94	6.37	80.50	12.49	8.83
8	82.39	7.52	6.20	82.62	12.15	8.59
8.5	83.35	7.05	5.88	83.55	11.52	8.14
9	84.59	6.39	5.40	84.76	10.59	7.49
9.5	85.15	5.76	4.90	85.29	9.61	6.80
10	85.55	5.16	4.42	85.67	8.65	6.12
11	85.88	4.53	3.89	85.97	7.63	5.39
13.5	86.54	3.20	2.77	86.58	5.42	3.84
16	89.32	2.87	2.57	89.36	5.03	3.56
21	89.63	2.84	2.55	89.67	5.00	3.53
26	89.07	2.71	2.41	89.10	4.73	3.35
36	90.32	2.45	2.21	90.35	4.33	3.06
46	89.47	2.34	2.09	89.49	4.09	2.90
56	88.19	2.35	2.07	88.21	4.07	2.88
66	88.79	2.37	2.10	88.82	4.12	2.91
81	86.31	2.45	2.12	86.33	4.15	2.93
96	81.62	2.59	2.12	81.65	4.15	2.93
111	77.04	2.76	2.12	77.06	4.16	2.94
131	70.13	2.87	2.01	70.16	3.95	2.79
145.6	66.30	2.93	1.94	66.33	3.80	2.69
147	66.71	2.92	1.95	66.74	3.82	2.70

Table 24. Results for 70% Power Near Stall at 30°

Position[mm]	Umean[m/s]	TI[%]	STD	RMS	U 95% Confidence Interval	TI 95% Confidence Interval
6	57.56	6.24	3.59	57.68	7.04	4.98
6.1	57.68	6.46	3.73	57.80	7.30	5.16
6.2	58.81	7.08	4.16	58.96	8.16	5.77
6.3	58.68	6.95	4.08	58.82	7.99	5.65
6.4	58.38	6.74	3.93	58.52	7.71	5.45
6.5	57.59	6.41	3.69	57.70	7.24	5.12
6.75	57.67	6.27	3.61	57.79	7.08	5.01
7	58.51	6.53	3.82	58.63	7.49	5.30
7.25	59.48	6.74	4.01	59.61	7.86	5.56
7.5	59.52	6.53	3.89	59.65	7.62	5.39
8	60.64	6.42	3.89	60.77	7.63	5.39
8.5	61.36	6.45	3.96	61.49	7.76	5.49
9	62.14	6.01	3.73	62.26	7.32	5.17
9.5	63.18	5.89	3.72	63.29	7.30	5.16
10	63.31	5.65	3.58	63.41	7.02	4.96
11	66.39	5.14	3.41	66.48	6.68	4.73
13.5	67.05	3.91	2.62	67.10	5.14	3.63
16	68.27	3.60	2.46	68.31	4.82	3.41
21	69.69	3.56	2.48	69.74	4.86	3.44
26	70.19	3.31	2.32	70.23	4.56	3.22
36	71.38	3.05	2.18	71.42	4.27	3.02
46	71.54	2.82	2.02	71.57	3.95	2.80
56	71.09	2.73	1.94	71.12	3.81	2.69
66	69.24	2.50	1.73	69.27	3.40	2.40
81	68.71	2.54	1.75	68.74	3.43	2.42
96	66.21	2.61	1.73	66.23	3.39	2.40
111	62.25	2.45	1.53	62.26	2.99	2.11
131	56.52	1.94	1.10	56.53	2.15	1.52
145.6	55.08	1.74	0.96	55.09	1.88	1.33
147	55.32	1.77	0.98	55.33	1.92	1.36

Table 25. Results for 85% Power Choked at 120°

Position[mm]	Umean[m/s]	TI[%]	STD	RMS	U 95% Confidence Interval	TI 95% Confidence Interval
6	121.29	6.06	7.35	121.51	14.40	10.18
6.1	119.96	6.00	7.20	120.18	14.11	9.97
6.2	118.68	5.92	7.02	118.89	13.76	9.73
6.3	118.75	5.82	6.91	118.95	13.54	9.57
6.4	119.71	5.85	7.00	119.91	13.72	9.70
6.5	119.67	5.78	6.91	119.87	13.55	9.58
6.75	119.88	5.64	6.76	120.07	13.26	9.37
7	122.03	5.45	6.66	122.21	13.05	9.22
7.25	121.24	5.22	6.33	121.40	12.41	8.77
7.5	122.64	4.99	6.12	122.79	12.00	8.48
8	123.40	4.73	5.84	123.54	11.45	8.10
8.5	124.58	4.53	5.64	124.70	11.06	7.82
9	124.63	4.32	5.38	124.74	10.55	7.46
9.5	124.64	4.13	5.15	124.75	10.09	7.14
10	123.86	4.02	4.98	123.96	9.76	6.90
11	124.56	3.76	4.69	124.65	9.19	6.50
13.5	125.34	3.56	4.46	125.42	8.74	6.18
16	126.22	3.35	4.23	126.29	8.28	5.86
21	125.95	2.94	3.70	126.00	7.26	5.13
26	128.23	3.05	3.91	128.29	7.65	5.41
36	128.13	3.10	3.97	128.20	7.79	5.50
46	127.51	2.77	3.53	127.56	6.92	4.89
56	126.80	2.71	3.43	126.84	6.73	4.76
66	125.08	2.73	3.41	125.13	6.69	4.73
81	124.48	2.67	3.32	124.53	6.51	4.60
96	120.12	2.56	3.08	120.16	6.04	4.27
111	113.50	2.56	2.90	113.54	5.69	4.02
131	104.98	2.78	2.92	105.02	5.72	4.05
145.6	97.28	7.97	7.76	97.58	15.20	10.75
147	96.37	2.83	2.73	96.41	5.35	3.78

Table 26. Results for 85% Power Intermediate Condition at 120°

Position[mm]	Umean[m/s]	TI[%]	STD	RMS	U 95% Confidence Interval	TI 95% Confidence Interval
6	108.92	5.48	5.97	109.08	11.70	8.27
6.1	109.75	5.80	6.36	109.93	12.47	8.81
6.2	110.03	5.72	6.29	110.21	12.34	8.72
6.3	109.52	5.55	6.08	109.69	11.92	8.43
6.4	109.72	5.69	6.24	109.89	12.23	8.65
6.5	109.28	5.50	6.01	109.44	11.77	8.32
6.75	109.21	5.38	5.87	109.37	11.51	8.14
7	110.29	5.11	5.64	110.44	11.05	7.81
7.25	110.50	5.05	5.58	110.64	10.94	7.74
7.5	110.83	4.82	5.35	110.96	10.48	7.41
8	111.21	4.35	4.84	111.32	9.49	6.71
8.5	111.90	4.15	4.64	111.99	9.09	6.43
9	111.91	3.96	4.44	111.99	8.70	6.15
9.5	112.91	3.79	4.28	112.99	8.39	5.93
10	112.91	3.65	4.12	112.98	8.07	5.71
11	113.97	3.49	3.97	114.04	7.79	5.51
13.5	115.62	3.23	3.73	115.68	7.31	5.17
16	115.78	3.09	3.57	115.83	7.00	4.95
21	118.00	2.80	3.31	118.05	6.48	4.58
26	118.63	2.60	3.08	118.67	6.04	4.27
36	119.02	2.53	3.01	119.05	5.91	4.18
46	118.76	2.39	2.84	118.79	5.57	3.94
56	116.79	2.18	2.55	116.82	5.00	3.53
66	117.26	2.24	2.63	117.29	5.16	3.65
81	115.65	2.28	2.64	115.68	5.17	3.65
96	109.95	2.34	2.58	109.98	5.05	3.57
111	103.45	2.21	2.28	103.47	4.48	3.17
131	94.69	2.21	2.10	94.71	4.11	2.90
145.6	91.78	2.54	2.33	91.81	4.58	3.24
147	91.56	2.41	2.21	91.59	4.33	3.06

Table 27. Results for 85% Power Near Stall at 120°

Position[mm]	Umean[m/s]	TI[%]	STD	RMS	U 95% Confidence Interval	TI 95% Confidence Interval
6	87.57	5.39	4.72	87.70	9.26	6.55
6.1	85.85	5.33	4.58	85.97	8.97	6.34
6.2	86.57	5.31	4.60	86.69	9.01	6.37
6.3	86.72	5.22	4.52	86.84	8.86	6.27
6.4	86.84	5.13	4.46	86.96	8.74	6.18
6.5	86.60	5.14	4.45	86.71	8.72	6.17
6.75	86.60	4.86	4.21	86.70	8.24	5.83
7	87.85	4.86	4.27	87.95	8.37	5.92
7.25	88.57	4.53	4.01	88.66	7.86	5.56
7.5	88.97	4.47	3.98	89.06	7.79	5.51
8	89.07	4.06	3.62	89.14	7.09	5.01
8.5	89.24	3.90	3.48	89.31	6.82	4.82
9	89.98	3.67	3.30	90.04	6.47	4.58
9.5	90.97	3.45	3.14	91.02	6.15	4.35
10	90.12	3.40	3.06	90.18	6.00	4.24
11	91.95	3.19	2.93	91.99	5.75	4.06
13.5	92.70	2.97	2.75	92.74	5.39	3.81
16	92.48	2.76	2.55	92.51	5.00	3.53
21	95.19	2.55	2.42	95.22	4.75	3.36
26	95.25	2.41	2.29	95.28	4.50	3.18
36	95.74	2.15	2.06	95.76	4.04	2.86
46	96.08	2.11	2.03	96.10	3.97	2.81
56	95.79	1.98	1.90	95.81	3.71	2.63
66	94.78	1.92	1.82	94.80	3.56	2.52
81	92.21	1.94	1.79	92.23	3.51	2.48
96	87.96	1.97	1.73	87.98	3.39	2.40
111	83.62	1.95	1.63	83.64	3.20	2.26
131	77.09	2.04	1.57	77.10	3.08	2.18
145.6	74.70	2.01	1.50	74.71	2.95	2.08
147	74.71	2.04	1.52	74.72	2.98	2.11

Table 28. Results for 70% Power Choked at 120°

Position[mm]	Umean[m/s]	TI[%]	STD	RMS	U 95% Confidence Interval	TI 95% Confidence Interval
6	96.26	5.36	5.15	96.40	10.10	7.14
6.1	96.59	5.61	5.41	96.74	10.61	7.50
6.2	96.34	5.41	5.21	96.48	10.21	7.22
6.3	96.83	5.34	5.17	96.97	10.14	7.17
6.4	98.20	5.30	5.21	98.34	10.20	7.21
6.5	98.77	5.16	5.10	98.91	9.99	7.06
6.75	99.07	4.79	4.75	99.18	9.30	6.58
7	100.08	4.90	4.90	100.20	9.61	6.80
7.25	100.48	4.43	4.45	100.58	8.72	6.17
7.5	100.59	4.33	4.35	100.69	8.53	6.03
8	101.24	3.94	3.99	101.32	7.83	5.53
8.5	101.78	3.47	3.53	101.84	6.92	4.89
9	101.78	3.36	3.42	101.83	6.70	4.74
9.5	100.84	3.17	3.20	100.89	6.26	4.43
10	101.98	3.11	3.17	102.03	6.22	4.40
11	102.07	2.90	2.96	102.11	5.80	4.10
13.5	102.47	2.83	2.90	102.52	5.69	4.02
16	101.61	2.58	2.62	101.65	5.13	3.63
21	101.39	2.40	2.44	101.42	4.78	3.38
26	103.24	2.44	2.52	103.27	4.93	3.49
36	104.52	2.40	2.50	104.55	4.91	3.47
46	104.27	2.29	2.39	104.30	4.68	3.31
56	102.32	2.30	2.35	102.35	4.61	3.26
66	99.49	2.26	2.25	99.52	4.41	3.12
81	97.22	2.25	2.19	97.25	4.29	3.03
96	94.38	2.31	2.18	94.41	4.28	3.03
111	90.07	2.50	2.25	90.10	4.40	3.11
131	82.37	2.50	2.06	82.39	4.03	2.85
145.6	79.47	2.44	1.94	79.50	3.80	2.69
147	79.88	2.48	1.98	79.90	3.88	2.74

Table 29. Results for 70% Power Intermediate Condition at 120°

Position[mm]	Umean[m/s]	TI[%]	STD	RMS	U 95% Confidence Interval	TI 95% Confidence Interval
6	85.16	5.06	4.31	85.27	8.45	5.98
6.1	85.49	4.92	4.21	85.59	8.24	5.83
6.2	85.01	4.99	4.24	85.11	8.32	5.88
6.3	85.02	4.98	4.23	85.13	8.30	5.87
6.4	85.09	4.93	4.19	85.19	8.22	5.81
6.5	85.34	4.80	4.10	85.44	8.04	5.68
6.75	85.68	4.43	3.80	85.77	7.44	5.26
7	85.35	4.26	3.64	85.43	7.13	5.04
7.25	86.28	3.98	3.43	86.34	6.73	4.76
7.5	86.60	3.81	3.30	86.67	6.47	4.57
8	86.42	3.47	3.00	86.47	5.87	4.15
8.5	86.27	3.24	2.79	86.31	5.47	3.87
9	86.18	3.01	2.59	86.22	5.08	3.59
9.5	87.21	2.87	2.51	87.25	4.91	3.47
10	86.89	2.76	2.40	86.93	4.70	3.32
11	87.78	2.59	2.27	87.81	4.45	3.15
13.5	87.74	2.37	2.08	87.76	4.07	2.88
16	89.20	2.40	2.14	89.22	4.19	2.96
21	89.65	2.34	2.09	89.67	4.10	2.90
26	89.77	2.09	1.87	89.79	3.67	2.60
36	90.73	1.99	1.80	90.75	3.53	2.50
46	90.48	2.06	1.86	90.50	3.65	2.58
56	89.07	1.96	1.75	89.09	3.42	2.42
66	87.85	1.94	1.70	87.87	3.33	2.36
81	86.26	2.06	1.78	86.28	3.48	2.46
96	82.59	2.09	1.73	82.61	3.38	2.39
111	78.46	2.12	1.67	78.48	3.26	2.31
131	72.04	2.20	1.59	72.06	3.11	2.20
145.6	70.15	2.19	1.54	70.16	3.01	2.13
147	70.20	2.21	1.55	70.21	3.05	2.15

Table 30. Results for 70% Power Near Stall at 120°

Position[mm]	Umean[m/s]	TI[%]	STD	RMS	U 95% Confidence Interval	TI 95% Confidence Interval
6	69.33	4.95	3.43	69.41	6.72	4.75
6.1	69.31	4.83	3.35	69.39	6.56	4.64
6.2	69.25	4.76	3.30	69.33	6.46	4.57
6.3	69.38	4.66	3.23	69.45	6.33	4.48
6.4	69.64	4.72	3.29	69.71	6.44	4.55
6.5	69.55	4.61	3.21	69.62	6.28	4.44
6.75	69.38	4.40	3.05	69.44	5.98	4.23
7	69.47	4.09	2.84	69.53	5.58	3.94
7.25	69.58	3.98	2.77	69.64	5.43	3.84
7.5	70.42	3.78	2.66	70.47	5.22	3.69
8	70.60	3.53	2.49	70.64	4.88	3.45
8.5	70.62	3.18	2.25	70.66	4.40	3.11
9	70.67	3.08	2.17	70.71	4.26	3.01
9.5	71.11	2.97	2.12	71.14	4.15	2.93
10	70.99	2.78	1.98	71.02	3.87	2.74
11	71.72	2.69	1.93	71.74	3.78	2.67
13.5	72.02	2.49	1.79	72.05	3.52	2.49
16	72.13	2.40	1.73	72.15	3.39	2.40
21	73.19	2.23	1.63	73.21	3.20	2.26
26	74.00	2.05	1.52	74.02	2.97	2.10
36	74.34	1.95	1.45	74.36	2.84	2.01
46	74.24	1.92	1.43	74.25	2.80	1.98
56	73.81	1.88	1.39	73.82	2.72	1.93
66	73.29	1.96	1.43	73.30	2.81	1.99
81	70.96	1.91	1.36	70.98	2.66	1.88
96	68.29	1.87	1.28	68.30	2.50	1.77
111	65.34	1.92	1.26	65.35	2.46	1.74
131	61.89	2.04	1.26	61.91	2.48	1.75
145.6	60.09	2.01	1.21	60.11	2.36	1.67
147	59.68	1.99	1.19	59.69	2.33	1.65

Table 31. Results for 85% Power Choked at 30° and Bellmouth Removed

Position[mm]	Umean[m/s]	TI[%]	STD	RMS	U 95% Confidence Interval	TI 95% Confidence Interval
6	131.20	7.74	10.15	131.59	19.89	14.07
6.1	130.45	7.80	10.18	130.85	19.95	14.10
6.2	128.22	7.92	10.15	128.62	19.90	14.07
6.3	129.87	7.77	10.09	130.26	19.77	13.98
6.4	130.19	7.77	10.11	130.59	19.82	14.02
6.5	130.47	7.82	10.20	130.87	19.99	14.13
6.75	130.69	7.94	10.37	131.11	20.33	14.38
7	131.39	7.69	10.10	131.78	19.80	14.00
7.25	130.51	7.44	9.71	130.87	19.03	13.46
7.5	129.91	7.08	9.20	130.24	18.03	12.75
8	131.71	6.29	8.29	131.97	16.25	11.49
8.5	132.24	5.78	7.65	132.46	14.99	10.60
9	133.46	5.22	6.97	133.64	13.65	9.65
9.5	134.12	4.78	6.41	134.27	12.56	8.88
10	134.73	4.29	5.78	134.86	11.34	8.02
11	134.73	3.90	5.26	134.83	10.31	7.29
13.5	134.53	3.13	4.21	134.60	8.25	5.84
16	135.25	2.92	3.95	135.31	7.74	5.47
21	136.81	2.83	3.87	136.87	7.59	5.37
26	136.59	2.50	3.41	136.64	6.68	4.73
36	137.47	2.13	2.93	137.50	5.74	4.06
46	138.26	2.07	2.87	138.29	5.62	3.98
56	137.08	2.28	3.13	137.12	6.13	4.34
66	134.30	2.02	2.71	134.33	5.31	3.75
81	131.74	2.55	3.36	131.78	6.58	4.65
96	128.68	2.67	3.44	128.73	6.74	4.76
111	124.43	2.58	3.22	124.47	6.30	4.46
131	116.06	4.28	4.97	116.16	9.75	6.89
145.6	105.93	10.60	11.23	106.53	22.01	15.56
147	105.78	8.25	8.72	106.14	17.10	12.09

Table 32. Results for 85% Power Intermediate Condition at 30° and Bellmouth Removed

Position[mm]	Umean[m/s]	TI[%]	STD	RMS	Confidence	TI 95% Confidence Interval
6	104.04	5.83	6.07	104.22	11.89	8.41
6.1	104.14	5.76	6.00	104.32	11.76	8.32
6.2	105.71	6.00	6.34	105.90	12.44	8.79
6.3	104.80	5.78	6.06	104.98	11.88	8.40
6.4	104.47	5.81	6.07	104.64	11.89	8.41
6.5	104.90	5.64	5.92	105.07	11.61	8.21
6.75	104.44	5.57	5.81	104.61	11.40	8.06
7	104.93	5.35	5.61	105.08	11.00	7.78
7.25	104.86	5.19	5.44	105.00	10.67	7.55
7.5	105.18	5.06	5.32	105.32	10.43	7.37
8	106.30	4.67	4.96	106.42	9.73	6.88
8.5	106.58	4.33	4.62	106.68	9.05	6.40
9	107.22	3.97	4.26	107.31	8.35	5.90
9.5	108.16	3.70	4.01	108.24	7.85	5.55
10	109.15	3.45	3.77	109.22	7.38	5.22
11	110.25	3.11	3.43	110.30	6.72	4.75
13.5	111.66	2.60	2.90	111.70	5.69	4.02
16	113.66	2.45	2.79	113.70	5.46	3.86
21	114.45	2.12	2.43	114.48	4.75	3.36
26	115.11	1.88	2.16	115.13	4.24	3.00
36	115.04	1.80	2.07	115.05	4.05	2.86
46	115.65	2.00	2.31	115.68	4.54	3.21
56	113.59	1.77	2.01	113.60	3.94	2.79
66	113.10	1.91	2.16	113.12	4.23	2.99
81	108.62	2.05	2.23	108.64	4.36	3.08
96	105.01	2.49	2.62	105.04	5.13	3.63
111	98.70	2.02	1.99	98.72	3.91	2.76
131	89.29	2.45	2.18	89.31	4.28	3.03
145.6	87.52	2.25	1.97	87.54	3.86	2.73
147	88.08	2.19	1.92	88.10	3.77	2.67

Table 33. Results for 85% Power Near Stall at 30° and Bellmouth Removed

Position[mm]	Umean[m/s]	TI[%]	STD	RMS	U 95% Confidence Interval	TI 95% Confidence Interval
6	84.24	5.47	4.61	84.37	9.03	6.39
6.1	83.01	5.29	4.39	83.13	8.60	6.08
6.2	82.98	5.26	4.37	83.09	8.56	6.05
6.3	83.31	5.19	4.32	83.42	8.47	5.99
6.4	83.28	5.20	4.33	83.39	8.48	6.00
6.5	85.10	5.32	4.53	85.22	8.88	6.28
6.75	84.78	5.16	4.38	84.90	8.58	6.06
7	84.34	5.01	4.22	84.45	8.28	5.86
7.25	84.18	4.75	4.00	84.27	7.84	5.54
7.5	84.18	4.55	3.83	84.26	7.50	5.31
8	85.53	4.40	3.77	85.61	7.38	5.22
8.5	86.98	4.13	3.59	87.05	7.03	4.97
9	86.38	3.81	3.29	86.44	6.45	4.56
9.5	86.23	3.44	2.97	86.28	5.82	4.12
10	86.71	3.24	2.81	86.75	5.51	3.90
11	88.18	3.00	2.64	88.22	5.18	3.66
13.5	88.98	2.69	2.39	89.01	4.68	3.31
16	89.87	2.52	2.27	89.90	4.44	3.14
21	92.00	2.16	1.99	92.03	3.90	2.76
26	94.28	1.84	1.73	94.30	3.39	2.40
36	93.88	1.65	1.55	93.89	3.04	2.15
46	93.73	1.83	1.72	93.74	3.36	2.38
56	92.29	1.70	1.57	92.31	3.07	2.17
66	89.66	1.79	1.61	89.67	3.15	2.23
81	86.34	1.77	1.53	86.35	3.00	2.12
96	83.81	1.92	1.61	83.83	3.16	2.23
111	78.93	1.76	1.39	78.95	2.73	1.93
131	74.29	1.86	1.38	74.30	2.70	1.91
145.6	72.68	1.90	1.38	72.69	2.71	1.91
147	71.63	1.86	1.33	71.64	2.61	1.84

Table 34. Results for 70% Power Choked at 30° and Bellmouth Removed

Position[mm]	Umean[m/s]	TI[%]	STD	RMS	U 95% Confidence Interval	TI 95% Confidence Interval
6	89.32	5.46	4.88	89.45	9.56	6.76
6.1	89.72	5.33	4.78	89.85	9.37	6.63
6.2	90.13	5.40	4.86	90.26	9.53	6.74
6.3	89.44	5.35	4.78	89.57	9.38	6.63
6.4	89.39	5.36	4.79	89.52	9.39	6.64
6.5	92.04	5.38	4.95	92.17	9.70	6.86
6.75	90.96	5.01	4.56	91.07	8.94	6.32
7	90.77	4.74	4.30	90.87	8.43	5.96
7.25	91.65	4.51	4.14	91.74	8.11	5.73
7.5	91.91	4.27	3.92	92.00	7.69	5.43
8	92.20	4.05	3.73	92.28	7.31	5.17
8.5	93.77	3.68	3.45	93.83	6.77	4.78
9	93.85	3.24	3.04	93.90	5.96	4.21
9.5	94.06	2.91	2.74	94.10	5.37	3.79
10	93.65	2.59	2.43	93.68	4.76	3.37
11	93.28	2.17	2.02	93.30	3.97	2.80
13.5	95.15	1.89	1.80	95.17	3.53	2.50
16	95.30	1.76	1.68	95.32	3.29	2.32
21	95.87	1.67	1.60	95.88	3.13	2.21
26	97.43	1.56	1.52	97.44	2.99	2.11
36	97.49	1.40	1.36	97.50	2.67	1.89
46	95.56	1.57	1.50	95.57	2.94	2.08
56	94.97	1.70	1.62	94.98	3.17	2.24
66	94.87	1.73	1.65	94.89	3.23	2.28
81	91.29	1.70	1.55	91.30	3.04	2.15
96	86.00	1.44	1.24	86.00	2.43	1.72
111	80.98	1.50	1.22	80.99	2.39	1.69
131	74.89	1.65	1.24	74.90	2.43	1.72
145.6	72.82	2.03	1.48	72.84	2.90	2.05
147	72.67	2.09	1.52	72.69	2.98	2.11

Table 35. Results for 70% Power Intermediate Condition at 30° and Bellmouth Removed

Position[mm]	Umean[m/s]	TI[%]	STD	RMS	U 95% Confidence Interval	TI 95% Confidence Interval
6	56.08	43.34	24.30	61.12	47.64	33.68
6.1	54.35	46.19	25.10	59.86	49.20	34.79
6.2	56.56	40.82	23.09	61.09	45.25	32.00
6.3	57.64	39.51	22.78	61.98	44.64	31.57
6.4	57.90	38.66	22.38	62.07	43.87	31.02
6.5	57.00	41.72	23.78	61.76	46.61	32.96
6.75	57.02	41.80	23.83	61.80	46.71	33.03
7	55.30	45.22	25.01	60.69	49.01	34.66
7.25	54.67	50.80	27.77	61.32	54.43	38.49
7.5	58.62	38.39	22.51	62.80	44.12	31.20
8	58.28	35.49	20.69	61.84	40.54	28.67
8.5	59.78	29.75	17.78	62.37	34.85	24.64
9	60.07	26.16	15.71	62.09	30.80	21.78
9.5	62.14	21.76	13.52	63.60	26.51	18.74
10	62.54	19.48	12.18	63.72	23.88	16.88
11	62.22	17.25	10.73	63.14	21.03	14.87
13.5	62.27	14.03	8.74	62.88	17.12	12.11
16	64.41	12.29	7.91	64.89	15.51	10.97
21	64.11	11.01	7.06	64.50	13.84	9.79
26	67.23	9.35	6.29	67.52	12.33	8.72
36	69.49	7.77	5.40	69.70	10.58	7.48
46	70.55	7.04	4.97	70.73	9.73	6.88
56	69.45	7.30	5.07	69.63	9.93	7.02
66	69.27	7.53	5.22	69.46	10.22	7.23
81	65.38	9.00	5.88	65.64	11.53	8.15
96	60.97	11.41	6.95	61.36	13.63	9.64
111	50.63	24.66	12.49	52.15	24.48	17.31
131	18.26	937.93	171.24	172.21	335.63	237.33
145.6	20.54	805.61	165.44	166.71	324.27	229.29
147	58.74	14.09	8.28	59.32	16.22	11.47

Table 36. Results for 70% Power Near Stall at 30° and Bellmouth Removed

Position[mm]	Umean[m/s]	TI[%]	STD	RMS	U 95% Confidence Interval	TI 95% Confidence Interval
6	64.99	4.17	2.71	65.04	5.31	3.75
6.1	64.88	4.15	2.69	64.93	5.27	3.73
6.2	64.64	4.11	2.66	64.70	5.21	3.68
6.3	64.94	4.29	2.79	65.00	5.46	3.86
6.4	64.69	4.17	2.70	64.75	5.29	3.74
6.5	65.05	4.24	2.76	65.10	5.41	3.83
6.75	65.48	4.17	2.73	65.54	5.36	3.79
7	65.68	4.03	2.65	65.74	5.19	3.67
7.25	66.17	3.94	2.61	66.22	5.11	3.61
7.5	66.15	3.80	2.51	66.19	4.92	3.48
8	66.15	3.41	2.26	66.18	4.43	3.13
8.5	66.86	3.30	2.21	66.90	4.33	3.06
9	67.05	3.00	2.01	67.08	3.94	2.79
9.5	67.22	2.73	1.83	67.24	3.59	2.54
10	67.32	2.48	1.67	67.34	3.27	2.32
11	68.12	2.29	1.56	68.14	3.06	2.16
13.5	69.28	1.91	1.33	69.29	2.60	1.84
16	69.80	1.82	1.27	69.82	2.49	1.76
21	70.79	1.65	1.16	70.79	2.28	1.61
26	71.29	1.44	1.03	71.30	2.02	1.43
36	71.65	1.33	0.95	71.66	1.87	1.32
46	71.91	1.42	1.02	71.92	2.01	1.42
56	70.54	1.40	0.99	70.55	1.94	1.37
66	69.80	1.42	0.99	69.81	1.95	1.38
81	68.07	1.48	1.01	68.08	1.98	1.40
96	65.26	1.41	0.92	65.27	1.80	1.27
111	61.81	1.37	0.85	61.82	1.66	1.18
131	58.69	1.29	0.75	58.70	1.48	1.05
145.6	58.11	1.31	0.76	58.12	1.49	1.05
147	58.08	1.30	0.76	58.08	1.48	1.05

Table 37. Results for 85% Power Choked at 0° and Bellmouth Removed

Position[mm]	Umean[m/s]	Tl[%]	STD	RMS	U 95% Confidence Interval	Tl 95% Confidence Interval
6	123.85	4.54	5.62	123.98	11.02	7.79
6.1	123.27	4.58	5.65	123.40	11.08	7.83
6.2	123.66	4.48	5.54	123.79	10.85	7.67
6.3	123.57	4.48	5.54	123.69	10.85	7.67
6.4	124.29	4.41	5.48	124.41	10.75	7.60
6.5	123.53	4.48	5.54	123.65	10.85	7.67
6.75	123.59	4.35	5.37	123.71	10.53	7.44
7	124.00	4.29	5.31	124.11	10.42	7.37
7.25	124.97	3.98	4.98	125.07	9.75	6.90
7.5	125.35	3.95	4.95	125.44	9.70	6.86
8	126.03	3.63	4.58	126.11	8.97	6.34
8.5	126.81	3.41	4.32	126.88	8.47	5.99
9	128.19	3.00	3.84	128.25	7.53	5.32
9.5	128.36	2.77	3.56	128.41	6.98	4.94
10	129.04	2.60	3.35	129.08	6.57	4.65
11	129.44	2.27	2.94	129.48	5.77	4.08
13.5	130.67	2.00	2.62	130.70	5.13	3.62
16	130.43	1.87	2.44	130.45	4.79	3.38
21	131.81	1.57	2.07	131.82	4.06	2.87
26	132.78	1.24	1.64	132.79	3.22	2.28
36	132.49	1.16	1.53	132.50	3.00	2.12
46	132.86	1.17	1.56	132.87	3.05	2.16
56	132.02	1.28	1.68	132.03	3.30	2.33
66	130.09	1.34	1.75	130.10	3.42	2.42
81	125.87	1.29	1.63	125.88	3.19	2.26
96	122.31	2.03	2.49	122.33	4.88	3.45
111	120.30	1.36	1.63	120.31	3.20	2.26
131	111.65	2.19	2.44	111.67	4.78	3.38
145.6	108.31	3.60	3.90	108.38	7.65	5.41
147	108.12	3.14	3.39	108.18	6.65	4.70

Table 38. Results for 85% Power Intermediate Condition at 0° and Bellmouth Removed

Position[mm]	Umean[m/s]	Tl[%]	STD	RMS	U 95% Confidence Interval	Tl 95% Confidence Interval
6	111.65	5.15	5.75	111.80	11.26	7.96
6.1	110.99	5.05	5.60	111.13	10.98	7.77
6.2	109.83	4.99	5.48	109.96	10.75	7.60
6.3	109.80	5.04	5.53	109.94	10.84	7.67
6.4	111.12	5.09	5.66	111.26	11.09	7.84
6.5	110.43	4.93	5.44	110.56	10.67	7.54
6.75	111.26	4.96	5.52	111.40	10.83	7.66
7	113.03	4.81	5.44	113.16	10.66	7.54
7.25	113.48	4.64	5.26	113.60	10.32	7.30
7.5	112.98	4.44	5.02	113.09	9.84	6.96
8	114.22	4.27	4.87	114.32	9.55	6.76
8.5	115.09	3.81	4.39	115.17	8.60	6.08
9	116.37	3.50	4.07	116.44	7.98	5.64
9.5	116.94	3.31	3.87	117.01	7.58	5.36
10	117.78	3.02	3.56	117.83	6.98	4.94
11	117.08	2.60	3.05	117.12	5.98	4.23
13.5	118.41	2.27	2.69	118.44	5.27	3.73
16	120.96	2.28	2.75	120.99	5.40	3.82
21	121.98	1.82	2.22	122.00	4.35	3.08
26	122.87	1.43	1.76	122.88	3.46	2.44
36	121.65	1.73	2.11	121.67	4.13	2.92
46	121.02	1.33	1.61	121.03	3.16	2.23
56	121.47	1.75	2.12	121.49	4.16	2.94
66	120.89	2.10	2.54	120.91	4.98	3.52
81	117.61	1.68	1.98	117.62	3.88	2.74
96	113.37	2.44	2.77	113.41	5.43	3.84
111	108.89	1.96	2.14	108.91	4.19	2.96
131	99.00	2.78	2.75	99.04	5.39	3.81
145.6	96.34	3.05	2.94	96.39	5.77	4.08
147	97.22	2.98	2.90	97.27	5.68	4.02

Table 39. Results for 85% Power Near Stall at 0° and Bellmouth Removed

Position[mm]	Umean[m/s]	TI[%]	STD	RMS	U 95% Confidence Interval	TI 95% Confidence Interval
6	93.40	5.99	5.59	93.57	10.96	7.75
6.1	93.93	5.91	5.55	94.09	10.89	7.70
6.2	93.94	5.94	5.58	94.10	10.94	7.74
6.3	93.89	5.85	5.50	94.05	10.77	7.62
6.4	94.16	5.84	5.50	94.32	10.79	7.63
6.5	94.08	5.79	5.45	94.24	10.67	7.55
6.75	93.06	5.63	5.24	93.21	10.28	7.27
7	93.67	5.50	5.15	93.81	10.09	7.14
7.25	95.54	5.63	5.38	95.69	10.55	7.46
7.5	96.63	5.43	5.24	96.77	10.28	7.27
8	97.49	5.10	4.97	97.61	9.75	6.89
8.5	98.33	4.61	4.53	98.43	8.88	6.28
9	99.08	4.26	4.22	99.17	8.27	5.85
9.5	98.59	3.89	3.83	98.66	7.51	5.31
10	100.03	3.59	3.59	100.10	7.03	4.97
11	101.49	3.18	3.23	101.54	6.33	4.48
13.5	102.21	2.73	2.79	102.25	5.47	3.87
16	102.31	2.60	2.66	102.35	5.22	3.69
21	105.03	2.19	2.30	105.06	4.51	3.19
26	107.09	1.79	1.92	107.11	3.77	2.66
36	107.42	1.80	1.93	107.44	3.78	2.67
46	106.77	1.98	2.12	106.79	4.15	2.94
56	105.57	2.71	2.86	105.61	5.60	3.96
66	104.97	1.68	1.76	104.99	3.45	2.44
81	101.62	1.65	1.68	101.63	3.29	2.33
96	98.78	1.93	1.90	98.80	3.73	2.64
111	94.16	1.82	1.72	94.18	3.36	2.38
131	86.80	2.04	1.77	86.82	3.47	2.45
145.6	84.06	2.01	1.69	84.08	3.30	2.34
147	84.00	2.03	1.71	84.02	3.35	2.37

Table 40. Results for 70% Power Choked at 0° and Bellmouth Removed

Position[mm]	Umean[m/s]	TI[%]	STD	RMS	U 95% Confidence Interval	TI 95% Confidence Interval
6	100.63	4.59	4.62	100.73	9.06	6.40
6.1	100.44	4.72	4.74	100.55	9.30	6.57
6.2	100.95	4.69	4.73	101.07	9.27	6.56
6.3	100.76	4.70	4.73	100.87	9.28	6.56
6.4	101.02	4.68	4.73	101.13	9.27	6.55
6.5	101.40	4.58	4.65	101.51	9.11	6.44
6.75	101.17	4.53	4.59	101.28	8.99	6.36
7	101.25	4.34	4.39	101.34	8.61	6.09
7.25	101.98	4.23	4.31	102.07	8.45	5.97
7.5	102.83	3.94	4.05	102.91	7.94	5.62
8	103.35	3.48	3.60	103.41	7.05	4.98
8.5	103.24	3.05	3.15	103.29	6.18	4.37
9	103.41	2.63	2.71	103.45	5.32	3.76
9.5	104.29	2.34	2.44	104.32	4.79	3.39
10	104.96	2.08	2.18	104.99	4.28	3.03
11	105.87	1.83	1.94	105.89	3.80	2.69
13.5	106.37	1.59	1.69	106.38	3.31	2.34
16	106.53	1.47	1.56	106.54	3.06	2.17
21	106.15	1.26	1.34	106.16	2.62	1.85
26	106.76	1.16	1.24	106.77	2.43	1.72
36	107.08	0.99	1.07	107.08	2.09	1.48
46	106.29	1.56	1.66	106.31	3.25	2.30
56	105.87	1.55	1.65	105.88	3.23	2.28
66	104.39	1.25	1.30	104.40	2.55	1.81
81	101.40	1.57	1.59	101.41	3.11	2.20
96	99.70	1.42	1.42	99.71	2.78	1.97
111	92.95	1.69	1.57	92.97	3.08	2.18
131	87.09	1.59	1.39	87.10	2.72	1.92
145.6	84.65	1.74	1.47	84.67	2.88	2.04
147	81.73	1.91	1.56	81.75	3.05	2.16

Table 41. Results for 70% Power Intermediate Condition at 0° and Bellmouth Removed

Position[mm]	Umean[m/s]	Tl[%]	STD	RMS	U 95% Confidence Interval	Tl 95% Confidence Interval
6	89.86	5.28	4.74	89.98	9.29	6.57
6.1	88.59	5.19	4.60	88.70	9.01	6.37
6.2	88.75	5.24	4.65	88.87	9.12	6.45
6.3	88.84	5.18	4.60	88.96	9.01	6.37
6.4	89.78	5.24	4.70	89.90	9.22	6.52
6.5	90.35	5.34	4.83	90.48	9.47	6.69
6.75	90.90	5.06	4.60	91.02	9.02	6.38
7	91.08	5.08	4.63	91.20	9.07	6.41
7.25	90.38	4.88	4.41	90.49	8.65	6.12
7.5	91.57	4.72	4.32	91.67	8.47	5.99
8	92.19	4.11	3.79	92.26	7.43	5.26
8.5	92.85	3.73	3.47	92.92	6.80	4.81
9	94.17	3.24	3.05	94.22	5.98	4.23
9.5	94.79	2.90	2.74	94.83	5.38	3.80
10	95.13	2.66	2.53	95.16	4.95	3.50
11	95.77	2.22	2.13	95.80	4.17	2.95
13.5	97.03	1.88	1.82	97.04	3.57	2.53
16	97.71	1.82	1.78	97.72	3.49	2.47
21	98.31	1.63	1.60	98.32	3.13	2.21
26	99.21	1.44	1.43	99.22	2.81	1.98
36	99.85	1.19	1.19	99.86	2.33	1.65
46	100.09	1.33	1.33	100.10	2.60	1.84
56	99.43	1.81	1.80	99.45	3.53	2.50
66	98.16	1.45	1.42	98.17	2.78	1.97
81	94.90	1.88	1.78	94.91	3.49	2.47
96	89.84	1.87	1.68	89.85	3.29	2.33
111	86.69	1.79	1.55	86.70	3.04	2.15
131	79.74	1.71	1.36	79.75	2.67	1.89
145.6	76.93	1.80	1.38	76.94	2.71	1.92
147	75.90	1.79	1.36	75.91	2.67	1.89

Table 42. Results for 70% Power Near Stall at 0° and Bellmouth Removed

Position[mm]	Umean[m/s]	TI[%]	STD	RMS	U 95% Confidence Interval	TI 95% Confidence Interval
6	74.11	5.39	3.99	74.21	7.82	5.53
6.1	74.02	5.32	3.94	74.13	7.71	5.45
6.2	73.99	5.51	4.07	74.10	7.98	5.65
6.3	74.04	5.53	4.09	74.15	8.02	5.67
6.4	74.57	5.34	3.98	74.68	7.80	5.52
6.5	73.93	5.39	3.98	74.04	7.81	5.52
6.75	74.77	5.28	3.95	74.87	7.73	5.47
7	75.02	5.26	3.95	75.12	7.74	5.47
7.25	75.23	4.98	3.75	75.32	7.34	5.19
7.5	75.78	4.86	3.69	75.87	7.23	5.11
8	75.32	4.42	3.33	75.40	6.52	4.61
8.5	76.00	3.96	3.01	76.06	5.90	4.17
9	76.67	3.60	2.76	76.72	5.40	3.82
9.5	76.71	3.21	2.46	76.75	4.83	3.41
10	77.20	2.87	2.22	77.23	4.35	3.08
11	78.08	2.54	1.98	78.10	3.89	2.75
13.5	79.61	2.11	1.68	79.63	3.29	2.32
16	80.74	2.00	1.62	80.75	3.17	2.24
21	80.63	1.71	1.38	80.64	2.71	1.91
26	81.60	1.55	1.27	81.61	2.49	1.76
36	82.68	1.32	1.09	82.68	2.14	1.52
46	83.24	1.39	1.15	83.24	2.26	1.60
56	81.25	1.56	1.27	81.26	2.48	1.75
66	80.54	1.56	1.25	80.54	2.46	1.74
81	78.51	1.60	1.25	78.52	2.46	1.74
96	75.77	1.65	1.25	75.78	2.46	1.74
111	72.82	1.75	1.27	72.83	2.50	1.77
131	66.70	1.81	1.21	66.71	2.37	1.68
145.6	64.74	1.88	1.21	64.75	2.38	1.68
147	64.50	1.92	1.24	64.51	2.43	1.72

THIS PAGE INTENTIONALLY LEFT BLANK

LIST OF REFERENCES

- [1] Camp, T. R. and Shin, H.W., 1994, “Turbulence Intensity and Length Scale Measurements In Multistage Compressors,” The American Society of Mechanical Engineers, New York, NY.
- [2] Hill, P.G., and Peterson, C., 1992, *Mechanics and Thermodynamics of Propulsion*, Pearson Education, Inc, NY.
- [3] Papamarkos, I., 2004, “Inlet Distortion Generation for a Transonic Compressor,” M.S. thesis, Department of Mechanical and Aerospace Engineering, Naval Postgraduate School.
- [4] Payne, T., 2005, “Inlet-Flow-Field Measurements of a Transonic Compressor Rotor Prior To And During-Steam Induced Rotating Stall.” M.S. thesis, Department of Mechanical and Aerospace Engineering, Naval Postgraduate School.
- [5] Frohnäpfel, D., 2019, “Methodology Development and Investigation of Turbofan Engine Response to Simultaneous Inlet Total Pressure and Swirl Distortion,” Ph.D. thesis, Department of Mechanical Engineering, Virginia Polytechnic Institute and State University.
- [6] Tennekes, H. and Lumley, J. L., 1972, *A First Course in Turbulence*, Massachusetts Institute of Technology, Cambridge, MA.
- [7] Bradshaw, P., 1971, *An Introduction to Turbulence and its Measurement*, Pergamon Press, NY.
- [8] Goldstein, R., 1983, *Fluid Mechanics Measurements*, Hemisphere Publishing, London, England.
- [9] Kulite., “Kulite Pressure Transducers Distinctively Different,” <https://kulite.com/technology/sensor-description>.
- [10] Siren, K., Rosen, G., Vad, J., and Nielsen., 2001, *Industrial Ventilation Guidebook*, Howard Goodfellow and Esko, Mississauga, Canada and Helsinki, Finland, Chap. 12.
- [11] TSI, Inc., 2000, IFA 300 Constant Temperature Anemometer System.” St Paul, MN.
- [12] Alford, N., 2008, “Evaluation of a Supersonic Compression Nozzle.” M.S. thesis, Department of Mechanical and Aerospace Engineering, Naval Postgraduate School.

- [13] Guimaraes, T., 2018, “Fluid Dynamics of Inlet Swirl Distortions for Turbofan Engine Research,” Ph.D. thesis, Department of Mechanical Engineering, Virginia Polytechnic Institute and State University.
- [14] TSI, Inc., “TSI Thermal Anemometry Probes Catalog,” http://www.tsi.se/documents/Hotwire_Catalog_2980465.pdf.
- [15] Harman, K., “Continued Modernization of the NPS Transonic Compressor Test Rig,” M.S. thesis, Department of Mechanical and Aerospace Engineering, Naval Postgraduate School.

INITIAL DISTRIBUTION LIST

1. Defense Technical Information Center
Ft. Belvoir, Virginia
2. Dudley Knox Library
Naval Postgraduate School
Monterey, California